IDENTIFICATION OF WHOLE CELL ACTIVE MOLECULES OF

MYCOBACTERIUM TUBERCULOSIS, ELUCIDATION OF MOLECULAR

MECHANISMS RESPONSIBLE FOR RESISTANCE, AND

CHARACTERIZATION OF RV0272: A POTENTIAL THERAPEUTIC TARGET

A Dissertation

by

RYAN C. HUGHES

Submitted to the Office of Graduate and Professional Studies of
Texas A&M University
in partial fulfillment of the requirements for the degree of

DOCTOR OF PHILOSOPHY

Chair of Committee:	James C. Sacchettini
Committee Members:	Tadhg Begley
	Paul Straight
	Hays Rye
Head of Department:	Gregory D. Reinhart

December 2016

Major Subject: Biochemistry

ABSTRACT

Current therapies for treatment of mycobacterial infections are adequate when diagnosis and pathology is well defined. Yet more evidence is beginning to accumulate for the multitude of reasons behind drug insensitive mycobacterial cases, especially for *Mycobacterium tuberculosis (M. tuberculosis)*. Drug resistant strains are not always the sole cause for complications in treatment. Heterogeneity of bacterial sub-populations and the micro environments they reside in can contribute to mycobacteria's ability to evade treatment. Elucidation of the mechanisms essential for bacterial virulence and persistence as well as developing antibiotics with more diverse mechanisms of action will allow clinicians to make more effective decisions regarding treatment regimens for each individual pathology.

One of the first stages in drug development is the identification of small molecules which effectively inhibit bacterial growth as well as determining their mechanism of action. The first part of this study focuses on establishing a High Throughput Screening (HTS) assay for the identification of growth inhibitors of *M. tuberculosis, Mycobacterium smegmatis (M. smegmatis), Mycobacterium abscessus (M. abscessus), and Mycobacterium fortuitum (M. fortuitum).* Pathogenesis is not exclusive to *M. tuberculosis* and these other non-tubercular species not only contribute to the disease epidemic, but can also serve as model organism(s) in a laboratory setting for *M. tuberculosis* due to their rapid growth rate and low infectivity in healthy individuals. A HTS of over 100,000 molecules was carried out against *M. tuberculosis, M. fortuitum, and M. abscessus.* The identified hits were validated in a dose response assay and

attempts to identify the intracellular target of inhibition were determined via selection of resistant mutants in *M. smegmatis, M. abscessus,* and *M. fortuitum.*

The second part of this study focuses on the characterization of a protein identified as a potential target of a growth inhibitor of *M. tuberculosis* identified in the original HTS. This enzyme, Rv0272, encodes for a hypothetical α/β hydrolase and has no significant sequence homology to any previously characterized enzymes. Purified recombinant Rv0272 was biochemically and biophysically characterized. The crystal structures of ligand bound Rv0272 combined with binding studies revealed the ligand promiscuity of Rv0272 and provided clues for potential enzymatic function(s). The enzyme has demonstrated binding affinity for small dicarboxylic acids, especially methylmalonate, phthalate, and maleate. Moreover, products of enzyme mediated reactions were observed in the active site of solved crystal structures after soaking with metabolites. These results suggest that Rv0272 is a previously uncharacterized serine hydrolase that may be functioning in the B12-dependent methylmalonate pathway for degradation of odd chain fatty acids. Additionally, Rv0272 may moonlight as an amidase, esterase, and/or thioesterase under certain physiological conditions.

DEDICATION

I would like to dedicate this work to my parents for their limitless support, love and patience throughout the years and for always being there for me my entire life and especially while I finish my degree.

ACKNOWLEDGEMENTS

TABLE OF CONTENTS

LIST OF FIGURES

Page

LIST OF TABLES

CHAPTER I

INTRODUCTION

HISTORY OF TUBERCULOSIS

It seems almost unbelievable to imagine that in the last 200 years, tuberculosis has been responsible for the deaths of approximately one billion people. The battle against the disease is one of the most important struggles in human history, yet its story appears to have been lost in modern times, replaced by the notion that tuberculosis is a ghost from the past. Nothing could be further from the truth as we face one of the worst epidemics ever recorded. Perhaps, in order to comprehend the magnitude of the disease itself, the origin of the bacterium and its relationship with human beings needs to be examined.

It is believed by many that tuberculosis evolved from a soil born micro-organism. The disease most likely first infected animals which inhaled or ingested it from the soil and was contracted by humans through eating of their flesh or drinking of their milk (1). The fossil record shows that human ancestry is only 3-5 million years old. In these records, evidence exists of several infections. A dental abscess was identified in a fossil skull from Homo erectus, dating back over 2 million years.[1] Also, a 40,000 year-old skull found in Broken Hill, Rhodesia, had a cavity indicative of a mastoid infection which would be easily recognizable by any ear, nose, and throat specialist today (3). Although neither infection was tuberculosis, it is suggestive that other infections were also present during these times.

---

[1] Personal communication between Keith Manchester and Frank Ryan. (2)

The first direct evidence of tuberculosis infection comes from investigating the remains of Egyptian mummies, some over 6,000 years old. *M. tuberculosis* has the capacity to eat away bone, especially vertebrae, which leads to the collapse of the spinal column, commonly referred to as "hunchback". The disease is easily recognizable by these disfiguring changes in many Egyptian mummies and re-affirmed from the "hunchback" depictions created by many Egyptian artists. Famously, the remains of a high priest of Amon still had signs of pus discharging from a spinal abscess along the course of the psoas muscle, unique to tuberculosis infections (4). Similar evidence has been found throughout grave sites dating from antiquity in Italy, Denmark, and the Jordan valley (5) (6). Therefore, it has been speculated that the first tuberculosis epidemic occurred during the Stone Age, paralleling the rise of the Egyptian empire.

By 2,500 BC, archeological evidence shows that tuberculosis was already well established in Europe and may have even been in Britain over a thousand years prior (7). Interestingly, there is clear evidence of the disease in skeletal remains from American Indians in Pre-Columbian America in what is now Ontario and New York State (8). Additional evidence of the disease was also found in a Peruvian mummies as well as in the skeletal remains from the ancient Ainu culture of Japan (9).

Tuberculosis has continued to persist and its prominence has been well documented for the last two thousand years throughout Europe. By the 1600's, the London Bills of Mortality recorded that consumption (older name previously used to describe tuberculosis) was responsible for one in five deaths. By the 19th century, seven million people a year died from tuberculosis while 50 million people were openly infected, the

worst areas being the metropolises of London and New York City. The course of the disease would remain steady, without any hope for treatment until the beginning of the 20th century, when the cause of tuberculosis was finally unraveled. However, to fully appreciate the strides which have been made in combating tuberculosis infections, one must first examine the foundation laid down previously by the generations of scientists whose perseverance and ingenuity led to the eradication of consumption, sepsis, gas gangrene, and pneumonia as the leading cause(s) of mortality in the U.S (2).

HISTORY OF ANTIBACTERIAL CHEMOTHERAPEUTICS

The stage was initially set by a totally unknown German doctor named Robert Koch on March 24, 1882 in Berlin. On this night he was set to address the German Physiological Society in front of many prominent attendees including Rudolph Virchow, Friedrich Loeffler, and Paul Ehrlich. Loeffler would later state "Koch was by no means a dynamic lecturer who would overwhelm his audience with brilliant words. He spoke slowly and haltingly, but what he said was clear, simple, logically stated – in short, pure unadulterated gold." Koch had done what so many before him and tried and failed, he discovered bacteria in organs which had been altered by tuberculosis. He had developed a new staining technique which allowed him to identify the characteristic rod shape of tuberculosis. He successfully detected tuberculosis bacilli in many varieties of animal and human tissues and had them on display for anyone to check the results for themselves. To every scientist or doctor at the time, the cause of tuberculosis was one of life's greatest mysteries. Koch ended his talk by saying, "All of these facts taken together can lead to

only one conclusion: that the bacilli which are present in the tuberculosis substances not only accompany the tuberculosis process, but are the cause of it. In the bacilli we have, therefore, the actual infective cause of tuberculosis." This was so profound that his speech would circulate around the world and in less than three weeks be enshrined in a Berlin medical journal. Paul Ehrlich would later confess, "I hold that evening to be the most important experience of my scientific life." Koch would go on to win the Nobel Prize in Medicine just 23 years later in 1905. [2]

Although Paul Ehrlich had already pioneered and perfected bacterial staining with his invention of methylene blue in the late 1800's, which Koch modified to in order to discover the bacterial origin of tuberculosis, his greatest contributions would come a little later. In the early 1900's, Ehrlich pioneered the idea of chemotherapy, through modification(s) of atoxyl, an arsenic derivative at the time believed to be an unmodifiable compound. Extensive chemical substitution and reduction products led to the creation of nr. 606, which became the first successful chemotherapeutic against syphilis, which he was awarded the Nobel Prize for Medicine in 1908 [Figure 1.1]. It was called Salvarsan, meaning "the arsenic that saves" and was known as the magic bullet of medicine at the time. Ehrlich donated 65,000 free samples for clinical testing which led to the development of a successful treatment method of Salvarsan for dementia and paralysis due to late stage syphilis at Rockefeller Hospital. [3]

---

[2] Taken from Professor Brock and Springer Verlag's biography of Robert Koch. Not Published. (2)
[3] Tuberculosis: The Greatest Story Never Told by Frank Ryan. Pages 88-90. (2)

A colleague of Ehrlich's, Williams Roehl, began working on a chemotherapeutic against African sleeping sickness based on azo-dyes from the textile industry. He theorized that the more intensely a dye stained textile fibers, the more likely it was to penetrate living cells. After testing more than 200 different agents, a carbide compound, "Bayer 205" was discovered which would later be world renown as "Germanin", the first potent treatment for sleeping sickness [Figure 1.2]. Since the 17th century, quinine has been used to treat malaria. In addition, Fritz Schoenhoefer synthesized a Plasmachin in 1924, a chinolin compound that was over 30 times more effective than quinine for treatment of malaria [Figure 1.3]. [4]

Figure 1.1. Salvarsan 606 and its formulation from Ehrlich's journal.

---
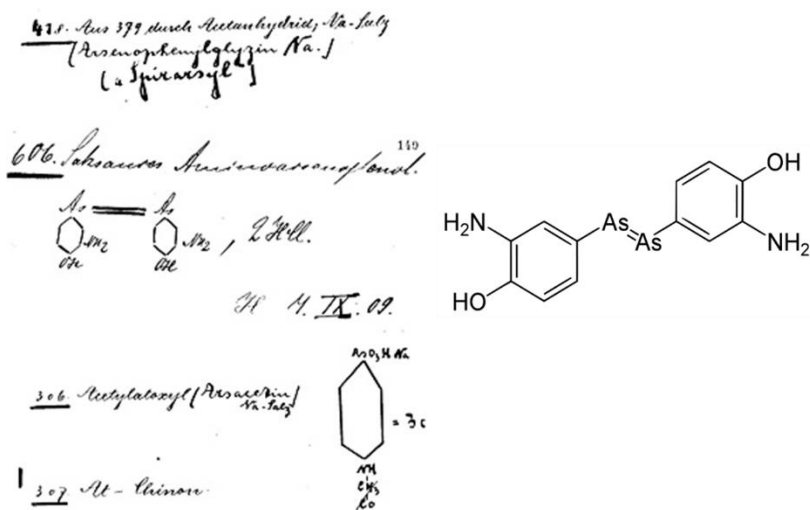
[4] Tuberculosis: The Greatest Story Never Told by Frank Ryan. Pages 74, 90-96. (2)

These prior successes set the stage for one of the single most important contributors to modern medicine, Gerhard Domagk. His first breakthrough came in 1932, when he discovered Prontosil rubrum, a relatively non-toxic azo derivative of chrysoidine for the treatment of streptococci infections [Figure 1.4]. Due to its low solubility, it had to be orally administered. However, he later developed a sodium sulfate version which could be topically applied. [5] In 1936, it was determined that an intermediate product of Prontosil was the bio-active form, thus the first discovery of a pro-drug. In 1935, Domagk identified an ethyl-dimethyl-vinyl ammonium chloride compound which was effective against a wide range of bacteria. "Zephirol" as Domagk called it, would become the world's primary disinfectant for decades [Figure 1.5] (10) .

Figure 1.2. Chemical structure of Germanin discovered by William Roehl.
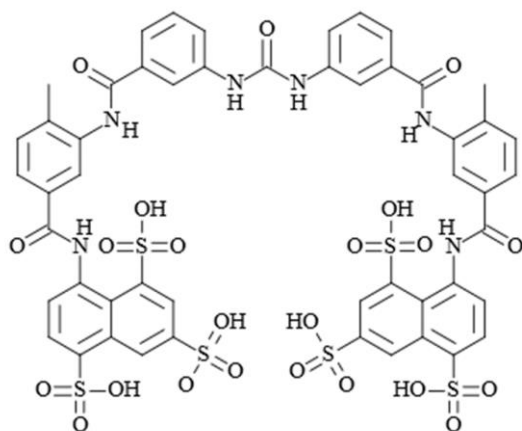
Then in 1941, Domagk identified sulfonamides that contained either a theodiazole or thiazole group which were active against tubercular bacilli *in vitro.* Around the same time, he developed three trial drugs, Conteben, Solvoteben, and Nikoteben for the treatment of Lupus Vulgaris, a disease which mercilessly decomposes a victim's face, often leading to patient suicide [Figure 1.6]. Conteben would later be proven to be a mildly effective treatment option for tuberculosis as well. However, these discoveries opened the door for the first therapeutics aimed at combating tuberculosis and coincided with the development of other equally important anti-tubercular chemotherapeutics. [6]

Figure 1.3. Compounds used for the treatment of malaria. Plasmochin (left) compared to quinine (right) which it surpassed in efficacy and potency.

Plasmochin   Quinine

---
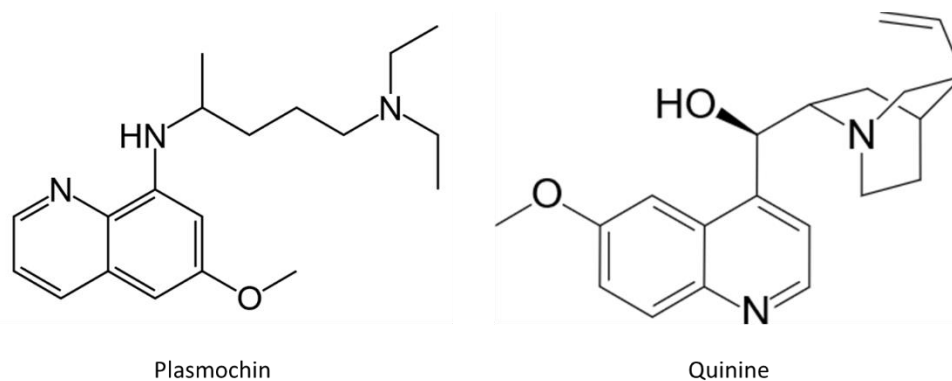
[6] Tuberculosis: The Greatest Story Never Told by Frank Ryan. Pages 342-348 (2)

HISTORY OF TUBERCULOSIS TREATMENT

The outlook for tuberculosis changed dramatically with the introduction of chemotherapy. The first discovery, para-amino salicylic acid (PAS), was made by Jorgen Lehmann in 1943 paralleled by Domagk's Conteben in in 1945. Unfortunately both drugs were found to be bacteriostatic. In 1944 Selman Waksman, Albert Schatz, and Elizabeth Bugie were the first to isolate streptomycin, the first bactericidal agent effective against *M. tuberculosis*. The first orally administered drug used for the treatment of tuberculosis was isoniazid, which was discovered to be effective against *M. tuberculosis* in 1952. This was followed 5 years later with the discovery of the rifamycins in 1957. These discoveries began a new chapter in the war on tuberculosis, where the disease could not only be managed, but cured.

CURRENT TREATMENT

As of 2015, The World Health Organization (WHO) recommends a cocktail of first line anti-tuberculosis drugs for all new patients for the first two months. It is made up of isoniazid, rifampicin, pyrazinamide, and ethambutol. This is followed by four months of isoniazid and rifampicin treatment. Taking each drug daily is recommended during the first two months, but can be switched to three times weekly dosing during the final four months. With high patient adherence to this prescribed regimen, treatment is effective over 95% of the time in eliminating the disease caused by antibiotic susceptible *M. tuberculosis*.

Figure 1.4. Chemical structure of Prontosil rubrum, one of the first highly effective general antibiotics.
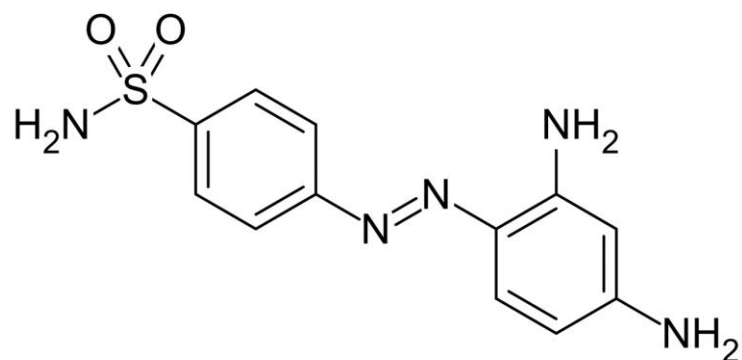
Figure 1.5. Comparison of the chemical structure(s) of Conteben, Solvoteben, and Nikoteben.
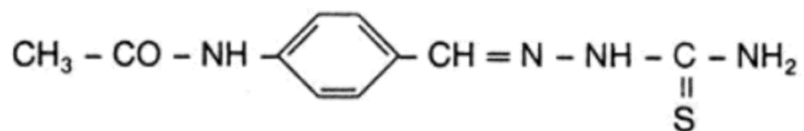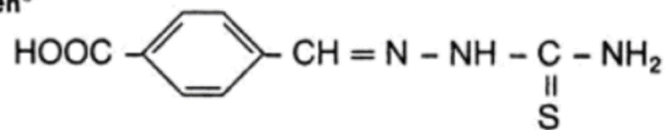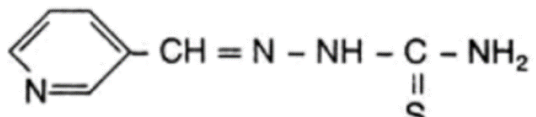
When *M. tuberculosis* has demonstrated resistance to at least two first line drugs, it is considered multi-drug resistant (MDR) and second line drug treatments must be implemented. Second line anti-tuberculosis drugs are less safe, more expensive, and call for a much longer treatment duration. These drugs include flouroquinolones, *para-*aminosalicylic acid, aminoglycosides, cyclic peptides, cycloserine, and ethionamide. Rational MDR tuberculosis (MDR-TB) treatment involves a minimum of four active drugs, a fluoroquinolone, an injectable aminoglycoside, and any first line drug to which the strain is sensitive. This treatment regimen should last for a minimum of 18 months and is estimated to cost over 160,000 euros. MDR strains which become resistant to key drugs from second line therapy, any fluoroquinolone and at least one injectable drug (Kanamycin, Capreomycin, Amikacin), are considered extensively drug resistant. (XDR). Treatment options for patients with XDR tuberculosis (XDR-TB) are extremely limited and it is estimated that 54% of XDR-TB patients die within a month of diagnosis (11).

Figure 1.6. Chemical structure of Zephirol, one of the first widely available disinfectants.
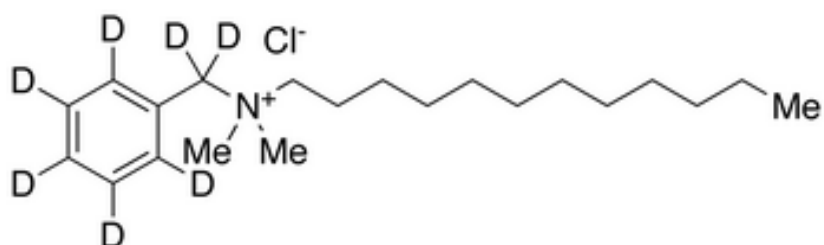
FIRST-LINE ANTIBIOTICS FOR DRUG-SUSCEPTIBLE *M. TUBERCULOSIS*

Isoniazid (INH)

General Information, Dosage, Adverse Effects

INH is a component of the first line drugs recommended by the World Health Organization for all anti-tuberculosis chemotherapeutic regimens. It can also be prescribed alone to be used as a prophylactic to help prevent transmission in areas or individuals at high risk. INH is generally taken orally at a dose of 100-300mg or in more severe cases as an injectable at a dose of 2ml of 25mg/ml. The maximum recommended dose is 300mg or 5mg/kg daily and is usually administered once a day for at least 6 months. Systemic or cutaneous hypersensitivity reactions can occur during the first weeks of treatment. Peripheral neuropathy, optic neuritis, toxic psychosis, and convulsions can occur in susceptible individuals but is exceedingly rare. Epilepsy can be provoked with in susceptible individuals. INH has a minimal inhibitory concentration (MIC) of 0.016-0.06 µg/ml against wild type tuberculosis H37rv (12).

Discovery

In 1949, two U.S. doctors, Corwin Hinshaw of Stanford and Walsh McDermott of Cornell Medical school traveled to Germany to investigate reports of a potent anti-tuberculosis drug. They discovered that Domagk had derived a synthetic chemical of the thiosemicarbazone series which had successfully treated well over 7,000 patients suffering from tuberculosis infection. They brought Conteben back to the US and proceeded to synthesize thousands of thiosemicarbazone derivatives in hopes of not only synthesizing

11

Conteben for themselves, but to improve on its potency. This endeavor was made possible because the U.S. declared that any German patent filed during the course of World War II was void. Conteben was quickly synthesized in the U.S. and renamed Amithiozone, without any compensation made to Bayer (2).

Figure 1.7. Chemical structure of isoniazid.
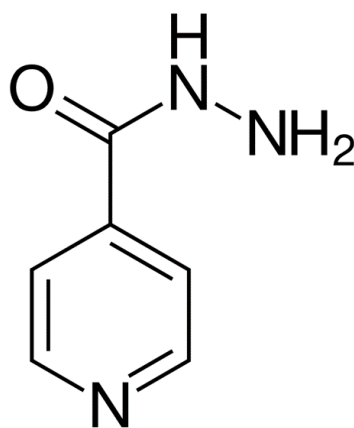
The thiosemicarbazones became the template to which many pharmaceutical companies targeted in order to create libraries of Conteben like molecules for treatment of tuberculosis. Simultaneous and independent work was on-going by Herbet Fox of Hoffman-La Roche and Jack Bernstein of E.R. Squibb & Sons in the US and Gerhard Bomagk of Bayer in West Germany. In 1951, all three arrived at the same chemical derivate, isonicotinyl hydrazine (isoniazid), and were able to demonstrate that isoniazid had a very high degree of anti-tubercular activity [Figure 1.7]. However, since the

synthesis had been published by Hans Meyer and Josef Mally of German Charles University in Prague in 1912 as part of their doctoral requirements, it was public domain and therefore no company could successful obtain a patent on isoniazid [Figure 1.7]. Regardless, it was soon hailed as one of the most potent, if not the most potent single anti-tuberculous drug available.

Mode of Action

From 1953 to 1980 many modes of action for INH were proposed. It was thought to interfere with cell division, pyridoxal-dependent metabolic pathways, lipid biosynthesis, fatty acid biosynthesis, nucleic acid biosynthesis, glycerol metabolism, NAD^+ biosynthesis, and NADH dehydrogenase activity (13-15). It wasn't until 1970 that Winder and Collins made a break through and showed that INH inhibited synthesis of mycolic acids, which are a critical component of the mycobacterial cell wall. In addition, they demonstrated that mycolic acid synthesis was unaffected by INH in an INH-resistant strain of *M. tuberculosis* (16). This was later confirmed in 1972 by Takayama et al who showed that in less than one hour after exposure to INH, the bacterium completely lost the ability to produce the individual mycolic acid components: alpha-mycolate, methoxymycolate, and beta-mycolate (17). In 1975, Takayama at al demonstrated that isoniazid inhibited the synthesis of long chain saturated and unsaturated fatty acids greater than C24. This led to the hypothesis that these fatty acids were precursors to mycolic acids and INH must be targeting an enzyme responsible for mycolic acid biosynthesis (18).

Then in 1979, Takayama and Davidson showed that INH led to the inhibition of the first specific reaction in mycolic acid synthesis, the desaturation of tetracosanoic acid (19). However, it wasn't until 1992 that the specific mode of action of INH was determined. Zhang et al discovered that mutations in a catalase-peroxidase encoding gene conferred resistance to INH. This gene, KatG was shown to restore sensitivity in INH-resistant isolates. Shortly after, it was discovered that INH is a pro-drug which requires the catalase peroxidase KatG to activate INH to form a hypothetical isonicotinoyl radical. This radical interacts with NAD^+ to form an INH-NAD adduct which then binds to the active site of the NADH-dependent enoyl-ACP reductase, InhA, disrupting mycolic acid synthesis (20).

In the early 2000's, the role of a β-ketoacyl synthase enzymes (KasA and KasB) were being evaluated for their contribution to INH resistance. KasA has been shown to be involved in both Type I and Type II fatty acid synthase systems in mycobacteria. The gene which encodes for KasA is part of the five-gene operon which is believed to be involved in mycolic acid synthesis. *In vitro* enzyme assays of KasA revealed that INH was able to inhibit KasA-associated fatty acid production by 41% at 10μg/ml. In addition, mutations in KasA have been identified in clinical isolates of *M. tuberculosis* resistant to INH (21). Constructs of KasA with these point mutations were made and tested for *in vitro* activity. It was shown that the individual mutations had at least a 29% reduction in activity compared to wild type. This result was recapitulated by creating mutant KasA recombinants and testing for activity of INH compared to wild type KasA. Strains which contained the plasmid with wild type KasA had a 5-fold decrease in MIC compared to the

mutant strains (22). These results implicated KasA in INH resistance and mutations in KasA may lead to a reduced enzymatic activity in exchange for drug resistance.

In 2007, the role of *M. tuberculosis* KasA mutations in INH resistance were again re-evaluated. There are two mutations in *kasA* seen in clinical isolates, G312S and G269S which are believed to contribute to INH resistance. Extensive analysis of 160 INH-resistant and drug-susceptible *M. tuberculosis* clinical isolates has shown that the G312S and G269S mutations occur at the almost the same frequency between both INH-resistant and drug-susceptible strains of *M. tuberculosis* . Further investigation revealed that all the isolates with the G312S mutation belonged to one evolutionary clade of the *M. tuberculosis* East-African-Indian (EAI) family, while all the G269S mutations belonged to the *M. tuberculosis* T family. The T family share a 13-band IS6110 restriction fragment length polymorphism. This suggests that KasA may not be directly related to INH resistance but represent a lineage of *M. tuberculosis* which are associated with these specific sequence polymorphisms. In further support of this hypothesis, 68 EAI and 30 T drug-susceptible *M. tuberculosis* isolates were sequence and analyzed looking for G312S mutations. Of the 69 EAI isolates, 28 had G312S mutations while the remaining were *kasA* wild type at 312 (23). A more recent study examined 609 INH-susceptible and 403 INH-resistant isolates were the T genotype is prevalent and found the G269S mutation in 9% of the INH-resistant strains and 14% in the INH-susceptible strains (24).

Mechanism of Resistance

There are two general mechanisms proposed to lead to resistance to INH in clinical isolates of *M. tuberculosis*. Preventing the activation of INH through mutation(s) in the activator, KatG or through mutation of transcription factors which regulate KatG expression (25). The most common mutation found in INH-resistant *M. tuberculosis* is a S315T mutation in KatG. The other mechanism is through mutations in the target, InhA which would prevent the binding of the INH-NAD adduct (26). Other mechanisms which may confer resistance but have yet to be extensively investigated include drug in-activators, alterations in redox, and efflux pumps.

One of the most studied mutations which leads to INH resistance is a S94A mutation in InhA. This mutation does not perturb the binding of the enoyl substrate to InhA, however it does increase the Km for NADH by 5-fold. This effectively allows for NADH to outcompete the INH-NAD adduct for binding and markedly reduce its effectiveness. Another well documented mechanism of resistance found in clinical isolates is a c-15t base pair change in the *inhA* regulatory region which increases expression of InhA by over 20 fold. This subsequently increases the minimum inhibitory concentration (MIC) of INH by up to 10 fold in *M. tuberculosis.* In one study this mutation was seen in 35% of INH-resistant, over 48% of MDR and 85% of XDR clinical isolates acquired from South Africa and is believed to be a marker for MDR (27).

Isolation of INH-resistant mutants *in vitro* has also revealed an additional site of mutation in Rv1854c, a gene which encodes for a type II NADH dehydrogenase. This enzyme functions by oxidizing NADH into NAD^+. Single point mutations have been

shown to reduce the enzyme's activity by 95% compared to wild type. This change in activity leads to higher levels of cellular NADH while maintaining similar levels of NAD^+. This increased pool of NADH concentration competes with the INH-NAD adduct for binding to InhA, leading to INH resistance (28).

There are five enzymes which are required to synthesize mycothiol, a detoxifying agent found in mycobacteria. Mutations in 2 of these genes, *mshA* and/or *mshC,* cause a drastic reduction in mycothiol levels which can lead to INH resistance. The relationship between mutations in *mshA* and *mschC* and INH resistance is ambiguous but it has been shown that reducing the amount of mycothiol in the cell is responsible for low levels of INH resistance (29).

There are more than 300 mutations in *katG* that have been identified throughout the open reading frame (ORF). The most frequently identified mutation is at codon S315 where each base can be mutated to make a different amino acid. The S315T mutation is identified in as high as 94% of INH-resistant clinical isolates in certain areas of the world (30). In addition, deletions in a gene encoding for an iron uptake protein, *furA*, lead to overexpression of katG and a hyper-susceptibility to INH in a laboratory setting. It was later shown that mutations in the intergenic region between *furA* and *katG* resulted in a decrease in INH oxidase activity and subsequently a two to four fold increase in INH resistance (31, 32). This data suggest that the *furA-katG* intergenic region should be examined in clinical isolates to possibly probe for low levels of INH resistance.

M. tuberculosis contains an arylamine N-acetyltransferase NAT2 which can acetylate INH and inactivate it. Mutations have been identified in the *nat2* gene which

confer low levels of INH resistance. However, these mutant Nat proteins are incapable of acetylating INH, so the obvious correlation between mutation and resistance is lacking in this case (33, 34).

Three genes which all encode for enzymes which contain an NAD^+ binding motif were found to confer low levels of INH resistance when overexpressed. The authors concluded that NAD-binding proteins may play a role in resistance by reducing the cellular levels of NAD^+, which in turn limits the amount of INH-NAD adduct which could potentially form (35). It has also been shown that expression of several efflux pumps are upregulated in the presence of INH which may play a role in drug resistance in *M. tuberculosis* (36).

Ethambutol (EMB)

General Information, Dosage, Adverse Effects

EMB is a primary component of the first line of anti-tubercular drugs recommended by WHO for short course treatment of drug susceptible *M. tuberculosis.* EMB is administered orally with a recommended dosage of 50mg/kg up to a maximum of 2.5g twice weekly. The plasma half-life has been shown to range from 2.5-4 hours in individuals with healthy renal function and is mainly eliminated in the urine (37). EMB does not appear to be extensively metabolized by the body and only 8-15% of an oral dose was found excreted as biologically inactive break-down products. However, the modifications that did occur appeared to involve oxidation of both alcohol groups corresponding to the dicarboxylic acid(s) (38). Although EMB failed to enter meninges or

spinal fluid of healthy patients, it surprisingly was able to enter the spinal fluid of patients with tuberculosis meningitis at therapeutic levels (>1µg/ml) (39). The lethal dose (LD_{50}) of EMB in mice and rats was determined to be 8.9 and 6.8 g/kg respectively (40).

Ocular toxicity has been observed in rare cases as well as other allergic manifestations including jaundice, skin rash, gastrointestinal upset, joint pain, numbness, fever, and headache. In general, these effects are reversible once the drug is discontinued (41, 42). EMB has been found to be active against all strains of *M. tuberculosis*, *Mycobacterium Bovis (M. Bovis)*, and *Mycobacterium Kansasii (M. Kansasii), Mycobacterium smegmatis (M. smegmatis), Mycobacterium ranei (M. ranei),* and *Mycobacterium phlei (M. phlei)* with an MIC of 0.5-2.0µg/ml (43). Additional susceptibility studies have shown that EMB is active against certain atypical mycobacteria such as *Mycobacterium aquae (M. aquae), Mycobacterium fortuitum (M. fortuitum), and Mycobacterium avium (M. avium)* on Lowenstein-Jensen medium (44). EMB is bacteriostatic and possesses little sterilizing ability but is active against *M. tuberculosis* strains resistant to INH and SM. It does not demonstrate activity against fungi, viruses, or other pathogenic bacteria.

Figure 1.8. Chemical structure of ethambutol.
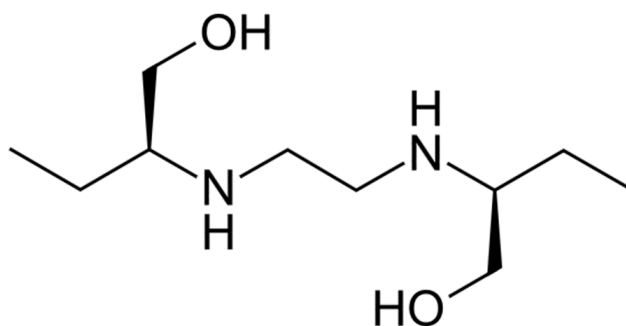
Discovery

In 1962, Shepherd and Wilkinson at Lederle Laboratories first discovered a molecule, N, N'-diisopropylethylenediamine, which had a very high activity against *M. tuberculosis.* This discovery was exciting because its chemical structure was completely unrelated to the other known anti-tuberculosis drugs at the time. This lead to extensive modifications and screening to synthesize an optimal drug from this parent compound. Shepherd and Wilkinson found that N-alkyl substitutions no bigger than *sec*-butyl groups were required for activity as well as branching on the diamine nitrogens. This led to the hypothesis that chelation was responsible for the observed anti-tuberculosis activity. From this theory, a series of N,N'-bis (hydroxyalkyl) alkyldiamines were made and tested for activity. The resulting compounds which demonstrated the most activity all contained a dextro-2-amino butanol moiety and dextro-2,2'-(ethylenediimino)-di-1-butanol dihydrochloride [Figure 1.8]. This was later shortened to ethambutol, which was four times more active *in vivo,* eight times more active *in vitro*, and less toxic than the original

lead molecule. It was concluded that EMB had a similar efficacy based on the ratio of drug tolerance to drug potency as INH and SM (45, 46)

Mode of Action

There have been several proposed mechanisms over the years and most studies have implicated EMB in detrimentally altering the mycobacterial cell wall structure. One such study demonstrated that EMB inhibited the transfer of arabinogalactan into the cell wall of *M. smegmatis* which led to the accumulation of trehalose mono- and dimycolates in the culture medium (47). In addition, EMB was shown to inhibit the transfer of glucose into the D-arabinose molecule of arabinogalactan. This leads to the accumulation of D-arabinofuranosyl-P-decaprenol, an intermediate in arabinogalactan biosynthesis (48). From these results, it was hypothesized that EMB blocks the transfer of arabinogalactan to the cell wall, resulting in the accumulation of mycolic acids. This agrees with the phenotypic observations that EMB treatment causes bacterial de-clumping and morphological changes (49).

The gene *embB,* which encodes for an arabinosyl transferase, an enzyme involved in the synthesis of arabinogalactan, is thought to be the target of EMB. In *M tuberculosis*, *embB* is located on an operon with *embA* and *embC*, sharing over 65% sequence identity with each and are predicted to encode for transmembrane proteins. This assumption was recapitulated by one study which showed that EMB-resistant *M. tuberculosis* isolates have frequent missense mutations in *embB* while EMB-sensitive *M. tuberculosis* did not (50).

However, EMB has also been reported to interfere with RNA metabolism, mycolic acid transfer, phospholipid synthesis, and spermidine biosynthesis (51-54)

Mechanism of Resistance

The mutation frequency which leads to EMB resistance is quite high and has been shown to occur at a frequency of 10^{-5} in both *M. tuberculosis* and *M. bovis.* However, the level of resistance achieved was never greater than five times the MIC, unless the cultures were passed and inoculated with fresh drug twice weekly for 10 weeks. In this case, a strain of *M. tuberculosis* was isolated that had an MIC of 120µg/ml, or about 60 times the MIC. In general these mutations are stable when passed into a drug free medium *in vitro* (55, 56).

EMB resistant *M. tuberculosis* strains usually have a mutation somewhere in the *embCAB* operon. The *embCAB* operon is comprised of three genes, *embC, embA,* and *embB.* Proteins EmbA and EmbB are believed to be charged with the proper terminal formation of hexaarabinofuranoside motif during arabinogalactan synthesis while EmbC is involved in lipoarabinomannan synthesis (57, 58). Mutations are most often found in *embB* but are occasionally seen in *embC* (59). Codon 306 in *EmbB* is the most commonly observed mutation in *M. tuberculosis* clinical isolates accounting for almost 70% of all resistant strains. Interestingly, a study on a large number of *M. tuberculosis* clinical isolates showed that mutations in *embB*306 were not necessarily conferring resistance to EMB (60). Instead the mutation appears to give the strain a predisposition to develop resistance to several other drugs, possibly an indicator of MDR-TB. Furthermore, the

authors found that it was specific amino acid substitutions which determine whether or not the strain would be EMB resistant or give rise to additional resistances. Additional mutations found implicated in EMB resistance are a Gln379Arg substitution in *embR* as well as mutations in *rmlD, rmlA2,* and Rv0340. There still remain almost 30% of EMB resistant strains where no known mechanism of resistance can be determined and mutations in the *embCAB* operon are absent (61).

Rifampicin (RIF)

General Information, Dosage, Adverse Effects

RIF is an orally administered, semisynthetic derivative of rifamycin and a primary component of the WHO recommended first line short course therapy for the treatment of tuberculosis. It is a potent bactericidal antibiotic with extensive sterilizing capacity against bacilli in both cellular and extracellular locales. Rifampicin is never used as a stand-alone anti-tuberculosis drug due to the high rate of resistance seen in clinical isolates. The overall prevalence of RIF-resistant *M. tuberculosis* strains is estimated to be as high as 25% among all infected patients, with nearly half of those being resistant to more than one drug (62). Rifampicin is lipid soluble and is readily absorbed and distributed amongst all bodily tissues and fluids. A maximum recommended daily dose of 600mg or 10mg/kg of RIF will have a peak serum concentration of 10µg/ml in 2-4 hours with a half-life of about 3 hours. RIF is recycled in the enterohepatic circulation and its metabolites are eventually secreted in the feces after extensively deacetylation occurs in the liver.

Minor gastrointestinal intolerances are common with RIF treatment and additional side effects such as skin rashes, fever, and thrombocytopenia can occur with intermittent use. Dose-related hepatitis can occur when patients exceed the recommended daily allowance of 600mg. Additionally, RIF can induce hepatic enzymes which could alter the dosage requirements for maximum effectiveness of other drugs. These include corticosteroids, steroid contraceptives, oral hypoglycemic agents, oral anticoagulants, phenytoin, cimetidine, quinidine, cyclosporine, and digitalis glycosides. RIF has an MIC of 0.25-0.5 µg/ml against *M. tuberculosis* in 7H10 growth media (12).

Discovery

Sensi et al at Dow-Lepetit Research Laboratories in Milan, Italy first synthesized rifampicin in 1957 as part of an extensive program design to chemically modify rifamycins, metabolites of *Norcardia mediterranei*. Rifamycins are a complex composed of 5 individual rifamycins (A, B, C, D, E). All molecules which demonstrated a capacity to kill mycobacteria were derived from rifamycin B, which itself is mainly inactive. It was shown that rifamycin B undergoes spontaneous "activation" in the presence of an aqueous, oxygenated environment. It was later realized this process converted rifamycin B into rifamycin O, which is reversibly converted into rifamycin S after the loss of one glycolic acid. Then through a mild reduction of rifamycin S, rifamycin SV was obtained. Rifamycin SV was extremely potent against gram-positive bacteria, especially *M. tuberculosis*. However, rifamycin SV was not orally bioavailable. Therefore, systematic structurally modifications of most of the functional groups of rifamycin SV eventually led

to the discovery of an orally available, anti-tubercular agent, rifampicin in 1965 [Figure 1.9]. However, it would not be commercially available until 1971 and its clinical evaluation would last an additional 10 years.

Mode of Action

RIF is highly lipophilic and easily passes across the *M. tuberculosis* cell membrane. Rif has been shown to inhibit mRNA synthesis by directly binding to bacterial DNA-dependent RNA polymerase (63). Bacterial RNA polymerase is composed of $\alpha_2\beta\beta'\omega$ subunits and is highly conserved among prokaryotes (64) (65). Structural studies have elucidated the mechanism by which RIF inhibits RNA polymerase. This data demonstrates the interaction between RIF and RNA polymerase from *Thermus aquaticus* and revealed that RIF binds in a pocket located between two domains of the RNA polymerase β subunit. This interaction effectively blocks the RNA transcript at the 5' end from elongating past the second or third nucleotide, inhibiting transcription (66).

Figure 1.9. Chemical structure of rifampicin.
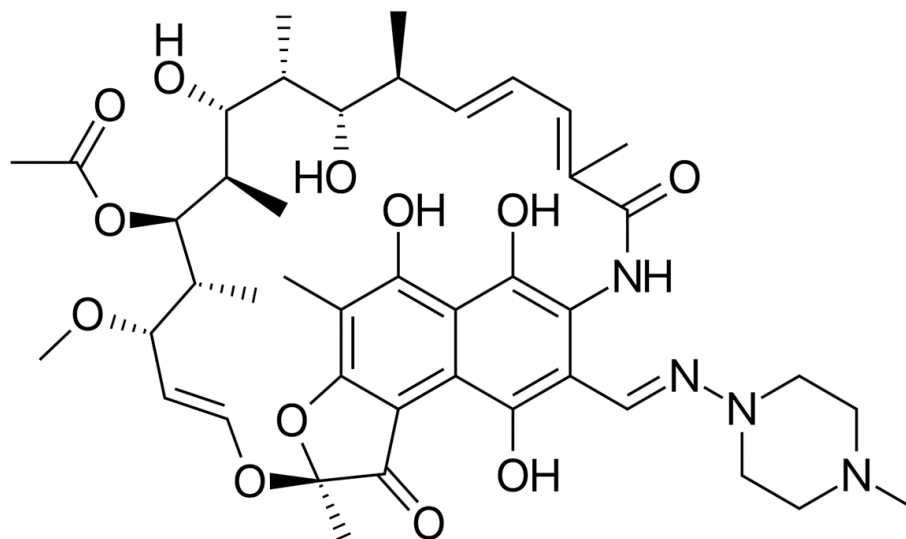
Even though the molecular target of RIF has been well characterized, the mechanism of how this interaction leads to cell death remains unclear. However, recent evidence has shown that the transcriptional inhibition of the toxin-antitoxin *mazEF* module by RIF leads to programmed cell death in *E. coli*. Inhibition of *mazEF* is believed to reduce the cellular levels of the antitoxic protein MazE, resulting in elevated levels of the toxic protein MazF, ultimately leading to cell death (67). Although *M. tuberculosis* contains homologues for these toxin-antitoxin proteins, it appears they are more involved in arresting cell growth and modulating persistence under adverse conditions rather than programmed cell death (68).

Mechanism of Resistance

Mutations leading to Rif resistance in laboratory strains occur at a frequency from 10^{-9} to 10^{-7} and develops in a single step. In Rif resistant *M. tuberculosis* clinical isolates, more than 85% are also resistant to INH, as it appears that resistance to Rif alone is rare (69). Similar to other bacterial species, over 95% of all Rif-resistant *M. tuberculosis* isolates have a mutation in the 81 base pair region of the *rpoB* gene, which encodes for the β subunit of RNA polymerase (70). Mutations at positions 531, 526, and 516 are the most frequent and generally result in high levels of resistance. Low level resistance to Rif is found in mutations at positions 511, 516, 518, and 522 (71, 72). At each of these loci, a single amino acid change was most common, with Serine-351 and Histidine-526 being the most frequently affected. The most common mutation found in clinical isolates is S531L (73). *In vitro* selection of spontaneous Rif resistance in *M. tuberculosis* also revealed mutations at Serine-351 and Histidine-526 as being the most dominant (74). Interestingly, mutations in codons 531 and 526 also confer high levels of cross-resistance to all rifamycins while mutations at codons 511, 516, and 522 only confer resistance to Rif and rifapentine, while still remaining susceptible to rifabutin and rifalazil (75, 76).

In rare cases mutations have been found in the 5' region of the *rpoB* gene with the V176F mutation conferring high levels of resistance to Rif. Several other mycobacterial species have the ability to confer low levels of resistance to Rif by inactivating it through ribosylation leading to innate antibiotic resistance (77). In a small percentage of Rif-resistant clinical isolates of *M. tuberculosis,* no identifiable mutation could be recognized which would explain resistance. This suggests that *M. tuberculosis* contains alternative

mechanisms of resistance which may affect the Rif's permeability or previously unidentified mutations may exist in other RNA polymerase subunits.

Pyrazinamide (PZA)

<u>**General Information, Dosage, Adverse Effects**</u>

PZA is a slightly bactericidal first line anti-tubercular drug recommended by WHO as a component for the treatment of drug sensitive *M. tuberculosis.* PZA is highly sterilizing, particularly in the acidic environments of macrophages and in areas of acute inflammation. It is orally bioavailable and reaches peak plasma concentrations two hours after ingestion. PZA has a half-life of 10 hours, is metabolized by the liver, and excreted primarily in the urine. PZA is usually well tolerated with little reported side-effects. In rare cases, hepato-toxicity, flushing of the skin, and moderate rises in serum transaminases can occur. More common adverse effects include hyperuricemia, gout, and arthralgia but are usually asymptomatic. The MIC for PZA in *M. tuberculosis* h37Rv in 7H12 liquid medium has been shown to be as high as 50µg/ml at pH 5.5 and 400µg/ml at pH 6.0 (78).

<u>**Discovery**</u>

PZA's discovery is interesting given that it has no activity *in vitro* against *M. tuberculosis* under normal growing conditions. It was originally synthesized in 1936 by Dalmer and Walter but its antimicrobial properties wouldn't be realized until 1952 [Figure 1.10]. What was known at the time was that nicotinamide displayed inhibitory activity against *M. tuberculosis.* This was later confirmed by Mckenzie et al at the Lederle

Laboratories of American Cyanamid and at Merck Laboratories. After extensive efforts, PZA was identified as the most active synthetic analogue of nicotinamide. Isoniazid, Ethionamide, and the first known anti-depressant, Marsilid, were also eventually derived from nicotinamide. Even more remarkable was that immediately following its synthesis, without additional investigation, it was tested in patients infected with *M. tuberculosis.* It demonstrated appreciable activity in humans in contrast to previous studies in the guinea pig. This led to extensive studies in the laboratories of Walsh McDermott at Cornell University which showed that PZA was only active against *M. tuberculosis* at an acidic pH [Figure 1.10]. They also were able to show that a combination of PZA and INH at high dosage was capable of inducing a sterile state in which tubercle bacilli could not be isolated by culture or animal inoculation from organs. However, the bacilli still were present in a persistent state and would eventually cause relapse and a future infection. McDermott later demonstrated that PZA is a prodrug which requires a bacterial amidase to convert it into the active molecule, pyrazinoic acid (POA) (79).

Figure 1.10. Chemical structure of pyrazinamide.
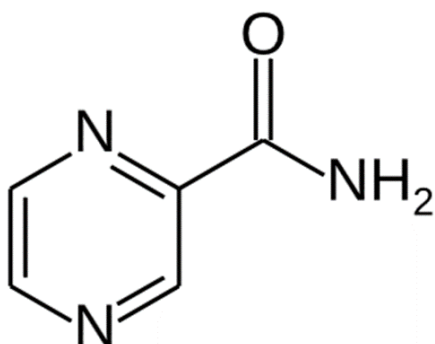
Mode of Action

PZA has been shown to be a pro-drug which requires a pyrazinamidase (PZase), encoded by the *pncA* gene to be converted into its active form, POA in *M. tuberculosis.* There have been several proposed mechanisms of action, but early hypothesis' state that POA can disrupt the mycobacterial membrane and interfere with energy production necessary for the bacilli to survive at the site of an infection (80). This is supported by the fact that PZA has increased activity against non-replicating bacteria with decreased membrane potential and the ability of POA to disrupt these membranes at acidic pHs (81). PZA shows little activity against intracellular *M. tuberculosis* in human monocyte-derived macrophages, but become highly active when these macrophages are activated with inferno gamma leading to the acidification of the phagosome (82). Another study suggest that PZA is only active against bacilli inside acidified lung compartments during the early stages of infection (83). This agrees with the current recommended treatment for PZA, which is usually limited to the first 2 months.

There is evidence which suggests that PZA enters the bacteria through passive diffusion, is converted to POA and excreted by an efflux pump. Under acidic conditions, POA becomes protonated and is re-absorbed into the cell where it accumulates faster than the efflux pump can remove it, causing cellular damage (84). A more recent study showed that PZA was able to inhibit the enzyme activity of quinolinic acid phosphoribosyltransferase, which is a key enzyme in the *de novo* synthesis of nicotinamide adenine dinucleotide (NAD) (85).

New evidence has confirmed the ribosomal protein S1 (RpsA) as a new target of POA. RpsA is involved in protein translation and the ribosome-sparing process of trans-translation. Shi et al demonstrated that POA binds to the 30S ribosomal protein S1 and inhibits protein synthesis. They also showed that mutations in *rpsA* resulted in altered binding profiles of POA to RpsA and resulted in PZA resistance (86). However, *rpsA* mutations from PZA-resistant clinical isolates have yet to be reported. Moreover, *rpsA* mutations have been identified in PZA-susceptible strains, making mutations in *rpsA* a poor indicator of PZA resistance in clinical strains (87).

There are several identified PZA-resistant strains which lack mutation in both *pncA* and *rpsA* and their regulatory regions. Sequence analysis of several mutants with low levels of PZA resistance were found to harbor mutations in the *panD* gene (88). *PanD* encodes for an aspartate-alpha-decarboxylase which is involved in the synthesis of β-alanine, a precursor for pantothenate and co-enzyme A biosynthesis (89). In agreement with these findings, PZA activity against laboratory strains of *M. tuberculosis in vitro* was

found to be antagonized when supplemented with β-alanine, pantothenate, and pantetheine (90).

Mechanism of Resistance

The hallmark of PZA resistant *M. tuberculosis* strains is the loss of pyrazinamidase and/or nicotinamidase activity. Mutations are found scattered across the entire *pncA* gene but there appears to be some localization at three distinct regions: 3-17, 61-85, and 132-142 (91, 92). However, new *pncA* mutations are identified frequently and there appears to be little correlation between *pncA* mutation genotypes and the resulting resistance phenotype. PZA is highly specific to *M. tuberculosis* and many species of mycobacteria are naturally resistant to PZA. In the case of *M. bovis,* the bacteria produces an inactive PZase protein, rendering the drug inactive because PZA is not converted into POA (93). In addition, PZA potentially has multiple cellular targets resulting in a varying correlation between the presence of mutations and resistance (94). Yet mutations in in the *pncA* gene or in its regulatory region are found in over 70% of PZA resistant *M. tuberculosis* isolates. Surprisingly, a recent study identified *M. tuberculosis* strains with high levels of resistance to PZA, with MICs above 1600µg/ml. Upon sequencing it was found that the strains contained large deletions in not only the *pncA* gene, but also several genes upstream and downstream (95).

SECOND-LINE DRUGS FOR THE TREATMENT OF MDR-TB AND XDR-TB

Streptomycin (SM)

<u>**General Information, Dosage, Adverse Effects**</u>

SM is a component of the second line of drugs recommended by WHO for the treatment of tuberculosis, usually reserved as part of a treatment regimen for MDR-TB. It is sometimes substituted for EMB depending on the type of infection, especially in the case of tuberculosis meningitis. SM is not absorbed in the intestinal tract and must be given as an intramuscular injection at 15mg/kg daily during the first 6-12 months of treatment. The plasma half-life is around 2-3 hours and is excreted unchanged in the urine. SM is not recommended in children due to the possibility of irreversible auditory nerve damage. It should not be used during pregnancy because it can cross the placenta and cause fetal nephrotoxicity. SM is bacteriostatic and has an MIC against wild type H37rv of 0.25-1.0µg/ml in 7H10 media (12).

<u>**Discovery**</u>

Selman Waksman with the help of his graduate students Rene Dubos and Albert Schatz, theorized that micro-organisms were capable of performing a vast number of biochemical reactions, which in the case of soil bacteria would be dependent on their environment. These potentialities could be induced by altering the environment, which led to the discovery of several potent antibiotics including Gramicidin. However, in 1943, they identified a new species of *Actinomyces* through a swab obtained from the throat of a sick chicken. This particular strain of *Actinomyces*, *Streptomyces griseus,* produced

streptomycin which was active against a broad range of bacteria [Figure 1.11]. Its anti-tubercular activity wasn't published until late 1944 after Dr. H. Corwin Hinshaw successfully tested streptomycin against guinea pigs infected with tuberculosis. In 1945, at a New Haven hospital, a child was successfully treated with streptomycin to cure a hopeless case of tuberculosis meningitis (2).

Mode of Action

SM has been shown to inhibit protein synthesis by binding to the 30S subunit of the mycobacterial ribosome, which would result in reading errors during translation. SM is believed to function by interrupting the initiation of protein synthesis by inhibiting the fusion of the 50S and the 30S particle by binding at the S12 and 16S rRNA junction in the 30S. This resulting complex is unstable which can lead to continuous frameshift mutations and ultimately cell death. At low concentrations, SM only inhibits bacterial cell growth (96).

Figure 1.11. Chemical structure of streptomycin.
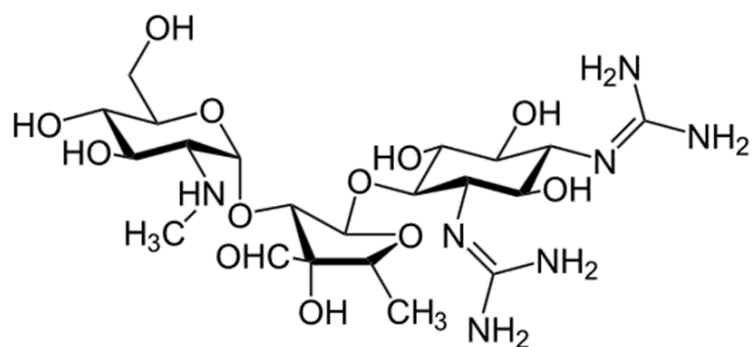
Mechanism of Resistance

In *M. tuberculosis,* the S12 protein and the 16S rRNA are encoded by *rpsL* and *rrs* genes respectively. Mutations in these two genes account for over 50% of all streptomycin resistance isolates. The most commonly observed mutation is a lysine to arginine mutation in codon 43 of *rpsL* which results in a high level of resistance. Mutations in codon 88 of *rpsL* are also quite frequent. Mutations in the *rrs* gene occur in the loops of the 16S rRNA and are centered in two distinct regions around nucleotides 530 and 915. SM-resistant *M. tuberculosis* arise due to a C insertion in the 530 loop. However, in about 20% of SM-resistant strains, mutations in either *rpsL* or *rrs* could not be identified. Recent evidence has shown that mutations in *gidB*, which encodes for a 7-methylguanosine methyltransferase confers low levels of resistance to SM in *M. tuberculosis.* Additionally, up-regulation of efflux pumps is another mechanism by which resistance to SM is believed to be achieved by.

Ethionamide (ETH)

General Information, Dosage, Adverse Effects

ETH is part of a group of second line drugs used in the treatment of tuberculosis when resistance or toxicity to any of the first line drugs has developed. It is orally administered and it is always given in combination with other antimycobacterial drugs. The daily recommended dose is 15-20mg/kg with the maximum allowance of 1g depending on body weight and tolerance. ETH is highly bactericidal against *M. tuberculosis in vitro* with an MIC range of 0.6 to 1.2μg/ml in 7H12 media (97). However, it is bacteriostatic within the recommended therapeutic window and at bactericidal concentrations is quite toxic. ETH has been shown to be active against other mycobacterial species such as *M. kansaii, M. leprae, and M. avium* (97).

ETH has several well documented side effects including toxic hepatitis, obstructive jaundice, acute hepatic necrosis, encephalopathy, peripheral and optic neuritis, hypoglycemia, and hypothyroidism. Plasma half-life is reported to be about 3 hours. ETH is completely metabolized in the liver and must be monitored or avoided in patients with hepatic impairment. Ethionamide-sulfoxide is a major metabolite of ETH and only 1% of ETH is excreted unchanged in the liver. Plasma protein binding is estimated to be 30% of total ETH (12).

Discovery

ETH is an isoniazid derivative developed by Grumbach et al while working at Theraplix in 1956 [Figure 1.12]. They were ultimately trying to improve on the

antimycobacterial properties of thioisonicotinamide (98). ETH was found to be active against INH, PAS, and SM-resistant *M. tuberculosis* strains.

Mode of Action

ETH is a structural analog of INH and also behaves as a prodrug. ETH is activated by the NADPH-specific Flavin adenine dinucleotide-containing monoxygenase EthA encoded by *Rv3854c* (99). Once activated, the mode of action mimics INH where it forms an Eth-NAD adduct which then binds and inhibits InhA, blocking mycolic acid biosynthesis. However, it differs from INH in that it requires two activation steps before it forms a covalently modified NAD-ETH derivative. EthA first converts ETH into a sulfoxide intermediate which is then converted again by EthA into a 2-ethyl-4-amidopyridine product (100). This final product demonstrates no anti-tubercular activity. In the case of ETH dependent inhibition of InhA, the addition of NAD^+ or NADH does not alter its inhibition profile. It has been suggested that the mode of action of the ETH mediated product differs from that of INH. Structural evidence has shown that an ETH-NAD adduct binds to InhA but the reaction leading to the ETH-NAD adduct is still unclear as to whether it is catalyzed by EthA alone or in conjunction with other enzymes (101). EthA also activates two other second line anti-tuberculosis drugs: thiacetazone and isoxyl, but they appear to inhibit a different final target other than InhA (102).

Figure 1.12. Chemical structure of ethionamide.
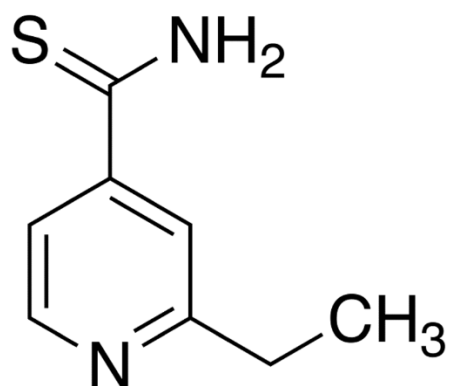
Mechanism of Resistance

There are a few documented mechanisms of resistance specific for ETH. These mechanisms of resistance involve mutations in the activator, *ethA,* the target, *inhA,* or the *ethA* regulator, *ethR.* To date, 85 *ethA* mutations have been identified with a wide range of demonstrated resistance. Mutations span the entire coding region in *ethA*, and unlike *katG* mutations, there does not appear to be a dominant mutation. Most of the observed nucleotide changes are missense mutations which results in amino acid substitutions, but insertions, deletions, and non-sense mutations have also been identified. It has been hypothesized that the lack of a dominant *ethA* mutation could be attributed to the presence of numerous monooxygenase homologs in *M. tuberculosis,* which could protect against a loss of EthA activity (103). A recent analysis concluded that 47% of all ETH-resistant *M. tuberculosis* clinical strains had an *ethA* mutation, while 62% had a mutation in the *inhA* gene or promotor region. Only 4% of ETH-resistant strains had mutations in *ethR,* and

many share additional mutations in the promotor region of *inhA* and in *ethA*. This study concluded that mutations in the target gene, *inhA,* were the main mechanism of ETH resistance in *M. tuberculosis* (104).

Para-aminosalicylic Acid (PAS)

<u>**General Information, Dosage, Adverse Effects**</u>

PAS a bacteriostatic against *M. tuberculosis* most commonly administered to patients with MDR-TB, XDR-TB or in place of RIF or INH when intolerance or resistance has occurred. PAS is never used as a stand-alone anti-mycobacterial drug and is usually accompanied by two other agents to which the strain which the strain is sensitive to. The recommended daily dosage is 4g for adults and 2g for children and should never exceed 4g. Approximately 50% of PAS is protein bound and penetration into the cerebrospinal fluid is rare. 80% of PAS is excreted in the urine with 50% in an acetylated form. PAS has a half-life of 2 hours and a MIC of 1µg/ml for *M. tuberculosis* grown in 7H12 media.

PAS has several rare but undesirable side effects including jaundice, hepatitis, optic neuritis, encephalopathy, hypoglycemia, hypothyroidism, vasculitis, and eosinophilic pneumonia. Additionally, PAS treatment reduces vitamin B12 absorption by over 50% and is often accompanied by vitamin B12 supplementation. PAS can also interfere with the overall serum levels of INH when taken in conjunction with INH serum levels being reduced by up to 20% (12).

Discovery

Jörgen Lehmann originally designed a chemical agent which was believed to not only act as a source of nutrition for tuberculosis, but would also impair their growth and kill them. His designs ultimately led to the synthesis of PAS, which on October 30, 1944 would be used to successfully treat a terminally ill Swedish woman infected with *M. tuberculosis* [Figure 1.13]. Although PAS was developed before streptomycin, it would not become an acceptable form of treatment until 2 years after the appearance of streptomycin (105).

Mode of Action

The exact mechanism through which PAS-mediate killing occurs has been highly speculative over the last 60 years. Given its structural similarity to *para-aminobenzoic acid (p*ABA)*, it has been proposed to inhibit dihydropteroate synthase (DHPS) in the folate biosynthetic pathway, which makes DHPS from *p*ABA (106). However, *in vitro* enzymatic data has not been able to show inhibition of DHPS by PAS. The folate pathway is ultimately responsible for generating tetrahydrofolate, a precursor for the synthesis of purine, thymidine, glycine, methionine, pantothenate, and formylmethionyl tRNA. The last step in the folate pathway is mediated by the enzyme dihydrofolate reductase (DHFR) which converts dihydrofolic acid to tetrahydrofolic acid. Recent evidence suggests that PAS is converted by the folate pathway into an "anti-metabolite" as a pABA mimic and inhibits DHFR activity. The PAS anti-metabolite has been shown to be a substrate for DHPS and converted into hydroxyl dihydropteroate. This product is then recognized by

dihydrofolate synthase (DHFS) to form hydroxyl dihydrofolate. Evidence shows that the hydroxyl dihydrofolate competes with dihydrofolate for binding to the active site of DHFR, blocking the production of tetrahydrofolate. Therefore, it has been speculated that PAS is a pro-drug for a metabolite which gets incorporated into the folate pathway, mimics essential substrates, and inhibits DHFR activity (107). However, more recent evidence has shown that although PAS is an *in vitro* inhibitor of DHFR, it did not affect *M. tuberculosis* growth through inhibition of DHPS. Instead, the data suggests that PAS modulates folate-dependent pathways entirely and irreversibly by serving as mimic substrate(s), product(s), and inhibitor(s) for enzymes subsequent to DHPS (108).

New data has shown that an additional enzyme exists in *M. tuberculosis,* RibD, which can function as a DHFR analogue and catalyze the turnover of DHF to THF. RibD is believed to function in the riboflavin biosynthetic pathway by converting 2,5-diamino-6-ribosylamino-4(3H)-pyrimidinone (DAROPP) to 5-amino-6-ribitylamino-2,4(1H,3H)-pyrimidinedione 5'-phosphate (ARIPP). Mutations upstream of the gene encoding for RibD were shown to be associated with PAS resistance in laboratory derived resistant strains. These mutations also demonstrated increased expression levels of RibD and enzymatic activity data demonstrated inhibition of RibD by known DHFR inhibitors. This may implicate RibD and the riboflavin biosynthetic pathway in PAS resistance and/or suggest that PAS acts as a metabolite mimic in more than just the folate-dependent pathway (109).

Mechanism of Resistance

Mutations in *dfrA,* the gene encoding DHFR have yet to be identified in PAS-resistant *M. tuberculosis* isolates. Other enzymes in the folate pathway, predominantly thymidylate synthase (ThyA) have been well described in contributed to PAS resistance. These include *thyA, folC, folP1, folP2, and thyX.* Additionally, three N-acetyltranssferase genes [*rhoA, aac(1), aac(2)]* have also been implicated in PAS resistance. ThyA catalyzes the reductive methylation of deoxyuridine monophosphate (dUMP) to yield deoxythymidine monophosphate (dTMP) and dihydrofolate. Mutations in *thyA* account for 37% of clinical isolates resistant to PAS with 24 distinct mutations currently annotated. The most prevelant mutation observed is AAC to GCC in codon 202. Most notably, over 60% of PAS-resistant isolates have no mutations which could explain resistance. This suggest PAS resistance in *M. tuberculosis* must involves additional targets or pathways which have yet to be elucidated (110).

Figure 1.13. Chemical structure of para-aminosalicylic acid.
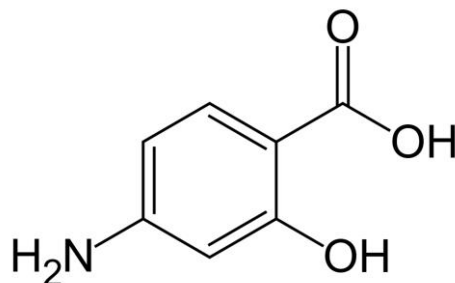
Fluoroquinolones (FQs)

General Information, Dosage, Adverse Effects

FQs are bactericidal antibiotics which are recommended by WHO as a second line therapy for the treatment of MDR-TB and XDR-TB. These include moxifloxacin, gatifloxacin, sparfloxacin, levofloxacin, ofloxacin, and ciprofloxacin. Moxifloxacin and gatifloxacin are currently being evaluated as potential first line therapeutics in order to shorten the duration of treatment. FQs have MICs against *M. tuberculosis in vitro* of 0.1 to 4.0µg/ml and have an early sterilizing effect. Levofloxacin and moxifloxacin are the most widely used FQs in treatment of MDR-TB with *in vivo* activity comparable to INH. The recommended daily dose ranges from 200mg to 800mg for 3-6 months. FQs have also been suggested as a prophylaxis for individuals who may be exposed to MDR-TB (111).

The most commonly reported adverse effects of FQs include tendonitis, tendon rupture, photosensitivity, and seizure. In less than 2% of cases, gastrointestinal issues can occur, hepatitis, renal dysfunction, hypoglycemia, vertigo, and insomnia. FQ absorption has been shown to be reduced when combined with antacids or multivalent cations (112). Non-steroidal anti-inflammatory drugs have also been shown to increase the possibility of seizures. The first generation of FQs (ofloxacin, ciprofloxacin, levofloxacin) are generally well tolerated and have a well-documented history of low toxicity and safety (113).

Discovery

The first synthesis of quinolones was an accident, a by-product from the synthesis of chloroquine, an anti-malaria drug commonly used in the treatment of malaria. In 1962,

at the Sterling-Winthrop Research Institute, George Lesher et al developed a series of 1,8-napthyridine derivatives from nalidixic acid which demonstrated good potency against a broad range of bacteria, most notably gram-negatives. This discovery led to the development of a library of quinolone compounds, which were first introduced into clinical practice in the early 1980s and are still highly used today due to their potent antimicrobial and anti-mycobacterial properties (114) [Figure 1.14].

Figure 1.14. Chemical structure of quinolone derivatives.

Nalidixic acid

Ciprofloxacin

Levofloxacin

Trovafloxacin
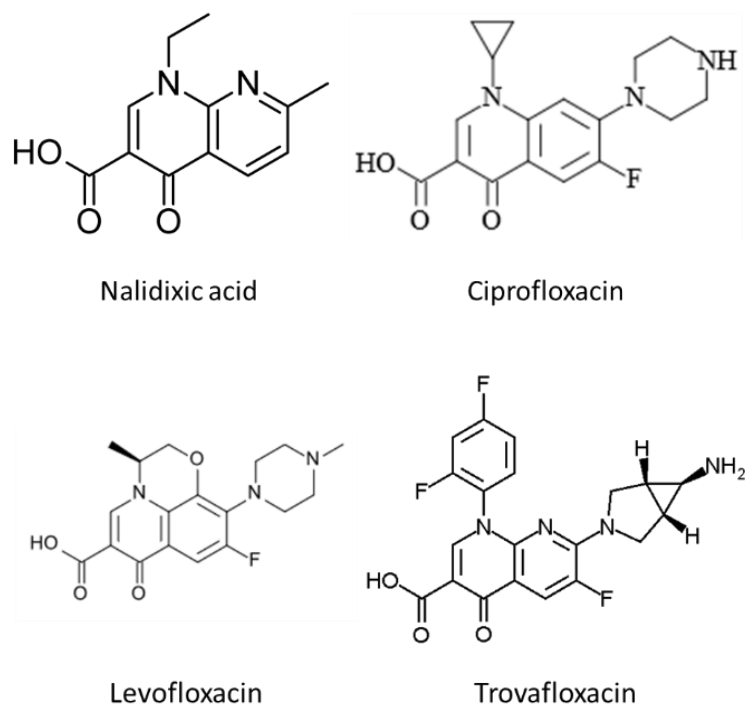
Mode of Action

FQs target and inhibit type II topoisomerases. The role of type II DNA topoisomerases is to introduce transient double-stranded breaks to force the passage of one segment of double stranded DNA through another. Most bacteria contain two type II topoisomerases, DNA gyrase and topoisomerase IV. DNA gyrase tends to be the primary target of FQs in gram-negative bacteria while topoisomerase IV is most often inhibited in gram-positive organisms. However, *M. tuberculosis* only contain one type II topoisomerase, DNA gyrase, which is therefore the sole target of FQs. Specifically, FQs target the catalytic core of DNA gyrase formed by the Toprim domain of the GyrB subunit and the BRD of GyrA subunit. Based on available data from crystal structures, it is believed that quinolones bind to a binary complex of gyrase and DNA. This interaction stabilizes the covalent enzyme tyrosyl-DNA phosphate ester bond and blocks DNA replication. In addition, hydrolysis of the tyrosyl-DNA linkage leads to the accumulation of double-stranded breaks, causing cell death (111, 115, 116).

Mechanism of Resistance

Mutations conferring FQ resistance in *M. tuberculosis* occur in the genes encoding the gyrase, frequently in the quinolone-resistance-determining region (QRDR) of *gyrA* but also in the QRDR of *gyrB*. The most commonly mutated residues are amino acids 89, 90, 91, and 94 in the QRDR-A and rarely amino acids 88 and 74 (117). Mutations in *gyrB* occur at amino acids 500, 538, 539, and 540 in QRDR-B. Several studies have looked at frequency of mutations outside of the QRDR regions in the entire *gyrA* and *gyrB* genes

and found that *gyrB* shows a higher propensity for mutations than *gyrA*. These mutations only lead to low levels of resistance, if any at all (118, 119). Often mutations outside of the QRDR region are accompanied by mutations inside the QRDR region of the other gyrase. For example, mutations found outside of the QRDR region in *gyrA* were often associated with mutations in the QRDR region in *gyrB*. N538D and E540V amino acid substitutions in *gyrB* confer the highest levels of resistance to FQs, while D500H, D500N, E540D, and T539P have all been found to confer lower levels of resistance (120, 121). Mutations outside of the gyrase genes have also been reported in clinical isolates resistant to FQs. The mechanisms by which resistance is obtain is still unknown. It is assumed that FQ resistant strains are cross resistant among many analogues. However, there are cases of strains resistant to moxifloxacin and gatifloxacin, but are still susceptible to oxfloxacin. It is possible that FQ resistance in *M. tuberculosis* can be caused by mutations which activate alternative resistance mechanisms, such as efflux pumps (122).

Cycloserine (CS)

General Information, Dosage, Adverse Effects

CS is a bacteriostatic antimicrobial recommended by WHO as a second line therapeutic for treatment of MDR-TB and XDR-TB. CS has a recommended daily dose of 250mg or 500mg three times a week with a maximum dose of 1000mg. CS has been shown to markedly deplete pyridoxine levels and therefore every 250mg of CS must be supplemented with 50mg of pyridoxine (123). CS has been shown to exacerbate some of the toxicities associated with ETH and INH co-administration. CS is often associated with

neurologic and psychiatric perturbations. These may include headaches, dizziness, nightmares, depression, anxiety, confusion, and coma. Severe kidney failure can also occur in individuals who frequently abuse alcohol (12). CS has an *in vitro* MIC against *M. tuberculosis* ranging from 5-20µg/ml (124).

Discovery

In 1955 while working at Merck, Kuekl et al discovered a metabolite from a new species of *Streptomyces* which demonstrated a broad range of antibiotic activity. They originally designated it "oxamycin" (125). This same team was also responsible for the total synthesis of oxamycin which they later termed cycloserine (126) [Figure 1.15]. At the same time, Hidy et al identified an identical metabolite from *Streptomyces orchidaceus* while working at Eli Lilly (127).

Mode of Action

CS, specifically the D enantiomer, is a structurally mimic of the amino acid D-alanine. This allows CS to infiltrate two different enzymatic reactions and prevent them from proceeding. CS has been shown to bind and inhibit both alanine racemase and D-alanine-D-alanine ligase. These are unique targets comparted to all known and previously reported inhibitors of *M. tuberculosis*. As such, CS displays no cross resistance to other approved anti-tubercular drugs currently employed. D-alanine-D-alanine ligase catalyzes the ATP-dependent formation of the amide bond between two D-alanine molecules, creating the dipeptidyl D-alanyl-D-alanine precursor for the peptidoglycan. Interestingly,

D-alanine-D-alanine ligase has two distinct and independent D-alanine binding sites, one on the N-terminus and one on the C-terminus of the enzyme. Recent studies have shown that CS binds exclusively to the C-terminal binding site, even in the absence of bound D-alanine at the N-terminus site (128, 129).

Figure 1.15. Chemical structure of cycloserine.
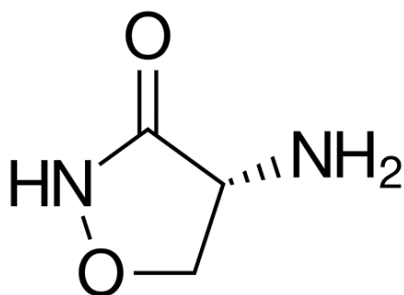
Mechanism of Resistance

The molecular basis of CS resistance in *M. tuberculosis* clinical isolates is incomplete and poorly understood. Studies in *M. smegmatis* have shown that overexpression of *alr* and *ddlA,* the genes which encode for alanine racemase and D-alanine-D-alanine ligase, confers resistance to CS (130). Furthermore, it is known that *M. bovis* is intrinsically resistant to CS, which is only partially explained by an identified mutation in *cycA,* a gene which encodes for an alanine transporter (131). A recent study

attempted to provide a more complete understanding of CS resistance found in *M. tuberculosis* clinical strains. It was found that CS resistance was most frequently due to a loss of function mutation in *ald*, which encodes for L-alanine dehydrogenase, followed by mutations in *alr*. Mutations in *ddlA* or *cycA* were only found in seven strains compared to 42 strains which contained an *ald* or *alr* mutation. Genetic background did not seem to influence the varying drug susceptibility phenotypes observed for each mutant. Clinical isolates with *ald* and *alr* mutations displayed the highest MIC compared to wild type *M. tuberculosis* which were found to be as high as 60µg/ml. Interestingly, *ald* and *alr* mutations were not additive and having both mutations did not confer a higher level of resistance to CS (132).

Aminoglycosides (Kanamycin, Capreomycin, Amikacin, Viomycin)

<u>**General Information, Dosage, Adverse Effects**</u>

These four aminoglycosides similar to SM, are highly bactericidal, have very poor oral bioavailability and therefore must be administered via intramuscular or intravenous injections. Aminoglycosides are a part of the second line group of drugs recommended by WHO used to treat MDR-TB and XDR-TB. The recommended daily dose is 15 to 30mg/kg with a maximum dose of 750mg for capreomycin and 1000mg for kanamycin. Resistance to aminoglycosides occurs at a high rate when administered as a single agent and as such is always used in conjunction with at least 4 other anti-mycobacterial drugs. Adverse effects include acute renal failure, ototoxicity, and hypersensitivity with kanamycin usually being the least tolerated of the four. Average peak serum

concentrations occur in less than one hour after treatment and the MIC range of the aminoglycosides is 4-10µg/ml against *M. tuberculosis in vitro* (12).

<u>Discovery</u>

Although kanamycin and amikacin are aminoglycosides and capreomycin and viomycin are polycyclic peptides, all four have a similar mechanism of action. Kanamycins were first discovered by researchers at the National Institute of Health in Tokyo, Japan in 1957. These antibiotics are produced by *Streptomyces kanamyceticus* and display a wide range of antibacterial activity, especially the most common form, kanamycin A. Capreomycin was first isolated in 1950 from *Streptomyces capreolus.* Amikacin is a synthetic derivative of kanamycin first published by the Bristol-Banyu research institute in Japan. Amikacin was developed to treat kanamycin resistant bacteria. Viomycin was first described by Alexandar Finlay along with 11 co-authors in 1951 and it was developed independently at both Pfizer and the Park, Davis Company (133) [Figure 1.16].

Figure 1.16 – Chemical structure of kanamycin, capreomycin, viomycin, and amikacin.
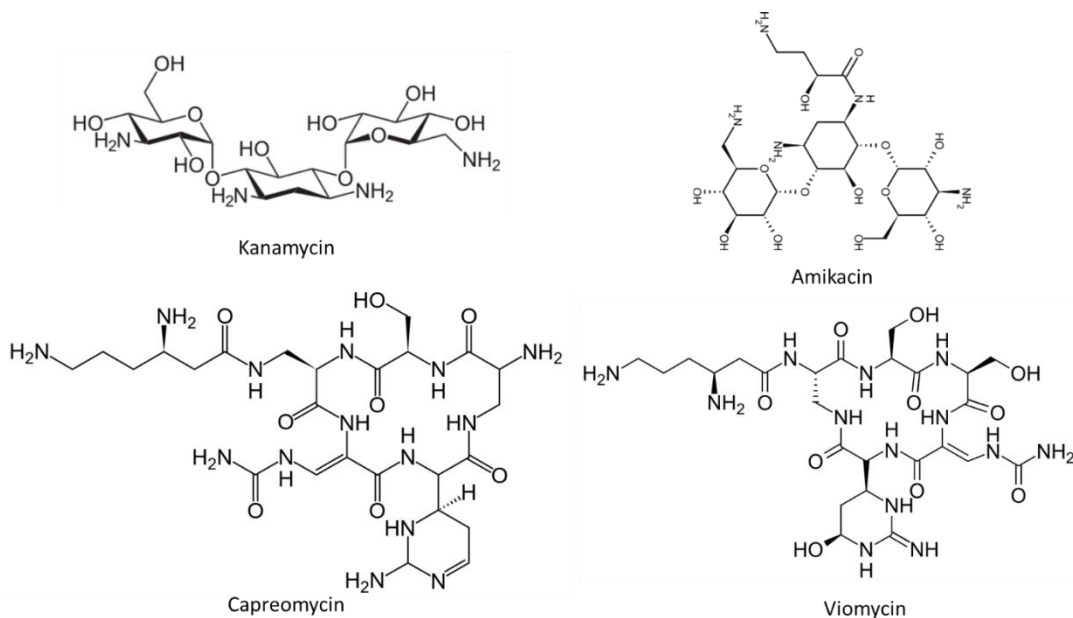
Mode of Action

Kanamycin and Amikacin are believed to bind to the A-site on the 16S rRNA and interferes with the accurate recognition of cognate tRNA by rRNA during translation. The translocation of tRNA from the A-site to the peptidyl-tRNA site is also thought to be perturbed. Capreomycin and Viomycin differ slightly in that they appear to bind across the ribosomal interface involving 23S rRNA helix 69 and 16S rRNA helix 44 (134).

Mechanism of Resistance

The most observed clinical mutation in kanamycin-resistant *M. tuberculosis* strains are at positions 1400 and 1401 of the *rrs* gene, which encodes for the 16S ribosomal

RNA subunit. Mutations at these two positions confer high levels of resistance to both kanamycin and amikacin. Additional mutations at position 1483 have also reported and there are resistant strains not cross resistant between the two antibiotics, suggesting other possible mechanism of resistance. To support this idea, mutations in the promotor region of the *eis* gene, which encodes for an aminoglycoside acetyltransferase, have been shown to confer low levels of kanamycin resistance but not to amikacin. These mutations have been reported in almost 80% of all isolates demonstrating resistance to kanamycin (135).

All reports of capreomycin resistant strains of *M. tuberculosis* show complete cross resistance to viomycin and vice versa. Mutations in the *tylA* gene, which encodes for a rRNA methyltransferase specific for 2'-O-methylation of ribose in RNA, is thought to be the sole progenitor of resistance to the cyclic peptides (136).

THIRD-LINE DRUGS USED FOR THE TREATMENT OF MDR-TB AND XDR-TB

Third line drugs most often have very poorly defined efficacy and undefined roles in the treatment of *M. tuberculosis* infections. The purpose of introducing many third line drugs is to reduce the treatment duration and to address the rise of XDR-TB cases which are less responsive to traditional therapies. Many third line drugs are previously well described to treat other bacterial or viral infections and are being repurposed for the treatment of tuberculosis.

Linezolid

Linezolid is a synthetic antibacterial from the oxazolidinone class which were first discovered in the 1970's at E. I. du Pont de Nemours & Co. They were initially investigated for their activity against methicillin-resistant bacteria. They were discontinued to due liver toxicity issues but were re-investigated in the early 1990s. In 1996, linezolid was discovered at Pharmacia & Upjohn and is under the Pfizer trade name Zyvox (137) [Figure 1.17].

Although the specific mechanism by which linezolid exhibits is antibacterial properties is not complete, it is known that oxazolidinones bind to the 23S portion of the 50S subunit of the ribosome, and prevents the initiation complex from maturing, blocking protein synthesis. It is unique among protein synthesis inhibitors in that it blocks at the step of initiation and not at elongation. This allows Linezolid to have very little cross resistance between other protein synthesis inhibitors (138).

Figure 1.17. Chemical structure of linezolid.
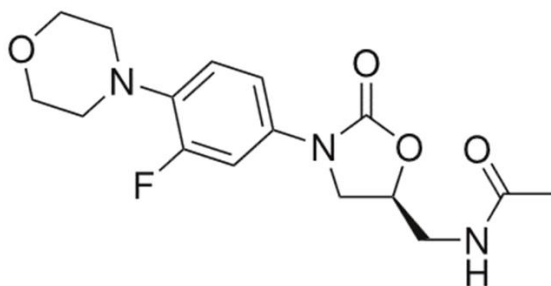
M. tuberculosis resistance to linezolid is quite unusual, but in a study analyzing over 200 MDR strains, it was found that 2% were resistant to linezolid. Mutations in the 23S rRNA of the resistant isolates were found to have a 4 to 8 fold increase in MIC. A more recent study found point mutations in *rpl*C, which encodes for the 50S ribosomal L3 protein. The most common base change was T460C in both *in vitro and* clinical isolates of *M. tuberculosis.* Other evidence suggest that efflux pumps are also involved in linezolid resistance (139).

Clofazimine

Vincent Barry et al originally synthesized Clofazimine in 1954 at Trinity College. It was originally investigated for anti-tuberculosis properties, but it failed to be effective. Five years later it was shown to be an effective treatment against leprosy. In 1969, Novartis launched clofazimine under the name Lamprene [Figure 1.18]. It was granted FDA approval in 1986 as an orphan drug (140).

The exact mechanism of clofazimine mediated antimicrobial activity has yet to be elucidated. However it is believed that the outer cell membrane appears to be the primary site of action while most likely interfering with the bacterial respiratory chain and ion transporters. It has been hypothesized that oxidation of reduced clofazimine generates reactive oxygen species (ROS), superoxide, and H_2O_2, which could lead to bacterial cell death. Conversely, clofazimine is also believed to interact with membrane phospholipids, which in turn promotes membrane dysfunction, ultimately leading to a suboptimal uptake of potassium ions, resulting in cell death (141).

There is currently very little characterization of clofazimine resistance in *M. tuberculosis.* However, it has been shown that in wild type H37Rv, mutations in the transcriptional regulator, Rv0678, resulted in an upregulation of MmpL5, a proposed efflux pump, which caused innate resistance to clofazimine (142).

Figure 1.18. Chemical structure of clofazimine.
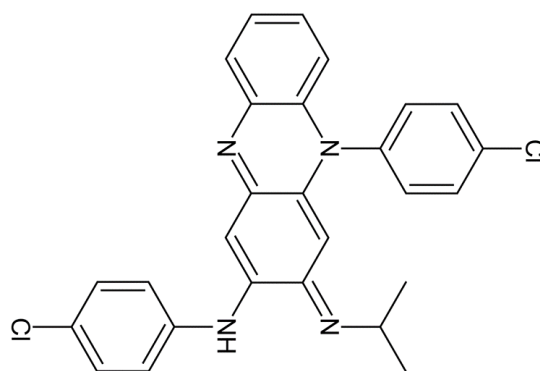
Beta-lactams

Amoxicillin and imipenem are broad spectrum antibiotics used in the treatment of aerobic, anaerobic, Gram-positive and Gram-negative bacteria [Figure 1.19]. Amoxicillin is broken down by β-lactamases produced by bacteria and therefore must always be co-administered with a β-lactamase inhibitor such as clavulanic acid. Imipenem is resistant to β-lactamases, but is susceptible to inactivation by the renal enzyme dehydropeptidase

1 and must be taken with cilastatin, a dehydropeptidase inhibitor. Although these combinations have demonstrated appreciable activity against *M. tuberculosis,* the pharmacokinetic properties, including a very short half-life, preclude its general use for the treatment of tuberculosis (143).

Figure 1.19. Chemical structure of amoxicillin and imipenem.

Amoxicillin   Imipenem
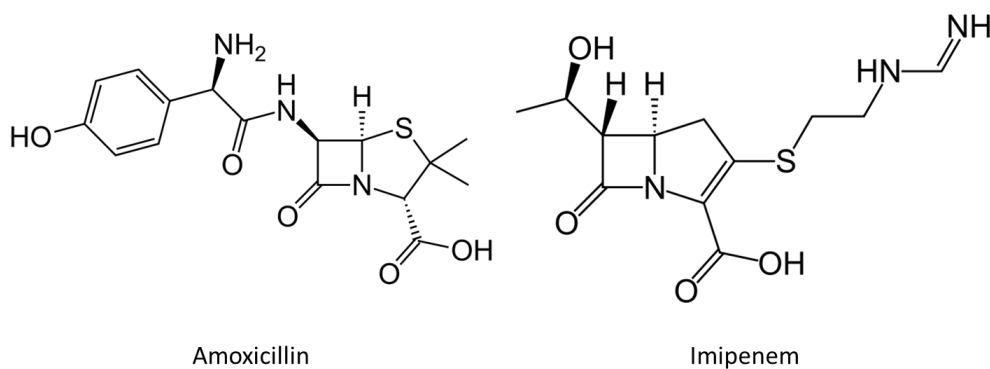
Thiacetazone

Thiacetazone is an old drug which was widely used due to its good *in vitro* activity against *M. tuberculosis* and low cost [Figure 1.20]. However, toxicity problems, especially drug-drug interactions with anti-retrovirals, makes it less than desirable. It is believed to inhibit mycolic acid cyclopropanation but it is no longer used in the United States (144)

Figure 1.20. Chemical structure of thiacetazone.
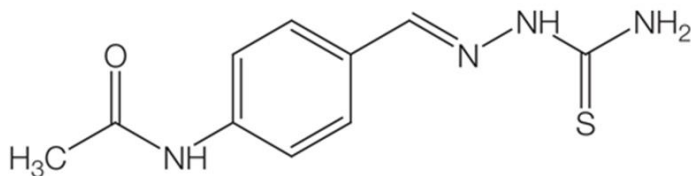
Macrolides

Intrinsic resistance to macrolides is often found in *M. tuberculosis* and as such is infrequently used in the treatment of tuberculosis. However, clarithromycin has been shown to reduce the MIC of first line drugs, notably EMB when co-administered [Figure 1.21]. A mutation in *emr37*, a gene which encodes a methylase at a specific site in the 23S rRNA, blocks the binding of antibiotics. Low permeability of the cell wall is another feature that makes macrolides very ineffective against *M. tuberculosis*, but they are surprisingly good at treating *Myccobacterium microti* infections (145).

Figure 1.21. Chemical structure of clarithromycin.

NEW CANDIDATES FOR TREATMENT OF TUBERCULOSIS

There are several criteria in which new drug candidates for the treatment of tuberculosis must fulfill in order to be considered. They must have a validated safety profile, be more potent than existing drugs, inhibit new targets, be compatible with anti-retroviral medications, and display no antagonism to other anti-mycobacterial drugs or drug candidates. In addition, new drug candidates should aim at inhibiting *M. tuberculosis* at various physiological stages including latent infections (146).

Bedaquiline

Bedaquiline was originally discovered in a High Throughput Screen (HTS) of thousands of compounds against *Mycobacterium smegmatis (M. smegmatis)* [Figure

1.22]. Originally named, TMC207, this compound demonstrated activity against *M. tuberculosis* in both *in vivo* and *in vitro* assays and was potent against both actively replicating and dormant bacilli (147, 148). It then proceeded to clinical trials and following the results of its phase II trial, it was given conditional approval by the FDA for the treatment of MDR-TB. However, it was issued a black box warning due to unexplained deaths following treatment. Bedaquiline is a diarlquinoline and it acts by inhibiting ATP synthase, a completely novel target in *M. tuberculosis* (149). Resistance to bedaquline has already been reported with the most prevalent mutations occurring in the *atpE* gene, specifically an A36P and I66M amino acid substitions. However, out of the 53 resistant isolates found, only 15 displayed mutations in the *atpE* gene (150). This suggests there are additional mechanisms of resistance that still need to be determined.

Figure 1.22. Chemical structure of bedaquiline.
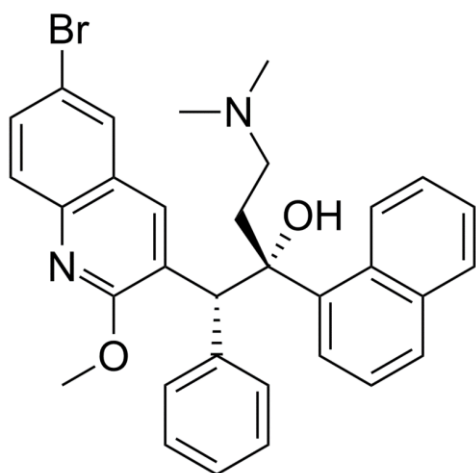
Delamanid

Delamanid is a derivative of nitro-dihydro-imidazooxazole that demonstrates activity against *M. tuberculosis*. It is currently in phase III clinical trials and has comparable activity to rifampicin with agreeable efficacy and safety for treatment of MDR-TB [Figure 1.23]. It is hypothesized to inhibit mycolic acid biosynthesis (151, 152).

PA-824

PA-824 is a nitroimidazole prodrug that needs to be activated by a nitro-reductase. Evidence suggests that it exerts its antimicrobial activity by inhibiting protein synthesis and perturbing cell wall lipids. It has demonstrated very good in vitro and in vivo activity and is currently undergoing clinical trials [Figure 1.24]. *M. tuberculosis* resistance to PA-824 have been associated with mutations in a glucose-6-phosphate dehydrogenase, dezaflavin cofactor F420, and in a nitroimidazo-oxazine-specific protein (153).

Figure 1.23 – Chemical structure of delamanid.
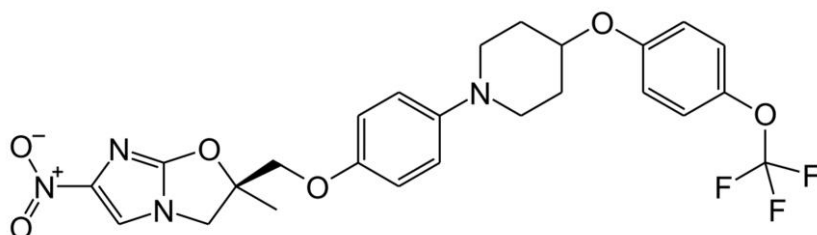
Benzothiazinones

A new class of drugs have emerged which are bactericidal and active against both drug-sensitive and MDR clinical isolates of *M. tuberculosis* [Figure 1.25]. It targets the gene products of Rv3790 and Rv3791 which catalyze the epimerization of decaprenylphosphorl ribose to decaprenylphosphoryl arabinose. These enzymes are known as DprE1 and DprE2. Recent studies have shown that reduction of an essential nitrogen group to a nitroso group, which allows benzothiazinones to interact with a cysteine residue in DprE1, inhibiting its function (154).

Figure 1.24. Chemical structure of PA-824.
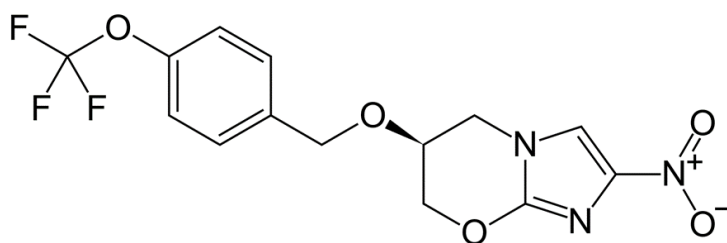
SQ-109

SQ-109 is an analogue of ethambutol, demonstrates good activity against both drug-sensitive and MDR *M. tuberculosis,* and has shown synergistic activity with other first line drugs [Figure 1.26]. SQ-109 and bedaquiline have been shown to act

synergistically against *M. tuberculosis in vitro,* effectively increasing the potentcy of

bedaquiline by more than 4 fold (155). It is currently in phase II clinical trials. Data

suggests that SQ-109 targets MmpL3, a possible transporter of trehalose monomycolate.

SQ-109 resistant *M. tuberculosis* isolates have mutations spanning the *mmpL3* gene (156).

Figure 1.25 – Chemical structure of the benzothiazinone, BTZ043.
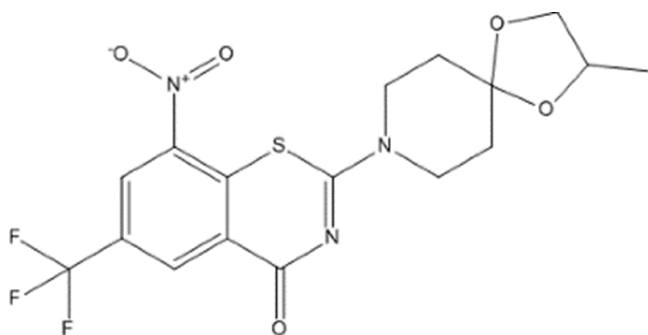
Figure 1.26 – Chemical structure of SQ-109.
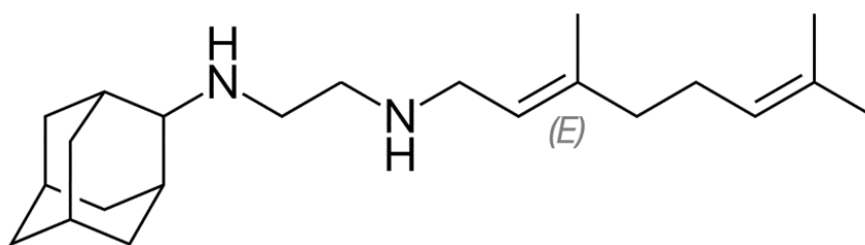
Despite the introduction to inexpensive and combinatorial therapies more than 40 years ago, tuberculosis still remains and has a footing in every corner of the world. It is apparent that even with abundance of chemotherapeutic options to treat *M. tuberculosis* infections, resistance will continue to arise as long as drugs are around. It can be argued that drug resistance in *M. tuberculosis* is a problem assisted by improper drug use and drug regimens. Drug resistance is a problem that does not have a single solution. In order to keep up with the evolving mycobacterial landscape, new drugs, new drug targets, and new mechanisms/ combinations of drugs must be identified and refined. There is need for shorter and less toxic treatment plans and quicker more efficient ways to evaluate plans for proposed drug therapies In addition, the mechanisms of resistance to current drugs need to be further elucidated, especially in the area of drug efflux pumps, to guide future drug discovery research.

CHAPTER II

IDENTIFICATION OF NOVEL GROWTH INHIBITORS AND ELUCIDATION OF POTENTIAL DRUG TARGETS IN *MYCOBACTERIUM TUBERCULOSIS*

BACKGROUND

Central Carbon Metabolism

Essential to the physiology of all bacteria, central carbon metabolism (CCM) is the enzymatic transformation of carbon through glycolysis, gluconeogenesis, the pentose phosphate shunt, and the tricarboxylic acid cycle (157).The transport and use of carbon substrates is afforded by multiple specific uptake systems and pathways which generate macromolecules such as proteins, nucleic acids, and cell wall components (158). The genes involved in CCM are controlled in part by transcriptional regulators which may sense key metabolites found in carbon metabolic pathways. Deconvolution of these global metabolic networks is challenging, yet sequence homology modeling, bioinformatics, mutation studies and transcriptional profiling have helped elucidate the structure and composition of CCM for *in-vitro* and *in-vivo* growth of intracellular pathogens.

Central Carbon Metabolism in *Mycobacterium tuberculosis*

CCM in *M. tuberculosis* diverges from most pathogens in that it is adapted to one host and one environment. *M. tuberculosis* has evolved interdependent physiological and pathological roles within the human macrophage and takes advantage of the metabolic flux which occurs during infection. Upon initial infection, *M. tuberculosis* has been shown

to perturb host cell glycolysis, engaging the metabolic pathways of the host cell and exploiting its ability to increase lipid accumulation and ATP synthesis (159). After initial infection, evidence suggests that *M. tuberculosis* primarily utilizes a diet of fatty acids derived from host lipids, then via beta-oxidation enters the TCA cycle as acetyl-CoA. In addition, *M. tuberculosis* has been shown to utilize carbon sources from glycerol, amino acids, and carbon dioxide fixation to feed central metabolism. Unique to *M. tuberculosis* is its ability to co-catabolize multiple carbon sources and direct individual components to distinct metabolic fates.

Drug Discovery in *Mycobacterium tuberculosis*

Traditional drug discovery in *M. tuberculosis* has followed a target-based approach. A target is usually a single gene, gene product, or molecular mechanism that has been identified on the basis of genetic or biological observations. In a target-based approach, HTS will facilitate identification of molecules that may interact with the target or target families. The benefit of a target-based approach is that the molecular mechanism of action (MMOA) is known. However, the most important obstacle to overcome is whether or not the identified inhibitors will translate into a phenotypic whole cell response. Therefore, phenotypic screens at the whole cell level have re-emerged as a much more successful strategy.

High Throughput Screening Assay

The challenge in identifying novel therapeutics for *M. tuberculosis* is recapitulating an *in vitro* environment which would directly translate to the complex *in vivo* conditions faced within a macrophage. Acetate and glucose are primary carbon sources which feed into gluconeogenic and glycolytic pathways. Gluconeogenesis and glycolysis are essential for the pathogenesis and persistence of *M. tuberculosis.* In order to probe as many physiologically relevant metabolic pathways as possible, a HTS assay must be able to identify inhibitor(s) of enzymes required for *M. tuberculosis* infection and/or persistence.

To identify more drug-like molecules, significant diversity is required among compound screening libraries in order to identify *in-vitro* screening conditions relevant to the conditions encountered by the bacteria during an infection. This platform carefully examines the required chemical diversity and *in vitro* growth conditions necessary to develop a HTS assay to systematically identify compounds which inhibit the growth of the bacteria. The versatility of the assay allows for the screen to accommodate many various *in vitro* growth conditions which may represent the nutritional milieu that mycobacteria encounter within its host.

Non-Tuberculous Mycobacteria (NTMs)

Interest in NTMs have grown significantly as a result of their infection in patients with AIDS and the recognition that disease caused by NTMs is also encountered among non-immunocompromised individuals. NTMs can be the cause of several clinical diseases

including pulmonary disease, lymphadenitis, disseminated disease, skin disease, soft tissue disease and bone disease. Several important observations have been made over the past two decades while monitoring pathogenesis of NTM infections. 1) In HIV infected individuals, disseminated NTM infections most often were seen only after the $CD4^+$ T-lymphocyte number had dipped below 50/µl. 2) In patients free of HIV infection, disseminated NTM infections were often found associated with specific mutations in interferon and interleukin synthesis and response pathways. 3) Pulmonary NTM infections were often associated with bronchiectasis in postmenopausal women with certain bodily habitus (pectus excavatum, scoliosis, mitral valve prolapse) (160-162). These data demonstrate that upon mycobacteria phagocytosis by macrophages, the proper regulation of interferon and interleukin, specifically IFN-γ and IL-12, is critical for the control of infection. Improper regulation of the IFN-γ/IL-12 pathways, either acquired or genetic, appears paramount for predisposition to NTM infection and dissemination of disease (163).

NTMs pose major challenges in diagnosis and treatment. NTMs share many characteristics with *M. tuberculosis* and appear identical upon microscopic examination. Additionally, the symptoms associated with NTM and *M. tuberculosis* infection often present in similar fashion, resulting in possible misdiagnosis and mistreatment. In a recent study, it was found that at least 10% and in some areas as high as 30% of suspected tuberculosis cases were in fact NTM infections. Furthermore, in a small clinical sample of 36 patients in Tanzania, 11.4% of patients with NTM infections were also found to be co-infected with *M. tuberculosis* (164). Often, anti-tuberculosis medications are administered

to patients suffering from NTM infections, leading to less than satisfactory outcomes. This is not unexpected given the diversity found within mycobacteria as well as the documented differences in their pathogenicity, virulence, mode of transmission, and antibiotic susceptibility.

Identifying potential therapeutics against NTMs is no small feat given the range of species which encompass the mycobacterial genus and their intrinsic resistance to antibiotics. Compounded by the realization that many NTM infections are associated with *M. tuberculosis* infections, treatment regimens may have to target multiple species of NTMs as well as *M. tuberculosis.* Ideally, a therapeutic would be identified by its ability to sterilize against a range of mycobacterial infections. Given the similarities among mycobacterial genomes, it may be possible to identify a chemotherapeutic that is active against a fast growing, non-pathogenic species such as *M. smegmatis,* that also demonstrates efficacy against other mycobacteria.

There is some debate as whether *M. smegmatis* could serve as a model organism for *M. tuberculosis* in a laboratory setting (165). *M. smegmatis* does not enter epithelial cells, does not persist in professional phagocytes, and has none of the pathogenic properties described by *M. tuberculosis* (166). However, *M. smegmatis* is saprophytic, shares 70% of the 4034 protein coding genes with *M. tuberculosis*, and displays a rapid *in vitro* doubling time of 2-3 hours. It has also been shown that 12 out of the 19 genes identified in *M. tuberculosis* as required for virulence share close homologues in *M. smegmatis* (167).

In order to evaluate *M. smegmatis* as a potential vaccine candidate for *M. tuberculosis*, one research group identified 38 genes which were significantly up-regulated during active, latent, and reactivated stages of infections. From this they identified 1367 T-cell epitopes and 140 B-cell epitopes on *M. tuberculosis* and compared those to *M. smegmatis* using a BLAST search. The results showed that the two shared 68 identical T-cell epitopes and 11 B-cell epitopes on 18 different proteins in *M. smegmatis* and 13 different proteins in *M. tuberculosis*. All 18 proteins have identified functions in *M. smegmatis* which correlate with the functions of the 13 identified proteins in *M. tuberculosis* (168).

In addition, several whole cell screens have been conducted which compare the results of identified active molecules between *M. smegmatis* and *M. tuberculosis*. The evidence shows that in over 75% of the whole cell active molecules against *M. smegmatis*, the compounds were also active against *M. tuberculosis*. However, the inverse was not quite as predictable. In one study, only 21% of the identified compounds active against *M. tuberculosis* showed activity against *M. smegmatis* while 86% of the compounds active against *M. smegmatis* were also active against *M. tuberculosis*. Although, many whole cell active compounds against *M. tuberculosis* may be lost when using *M. smegmatis* as a model organism, the molecules which demonstrate activity on *M. smegmatis* will often demonstrate potency against *M. tuberculosis*. Interestingly, *M. abscessus* shares more growth characteristics with non-pathogenic mycobacteria such as *M. smegmatis*, but it also shares 1675 protein coding regions with the pathogenic mycobacteria, *M. tuberculosis* and 2117 with *M. smegmatis* (168-172). Therefore, utilizing a fast growing pathogenic

mycobacterial species in screening assays serves two purposes; a model organism for *M. tuberculosis* and also as a model for itself. As such, screening against NTMs could be a promising avenue for the discovery of *M. tuberculosis* and NTM therapeutics simultaneously.

Methods for Target Identification

When using phenotypic whole cell screening techniques as a tool for drug discovery, the need to identify precise protein targets or mechanisms of action responsible for the phenotype(s) observed becomes critical. There are several methodologies employed for discovering target(s) of whole cell active small molecules: genetic interaction methods, classical genetic methods, computational inference methods, and direct biochemical methods (173). Genetic interaction works by modulating hypothesized targets in cells, presumably changing the sensitivity to the small molecule. This requires additional insight into the biological target and may be more practical when screening against known classes of compounds.

Computational inference or target hypotheses, uses pattern recognition to compare sets of molecules and their effects to known reference molecules. Many times this only leads to pathway inferences and must await secondary confirmation of the actual protein receptor. Direct methods involve labeling of the small molecule or protein and attempting to observe a physical interaction between the two. The biggest drawback to the method is the label itself, which many times can interfere with binding or cause instability when ligated to a protein or small molecule. Classical genetics involves applying an

experimental selection pressure in order to identify a phenotype of interest. This is followed by identification of the gene responsible for the observed phenotype.

Classical Genetics Method of Target Identification

Bacterial antibiotic resistance can be achieved by horizontal acquisition of resistance genes, by recombination of foreign DNA into the chromosome, or by mutations in the chromosomal loci. Mutation rate is defined as the *in vitro* frequency at which bacterial growth appears within a population in the presence of a given antibiotic (174). In order to understand the mechanism of resistance within a population, each individual genotype which gave rise to the specific phenotype must be examined. This mutation selection process within the bacterial population is incredibly dynamic. Much work has been done to show that many factors play a role in varying the mutation frequency. Antibiotic concentration, growth media, oxidative stress, and population density all influence the genotype and phenotype(s) of the bacteria's mutability.

In regards to target identification, the selection pressure would be applied in the form of a small molecule which demonstrated a reduction in cell viability, and the expected phenotype would be lack of bacterial growth. However, in the event that a mutation occurred, which limited the efficacy of the compound while still maintaining an adequate level of fitness, bacterial growth may still occur. This population would be considered resistant against the compound used as selection pressure. Spontaneous mutation is rare and only occurs in $1x10^{-4}$ to $1x10^{-11}$ bacteria. In order to increase the rate of mutation, a mutagen can be added to the bacteria culture, effectively increasing the

frequency by up to 1000 fold. Ethyl methanesulfonate (EMS), methyl methanesulfonate, and ultraviolet (UV) light are commonly used mutagens.

Model Organism(s) of *M. tuberculosis* for Target Identification

Given the draw backs displayed by many of the described target identification methods combined with the advent of modern whole genome sequencing technology, classical genetics becomes the most practical approach. In order to successfully probe for desired phenotypes, the organism must first lend itself to genetic manipulation. It is quite difficult and time consuming to modify wild type *M. tuberculosis* (H37Rv) to the extent that a BSL3 laboratory would be required. The non-pathogenic strains of *M. tuberculosis* (BCG, $MC^2 7000$) are possible candidates, but their long doubling time and low frequency of resistance, make them less than ideal (175). The fast growing mycobacteria share similar genome sequences, have shorter doubling times, and are relatively non-pathogenic. These traits make them ideal candidates as a model organism for *M. tuberculosis. M. smegmatis, M. fortuitum, and M. abscessus* were selected as candidates for *in vitro* target identification. They are more susceptible to spontaneous *in vitro* mutation, have a doubling time of about 2-4 hours, and share many homologous proteins to *M. tuberculosis*. The homology of NTMs to *M. tuberculosis* has been demonstrated not only by whole genome sequencing, but also through the compounds which were active across multiple species of mycobacteria shown in the previous HTS assay.

Whole Genome Sequencing

Whole genome sequencing technology allows researchers to interrogate mutated genes and hypothesize on the mechanism of resistance based on the observed genotypes. Analysis of genome sequencing data is less complicated when the population is clonal, or void of genetic variation. This can be accomplished when the selection process takes place on solid agar media. Each colony which appears would be clonal and contain a uniform genotype. However, growth and selection in a liquid culture makes it more difficult to de-convolute the sequencing data and pinpoint specific genes responsible for resistance. The advantage to liquid culture selection is that each mutant sequenced would theoretically give a snapshot of all the mutations within the mixed population. This is incredibly useful when one considers the cost per sequencing run as well as the time involved for preparing and sequencing individual clonal samples.

MATERIALS AND METHODS

Bacterial Strains

M. abscessus (strain SYU3)*, M. fortuitum* (strain PN)*, M. smegmatis* (strain MC^{2}155) were obtained from Dr. Eric Rubin at Harvard Medical School. MC^{2}7000 was obtained from Dr. William Jacobs. MC^{2}7000 is a genetically engineered attenuated strain of wild type *M. tuberculosis (H37Rv)* which is deficient in several genes (ΔpanCD ΔRD1), PanC and PanD are two genes involved in the biosynthesis of pantothenic acid and coenzyme A, which are required for intracellular replication and persistence (176). RD1

is an operon containing 9 genes essential for *M. tuberculosis* virulence and are missing in all attenuated strains (177).

Compound Library Creation

Two chemically diverse, small molecule libraries, with Tanimoto scores <0.7, were created following Lipinski's rule of 5 and purchased from ChemBridge, Enamine, Asinex, Maybridge, ChemDiv, and Life Chemicals (178). The compound libraries were also filtered for molecules which are known to contain reactive R groups or demonstrate any known problems of instability such as isonitriles, aliphatic aldehydes, sulfamates, thiosulfates, and oxiranes. Library 1 (Sac1) contains 51,780 compounds and Library 2 (Sac2) contains 52,781 compounds. Solid material of each individual compound was dissolved into 100% dimethylsulfoxide (DMSO) to a concentration of 10mM and aliquoted into 96 well plates in order to create stock solutions (Mother Plates). Subsequently, working stock solutions (Daughter Plates) were created by making a 10:1 dilution in 100% DMSO from the mother plates into 384 well daughter plates to a final concentration of 1mM.

Chemicals, Media, Equipment and Supplies

384 well and 96 well polypropylene and polystyrene plates were purchased from Costar. Middlebrook OADC Growth supplement (Oleic Albumin Destrose Catalase) was purchased from Fisher Scientific. Pantothenic Acid (PAN), Malachite Green (MG), Sodium Acetate (NaOAc), Dextrose, Sodium Chloride (NaCl), Calcium Chloride ($CaCl_2$),

Magnesium Sulfate (MgSO$_4$), Resazurin, Tween 80, Tyloxapol, Ethyl methanesulfonate (EMS), M9 Minimal Media, and Middlebrook 7H9 growth media were purchased from Sigma. HTS assays were carried out using a CyBio Vario and an inline 8+1. Results were monitored and recorded using a POLARstar Omega plate reader from BMG Labtech.

Bacterial Media and Growth Conditions

M. abscessus, M. fortuitum, M. smegmatis were grown in Middlebrook 7H9 media supplemented with 0.2% dextrose, 0.01% NaCl, 0.2µ/ml MG, and 0.04% Tween 80 until an optical density at 600nM (OD$_{600}$) of about 1.0 was reached. The cells were passed into M9 minimal media supplemented with 1.0% NaOAc, 0.1mM CaCl$_2$, 2mM MgCl$_2$, 0.2µg/ml MG, and 0.04% Tween 80. The cells were grown again to an OD$_{600}$ of 1.0 and then diluted to a final working concentration of OD$_{600}$ of 0.005 into M9 minimal media supplemented with 1.0% NaOAc, 0.1mM CaCl$_2$, 2mM MgSO$_4$, 0.2µg/ml MG, and 0.04% Tween 80.

MC^{2}7000 was grown in Middlebrook 7H9 media supplemented with 0.2% dextrose, 0.01% NaCl, 0.2µl MG, 0.04% Tyloxapol, 100µg/ml PAN, and a 1:10 dilution of Middlebrook OADC grown to an OD$_{600}$ of 1.0. Using NaOAc as the only carbon source, the cells were passed into M9 minimal media containing 1.0% NaOAc, 0.1mM CaCl$_2$, 2mM MgSO$_4$, 0.2µg/ml MG, and 0.04% Tween 80, and 100µ/ml PAN to a final working concentration of OD$_{600}$ of 0.05. Using mixed carbon sources of dextrose and NaOAc, the cells were passed into M9 minimal media containing with 0.2% dextrose, 0.2% NaOAc,

0.01% NaCl, 0.2µl MG, 0.04% Tyloxapol, and 100µg/ml PAN to a final working concentration of OD_{600} of 0.05.

HTS Assay Conditions

Using the CyBio Vario, either 1.0µL (single carbon source) or 0.5µL (mixed carbon source) of compound from each well of a Daughter Plate was pipetted into a 384 well polypropylene assay plate. Columns 3-22 were reserved for compounds (320/plate) and columns 1,2, 23 and 24 were reserved for positive and negative controls (Rifampicin, Streptomycin, and DMSO) Next, 49µL of the working stock culture was added to each well, resulting in a final concentration of 1-2% DMSO, and 10-20µM of compound per well. Plates were then sealed with a semi-porous film and then placed into a 37°C non-shaking incubator. MC^27000 was grown in a CO_2 jacketed incubator, negating the need to apply a seal.

The fast growing mycobacteria (*M. smegmatis, M. fortuitum, M. abscessus)* were grown for 24 hours, removed from the incubator and 1.25µl of resazurin added to every well. The plates were then resealed and placed back into the incubator. The slow growing mycobacteria (MC^27000*)* were incubated for 7 days when grown on a mixed carbon source of NaOAc and dextrose or for 21 days when grown on NaOAc alone, before the addition of resazurin. After an additional incubation of 24-48 hours, the plates were removed from the incubator and cell viability was determined by either measuring the difference in absorbance at 573nM and 603nM or by fluorescence using an excitation wavelength of 579nM and an emission wavelength of 584nM

HTS Data Analysis

Metabolically active cells will reduce Resazurin in a NADH dependent manner producing Resorufin (179) [Figure 2.1]. Resazurin has an absorbance maximum at 605nM while Resorufin has an absorbance maximum at 573nM. Taking the difference of the two values will give a fairly accurate estimate for the amount of viable cells present in each well. Alternatively, Resorufin is a fluorescent product of Resazurin, therefore measuring the resulting emission at 584nM when using an excitation wavelength of 579nM will also yield an estimate to the amount of viable cells in each well. Both methods were used and values for cell viability were calculated by comparing unknowns to positive and negative controls. The assay was validated on a plate by plate basis using SM and RIF as positive controls with known MICs. Z-values were calculated for each plate and scores above 0.7 were considered acceptable.

Figure 2.1. Reduction of resazurin to resorufin. Actively respiring cells are shown in pink, which have oxidized resazurin to resorufin. Cells which are no longer respiring are shown in blue. A gradation of blue to pink (shades of purple) represents wells which either contain very few actively respiring cells or they are respiring very slowly.
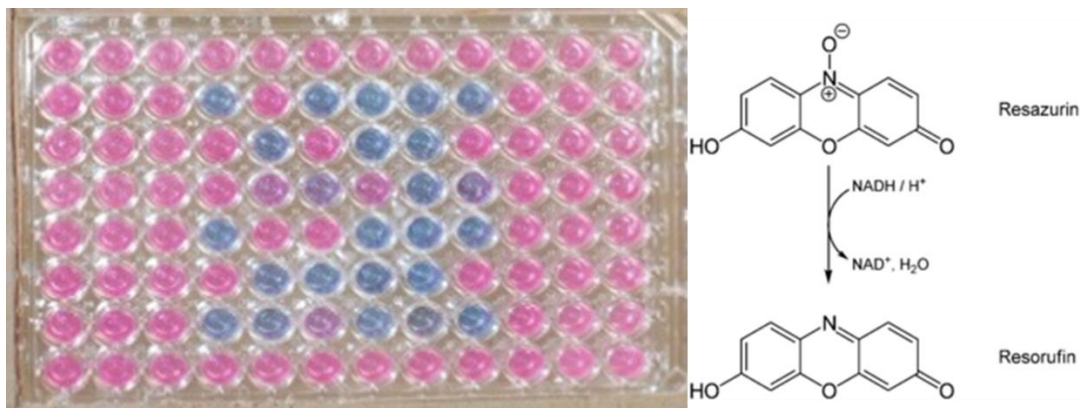
Percent viability, or percent control was calculated using the following [% Control = $100*(1-((\text{sample} - \text{negative control})/(\text{positive control} - \text{negative control})))$] Values that were at least three standard deviations away from the mean were used as criteria for determining which compounds gave a statistically significant phenotypic response, corresponding to decreased cell viability and respiration. Compounds which decreased cell viability were deemed "hits" and further validated using a dose response assay in order to determine approximate Minimum Inhibitory concentration of 50% growth (MIC_{50}) values against each organism.

Selection of Resistant Mutants

Compounds were selected from the hits generated during the HTS which demonstrated activity against *M. tuberculosis* and at least one additional fast growing mycobacterium. *M. abscessus, M. fortuitum, M. smegmatis* were grown in Middlebrook 7H9 media supplemented with 0.2% dextrose, 0.01% NaCl, 0.2μ/ml MG, and 0.04% Tween 80 until an optical density at 600nM (OD_{600}) of about 1.0 was reached. The cells were passed into either M9 minimal media supplemented with 1.0% NaOAc, 0.1mM $CaCl_2$, 2mM MgCl2, 0.2μg/ml MG, and 0.04% Tween 80, or 7H9 media supplemented with 0.2% dextrose, 0.01% NaCl, 0.2μg/ml MG, and 0.04% Tween 80. Media selection was based on the activity profile of the compounds used during the original HTS. The cells were grown again to an OD_{600} of 1.0 and then incubated with EMS for a period of time. The cells were then diluted to a final working concentration of OD_{600} of 0.01 into the same media used during the growth in the presence of EMS.

MIC$_{50}$s of the selected compounds were used to determine working concentration for the assay. 10 compounds were used in each 96 well plate. Columns 1 and 12 were used as positive and negative controls (Rifampicin, DMSO). The 10 compounds were diluted to a final working concentration that was equal to 100x their MIC for a total of 8 dilutions. These values and concentrations were determined for each individual compound and for each bacterial strain being tested. Growth media was added to each well for a final concentration of 200µL. The plates were sealed and placed into a shaking incubator at 37°C for 5 days. After 5 days, the plates were removed, and 2.5µL of resazurin was added. The plates were returned to the incubator and every 24 hours were checked to determine if the culture in any well displayed growth at a concentration greater than the original MIC of the compound. If so, the culture was aspirated from the well and split into two fractions. One was frozen at -80°C in order to preserve stock of the original mutant culture, and the other was diluted into the same growth media to a total volume of 5ml in the presence of the compound the resistant mutant was selected against at a concentration greater than the original MIC.

Once the culture was grown to late log phase, preparation for genomic DNA extraction began with the addition of glycine to a final concentration of 1%. The culture was grown for an additional 24 hours. To complete the process of DNA extraction, methods from a previously published protocol were used (180)

Whole Genome Sequencing and Data Analysis

Each individual genomic isolate was sequenced using an Illumina Genome Analyzer IIx, as previously described (181, 182). The results were analyzed by a comparative genome assembly method using proprietary software developed in our lab by Dr. Tom Ieorger. Mutations were identified by searching for single nucleotide polymorphism(s) (SNPs) in essential genes. Since the genomic population was a mixture of various resistant mutants, SNPs were often inferred in terms of heterogeneity between individual reads. SNPs and insertions/deletions were determined by comparing multiple sequence runs between each isolate and H37Rv. Mutations found in genes deemed essential were clustered and subjected to secondary assays for validation. Gene essentiality was determined from transposon site hydridization assays (TraSH) done previously (183, 184). Genetic recombineering and over-expression studies were secondary assays employed to validate the individual genetic mutations responsible for resistance (185).

RESULTS

HTS of Sac1 Library

Compounds from the Sac1 library were screened against MC^{2}7000 at a concentration of 20μM and against *M. smegmatis, M. fortuitum,* and *M. abscessus* at a concentration of 10μM using NaOAc as a primary carbon source. 1255 compounds hits were obtained from the primary screen against MC^{2}7000 (2.42%), 1236 compounds against *M. abscessus* (2.39%), 929 compounds against *M. fortuitum* (1.79%), and 545 compounds against *M. smegmatis* (1.05%). MC^{2}7000 had 325 hits shared with *M.*

fortuitum, and 406 shared with *M. abscessus*. There were 251 hits shared between all three

mycobacteria and 179 of the 251 compounds were also active against *M. smegmatis*

[Figure 2.2]. These numbers are consistent with what has been reported in a recent study

which showed that only 50% of compounds which kill *M. tuberculosis* could be detected

when using *M. smegmatis* as a model organism (168).

The 1255 hits against MC^27000 were further validated in a dose response assay

using NaOAc as a primary carbon source. Re-screening using NaOAc as the primary

carbon source, 880 compounds demonstrated greater than a 50% reduction in cell viability

at 20µM. 646 compounds at 10µM, 560 compounds at 5µM, 337 compounds at 2.5µM,

and 297 compounds at 1.25µM. This represents a 70% re-test rate from the primary screen

with 880 out of the 1255 compounds re-testing at a concentration of 20µM.

Figure 2.2. Venn diagram of the Sac1 screen results. SYU3 = *M. abscessus*. PN = *M. fortuitum*. Mtb = *M. tuberculosis*. 1255 compounds were active against *M. tuberculosis,* with 406 of those also being active against *M. abscessus*¸ and 325 of the 1255 also active against *M. fortuitum*. 251 out of the 1255 were active against all three mycobacteria. There were 1236 compounds active against *M. abscessus* alone and 929 active against *M. forutitum alone*. 523 compounds were active against both *M. fortuitum* and *M. abscesssus*.
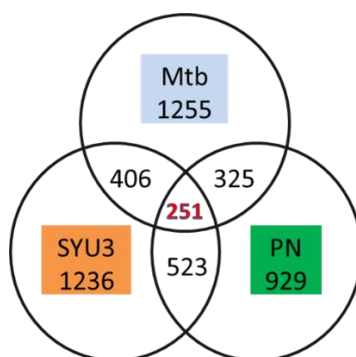
A comparison of the top 200 hits at 1.25µM with a subset of 200 random molecules which did not show inhibition at 20µM displayed very little differences between the two sets except in three criteria, average log P, average polar surface area and average pKa. Although pKa is a key physiochemical parameter influencing many biopharmaceutical characteristics, its absolute value does not lend itself to simple calculations and comparison. However, the active molecules have an average pKa of 6.53 while the inactive molecules have a slightly higher average of 7.23. In the case of the active molecules, at a neutral pH, they will exist primarily in a deprotonated form. This observation for the group of molecules reveals very little, but pKas when investigated on an individual basis can give insight into a drug's absorptivity. This is because most drugs are weak acids or weak bases, and from a calculated pKa, the percent unionized or percent ionized of the molecule at varying biological pHs can be determined. The ratio of ionization to unionization can be used to determine how well the drug will be absorbed as well as predict its solubility at neutral pHs, such as blood plasma or acidic pHs, such as in the stomach.

On the other hand, log P values have direct correlation to a molecule's lipophilicity and cellular absorptivity. Therefore, the higher the log P value, the lower the hydrophilicity of the molecule which translates into poor cellular absorption. It has been shown that most compounds should have a log P less than 5 in order to have a reasonable probability of being well absorbed. The average log P for the active molecules was 4.05 compared to 3.08 for the in-actives. Several active molecules lay outside the average by a great deal with a range of 8.22 to 0.38 [Figure 2.3]. The compound with a log P of 0.38 is

also active against *M. abscessus* at 1.25µM, but not *M. fortuitum.* In order to determine if the average log P of the hits were affected by these outliers, a cut off of 1-7 was used and the log P was re-calculated. By removing the outliers below 1 and above 7, the average log P was only slightly affected with an average of 4.07. This would seem to indicate that on average, the active molecules are slightly hydrophobic and may partition more efficiently into cellular compartments like the lipid bilayer of cells. Although a lower log P is usually preferable, there are several compounds which demonstrate anti-tuberculosis activity that are slightly more lipophilic than inactive ones. These include: bedaquiline, 6.37; delamanid, 6.14; rifapentine, 4.83; SQ-109, 4.64; rifampin, 3.85. However, three of the four first line drugs are hydrophilic; isoniazid, -0.71; ethambutol, -0.12; and pyrazinamide, -0.71 (186). A recent study showed that combinations of mostly lipophilic anti-tubercular drugs were highly sterilizing against *M. tuberculosis* in mice infections (187, 188). Therefore, a slightly higher log P may be a good indicator of molecules which may show promising activity against *M. tuberculosis.*

Figure 2.3. Log P of hits from Sac1 screened against *M. tuberculosis* at 1.25µM.

CD:000L-4290
Log P = 8.22

CD:8012-7376
Log P = 0.38
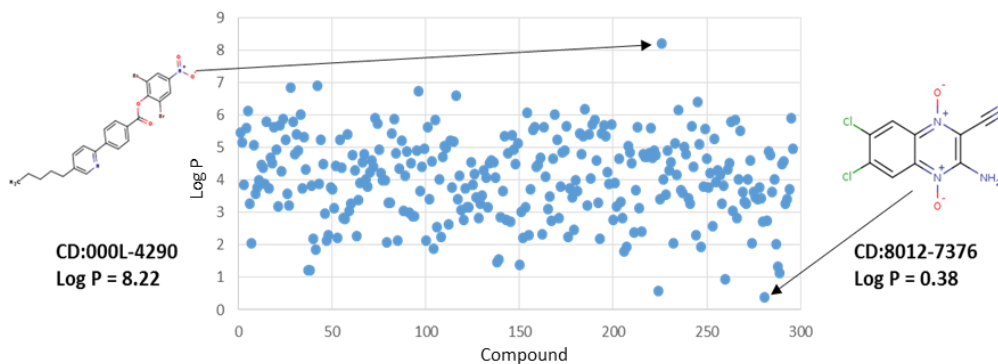
Values for acceptable polar surface area for ideal drugs are usually in the range of 75 Å^2 to 140 Å^2, with values above 140 Å^2 being associated with poor membrane permeability and values below 75 Å^2 being associated with an increased risk of non-specific cytotoxicity (189, 190). Interestingly, the average polar surface area was about 10 Å^2 lower for the active molecules than for the non-actives. There were a few molecules which deviated from the average with the highest PSA being 142.05 and the lowest at 6.48 [Figure 2.4]. The molecule with the PSA of 142.05 was also active against *M. fortuitum* at 1.25µM, but not *M. abscessus.* Setting a cut off from 20 to 120, the average PSA was re-analyzed and did not vary much from the original with a value of 62.08.

Figure 2.4. PSA of hits from Sac1 screened against *M. tuberculosis* at 1.25µM.
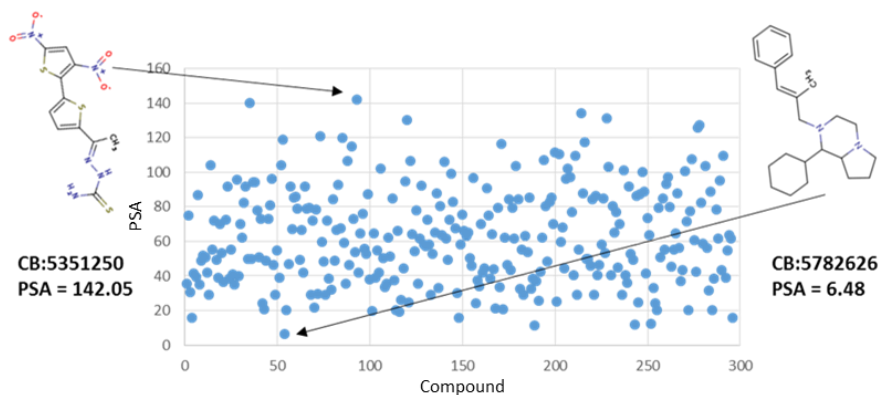
From a predictive and comparative stand point, there is very little that separates the two subsets. This may be more of a reflection of the selection criteria used in the creation of the library more than the differences between active and inactive molecules. Since similar values were obtained between the two data sets with only minor discrepancies found for all of the compared sets of molecules it is difficult to differentiate between active and inactive molecules based solely on predicted chemical properties [Table 2.1].

The 297 hits found against *M. tuberculosis* at 1.25µM were cross referenced for activity against *M. abscessus* and *M. fortuitum* and 140 and 112 actives were found respectively. The 140 actives against *M. tuberculosis* and *M. abscessus* at 1.25µM had an average PSA of 65.67, an average log P of 4.19, and an average molecular weight of

350.75. The 112 actives against *M. tuberculosis* and *M. fortuitum* at 1.25 µM had an average PSA of 64.34, log P of 4.23, and an average molecular weight of 347.39. Among the same pool of hits, the trend seems show that molecules active against *M. fortuitum* seem to be slightly smaller, less polar, and more lipophilic than molecules which are active against *M abscessus.*

Table 2.1. Average statistics of the top hits from Sac1 against *M. tuberculosis.*

Sac1 Library Comparison	Avg. MW	Avg. Log P	Avg. H-Bond Donors	Avg. H-Bond Acceptors	Avg. pKa	Avg. Number of Heavy Atoms	Avg. Number of Rotatable Bonds	Avg. Polar Surface Area
Top 200 hits at 1.25µM	344.68	4.05	1.17	3.31	6.53	23.32	4.29	63.19
200 Molecules with no activity at 20µM	249.86	3.08	1.14	3.94	7.23	24.38	4.29	72.24

The 112 compounds which demonstrated activity against *M. fortuitum* and *M. tuberculosis* were clustered using a binary clustering tool with a similarity score of 0.4.

This led to very little clustering based on molecular similarity except with one group of seven compounds. These seven compounds are all composed of poly-cyclic ring systems with only one compound containing a halogen R group [Figure 2.5]. Surprisingly, four out the seven were also active against *M. abscessus* at 1.25µM. These seven compounds had an average PSA of 58.12 and an average log P of 3.92. These values for the cluster are significantly lower than the values determined for all active molecules against *M. fortuitum* and *M. tuberculosis* at this concentration.

The 140 compounds which demonstrated activity against *M. abscessus* and *M. tuberculosis* were clustered in the same manner as above. This led to single compound clustering except in the case of two groups of three compound and four compounds. The cluster of four compounds were compound of poly-cyclic ring systems all containing a nitro group. Three out of the four compounds were also active against *M. fortuitum.* The three compound cluster were composed of poly-cyclic ring systems with multiple halogen R groups. Only one of the three was also active against *M. fortuitum* [Figure 2.6]. The seven compound had an average PSA of 75.13 and an average log P of 4.40. These values are significantly higher than the averages found for the active molecules against *M. fortuitum* and *M. tuberculosis* which clustered together as well as the 297 hits which were active against *M. tuberculosis* at 1.25µM. The two compounds which had the highest PSA or 111.43 and 91.63, were not active against *M. fortuitum.* This is consistent with all the compounds which were active against *M. abscessus* and *M. tuberculosis.* There seems to be a preference for molecules with a higher log P and larger surface area for *M. abscessus* compared to *M. fortuitum* and *M. tuberculosis*

Figure 2.5. Seven molecules which are active against *M. tuberculosis* and *M. fortuitum* at 1.25µM. The top four compounds are also active against *M. abscessus* at 1.25µM.
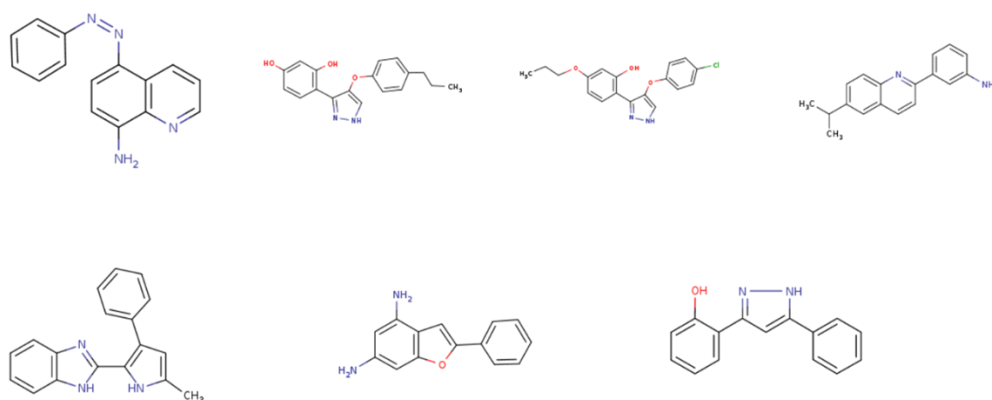
Figure 2.6. Two clusters of four and three molecules respectively that were active against *M. abscessus* and *M. tuberculosis* at 1.25µM. Compounds which are also active against *M. fortutium* at 1.25µM are boxed in.
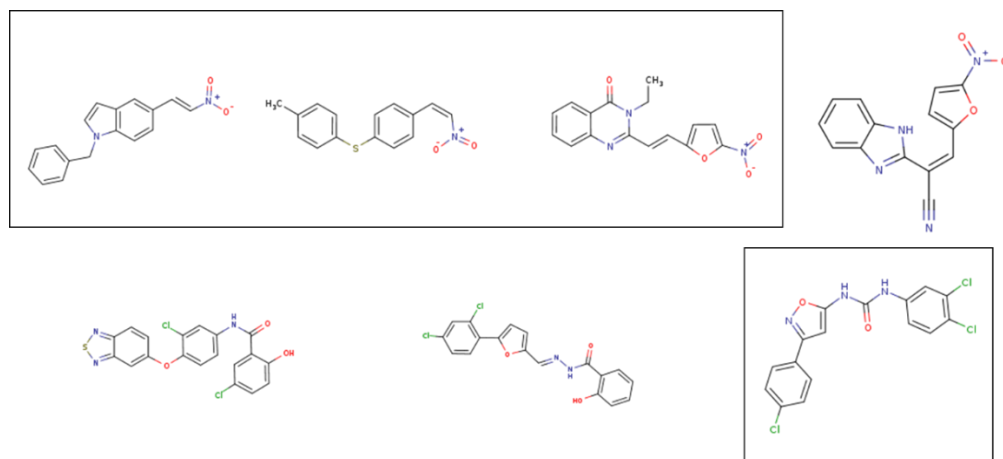
HTS of Sac2 Library

Compounds from the Sac2 library were screened against MC^{2}7000 at a concentration of 10µM using a mixed carbon source of NaOAc and dextrose. 542 compounds were obtained from the primary screen (1.03%). The hits were re-screened using NaOAc and dextrose as carbon sources in a dose dependent assay. 465 compounds retested for a greater than 50% reduction in cell viability at 10µM, 354 compounds at 5µM, 156 compounds at 2.5µM, and 104 compounds at 1.25µM. In order to determine if chemical properties could be a predictor of potency, the hits at every concentration of the dose response were compared against one another as well as against 500 random molecules that displayed no activity. In contrast to the results from the Sac1 analysis, there were significant trends observed among most of the compound's molecular properties. The average molecular weight, the average log P, the average number of hydrogen bond donors and acceptors, the average number of heavy atoms, the average number of rotatable bonds, and the average polar surface area decreased as the molecule's potency increased [Table 2.2]. The average log P was 4.46 for the 104 active molecules at 1.25µM while it was 3.46 for inactive molecules. The log P values ranged from 7.12 to 0.37 and these outliers were removed before re-calculating the average log P which deviated just slightly with a new value of 3.57 [Figure 2.7]. The average PSA was 57.71 which ranged from 127.55 to 3.88. These outlier were removed and the average PSA was re-calculated to a new value of 58.05 [Figure 2.8]. These observations seem to suggest that the most potent molecules against *M. tuberculosis* tend to have smaller molecular weights, which lead to a decrease in many of the other chemical properties.

Table 2.2. Average statistics of the top hits from Sac2 against *M. tuberculosis*.

Sac2 Library Comparison	Avg. MW	Avg. Log P	Avg. H-Bond Donors	Avg. H-Bond Acceptors	Avg. pKa	Avg. Number of Heavy Atoms	Avg. Number of Rotatable Bonds	Avg. Polar Surface Area
104 hits at 1.25µM	330.69	3.46	0.93	2.96	6.62	21.76	3.82	57.70
156 hits at 2.5µM	334.76	3.46	0.98	3.05	6.98	22.11	3.97	59.70
354 hits at 5.0µM	344.17	3.39	1.04	3.26	6.89	23.24	4.21	62.73
465 hits at 10µM	346.02	3.39	1.04	3.32	6.78	23.4	4.23	63.22
500 molecules with no activity	355.17	2.77	1.07	3.92	6.72	24.49	4.68	70.97

Figure 2.7. Log P of hits from Sac2 screened against *M. tuberculosis* at 1.25µM.

LC:F1301-0392
Log P = 7.12

LC:F2135-0092
Log P = 0.37
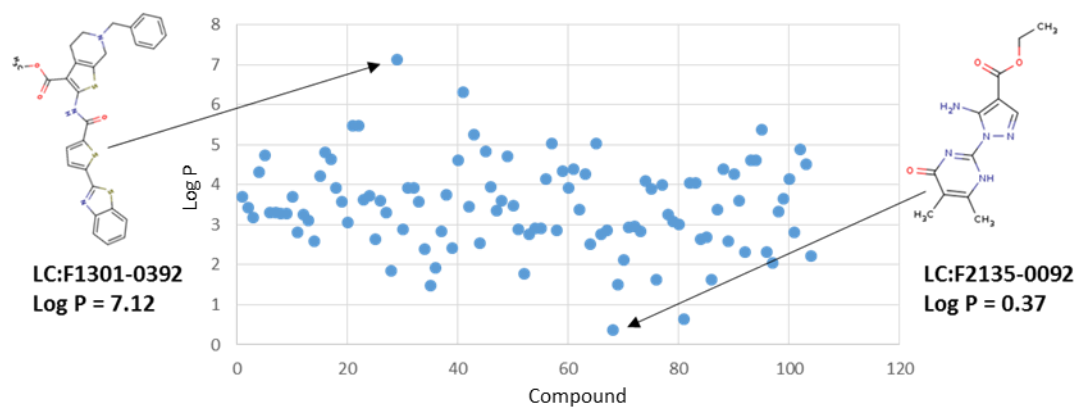
Figure 2.8. PSA of hits from Sac2 screened against *M. tuberculosis* at 1.25µM.

LC:F5305-0154
PSA = 127.55

AS:BAS00127456
PSA = 3.88
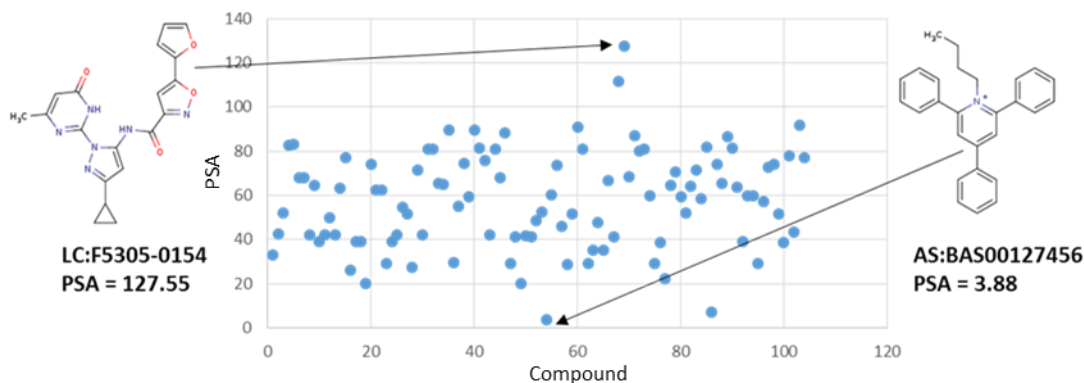
Selection of Resistant Mutants

There were 179 compounds which demonstrated whole cell activity against *M. abscessus, M. smegmatis, M. fortuitum, and* MC^{2}7000. These compounds were screened in an attempt to select for resistance in the NTMs. Thirty-six compounds were identified in which resistance could be selected for in at least one of the NTMs. From those 36 molecules, a total of 122 resistant isolates were selected, sequenced, and subjected to genotypic analysis. 104 mutants were selected from *M. smegmatis,* 10 from *M. fortuitum,* and 8 from *M. abscessus* [Table 2.3].

Mechanism of Resistance

SNPs were successfully identified in 28 of the 122 samples submitted for whole genome sequencing. SNPs which resulted in synonymous substitutions were eliminated

and the remaining genes were separated into two groups based on essentiality. Since gene essentiality is often variable and dependent on experimental conditions, genes considered non-essential *in vitro* were not entirely eliminated as a possible genotype conferring resistance. Essential genes which did not have an orthologue in H37Rv were also removed from consideration. 18 resistant isolates were identified containing SNPs in genes essential for growth and as well as being orthologous in H37Rv. From these 18 isolates, three genes were eventually selected for further study, Rv0206, Rv0272, and Rv2857 [Table 2.4].

Table 2.3. Compounds which resistant mutants were successfully selected against.
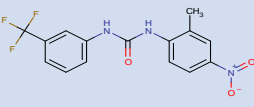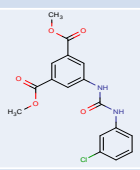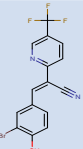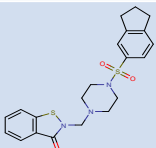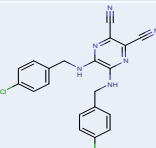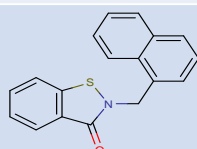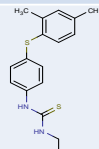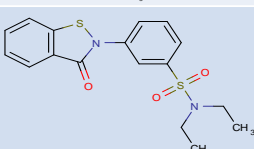
Molecule Name	Structure	Active against M. fortuitum @ 10μM	Active against M. abscessus @ 10μM	MIC in MC²7000	Resistant Isolates in MC2155	Resistant isolates in M. fortuitum	Resistant isolates in M. abscesssus
GATB_SAM002705352		Yes	Yes	2.5 μM	2	2	0
GATB_SAM002705130		Yes	Yes	2.5 μM	2	0	0
EN:T6067980		Yes	Yes	5 μM	2	0	0
EN:T5806624		Yes	Yes	1.25 μM	2	0	0
EN:T5481663		Yes	Yes	5.0 μM	2	0	0
EN:T5438905		Yes	Yes	5.0 μM	2	0	0
EN:T5256576		Yes	Yes	1.25 μM	2	0	0
EN:T5240565		Yes	Yes	1.25 μM	4	2	0
EN:T0513-3325		Yes	Yes	10 μM	2	0	0

Table 2.3 Continued
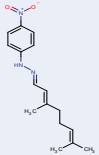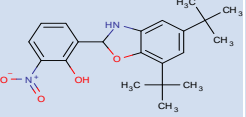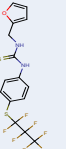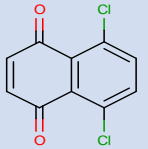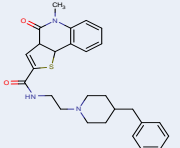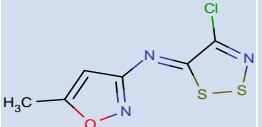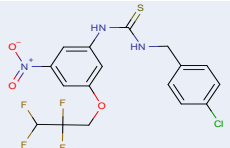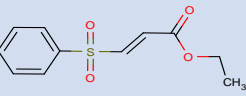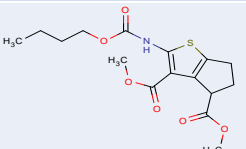
Molecule Name	Structure	Active against M. fortuitum @ 10μM	Active against M. abscessus @ 10μM	MIC in MC²7000	Resistant Isolates in MC2155	Resistant isolates in M. fortuitum	Resistant isolates in M. abscesssus
EN:T0509-9548		Yes	Yes	10 μM	8	0	0
EN:T0503-5068		Yes	Yes	5 μM	2	0	0
EN:T0501-3547		Yes	Yes	1.25 μM	16	2	0
CD:R091-0019		Yes	Yes	5 μM	2	0	0
CD:C066-3108		Yes	Yes	5 μM	2	0	0
CD:8001-2971		Yes	Yes	5 μM	2	0	0
CB:7825760		Yes	Yes	No	0	2	0
CB:6691134		Yes	Yes	10 μM	0	0	2
CB:6675077		Yes	No	10 μM	1	0	0
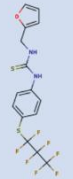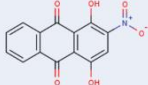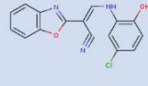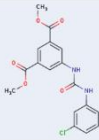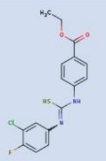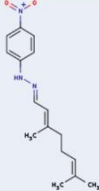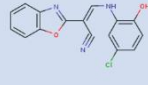
Table 2.3 Continued

Molecule Name	Structure	Active against M. fortuitum @ 10µM	Active against M. abscessus @ 10µM	MIC in MC²7000	Resistant Isolates in MC2155	Resistant isolates in M. fortuitum	Resistant isolates in M. abscesssus
CB:6593752		Yes	Yes	10 µM	13	0	0
CB:6429284		Yes	Yes	10 µM	0	0	2
CB:6313742		Yes	Yes	10 µM	2	0	0
CB:5944406		Yes	No	10 µM	4	0	0
CB:5660393		No	No	5 µM	0	0	2
CB:5650154		Yes	Yes	2.5 µM	4	0	0
CB:5649218		Yes	Yes	Not Active	4	0	0
CB:5646983		Yes	Yes	5 µM	3	0	0
CB:5551271		Yes	No	5 µM	2	0	0

Table 2.3 Continued

Molecule Name	Structure	Active against M. fortuitum @ 10µM	Active against M. abscessus @ 10µM	MIC in MC²7000	Resistant Isolates in MC2155	Resistant isolates in M. fortuitum	Resistant isolates in M. abscesssus
CB:5302942		Yes	No	2.5 µM	2	0	0
CB:5302408		Yes	Yes	5 µM	2	0	0
CB:5275017		Yes	Yes	10 µM	2	0	0
CB:5224399		No	No	2.5 µM	2	0	0
CB:5217488		Yes	Yes	Not Active	2	0	0
CB:5210732		Yes	Yes	1.25 µM	2	2	0
CB:5130983		Yes	Yes	1.25 µM	3	0	0
CB:5104304		Yes	No	Not Active	2	0	2
306373		No	No	1.25 µM	2	0	0

96

Table 2.4. Identified SNPs in 28 resistant isolates via whole genome sequencing.

Compound	Structure	Resistant Isolates	Genes Identified with Mutations	Mtb Orthologue Gene Product	Identified SNPs
EN:T0501-3547		2	MSMEG_3217 MSMEG_6330	Rv1609 (TrpE) Rv3754 (TyrA)	P498L A281V
CB:5302794		4	MSMEG_6759 MSMEG_0064 MSMEG_1515 MSMEG_3531	Rv3696 (GlpK) Rv3873 (PPE68) Rv3764 (HK) Rv1887 (Hyp)	A264T A120V R311K V142A
CB:5646983		8	MSMEG_6362 MSMEG_3065 MSMEG_3108 MSMEG_3200 MSMEG_4301 MSMEG_5350	Rv2196 (CytB) Rv1407 (Fmu) Rv2832 (ugpC) Rv1595 (NadB) Rv1925 (FadD31) Rv3539 (PPE63)	M120I A238S D25* L302R S354D A127T
CB:7252875		4	MSMEG_0250 MSMEG_6834 MSMEG_5912 MSMEG_4757	Rv0206 (MmpL3) Rv3045 (AdhC) Rv1731 (GabD2) Rv2524 (FAS)	A326T Q131* Q132* P206S
CB:7794244		2	MSMEG_0250 MSMEG_2598	Rv0206 (MmpL3) Rv2857 (Hyp)	T39M A24V
EN:T0509-9548		6	MSMEG_0605 MSMEG_1895 MSMEG_2459 MSMEG_2584 MSMEG_4175 MSMEG_4295	Rv0272 (Hyp) Rv0117 (OxyS) Rv2397 (CysA1) Rv2864 (R160H) Rv0576 (ArsR) Rv2223 (Pro)	S333F G254E W183* R160H G27D T27P
CB:6593752		2	MSMEG_1161	Rv3756 (ProZ)	V216A

Examination of the Identified Target(s): Rv0206

One of the more intriguing targets identified was MSMEG_0250, which is orthologous to Rv0206. Rv0206 has been previously annotated as a large transmembrane transporter (MmpL3) belonging to a family of transmembrane proteins, specific to mycobacteria. Previous work has shown that MmpL3 may be involved in the transport of mycolic acids (156). Other work has demonstrated that MmpL3 may play a role in sequestering heme across the cell membrane (191). MmpL3 has also been the focus for drug development and increasingly more evidence suggest its importance for the survival of *M. tuberculosis* (192) (193). However, the abundance and diversity displayed by the multiple pharmacophores targeting MmpL3 have called into question its validity as a drug target.

Considerable work has been done in order to pinpoint a single mutation or an area of mutations in Rv0206 which may lead to resistance. To date, resistant isolates in both *M. smegmatis* and *M. abscessus* have been selected against 3 different whole cell active molecules [Figure 2.9]. In addition, other members of the lab have been successful in identifying mutations in Rv0206 from resistant isolates of MC^{2}7000 selected against 10 compounds [Figure 2.10]. Furthermore, cross resistance has been demonstrated towards several of these molecules in *M. smegmatis* isolates with known mutations in Rv0206 [Figure 2.11]. Yet, these efforts have so far failed to yield a definitive mechanism of resistance due to the diversity of compound chemo types and mutations identified. However, it can be conclusively stated that mutations in MmpL3 lead to resistance against a considerable amount of anti-tuberculosis compounds and the mutations are spread

throughout the gene (data not shown). This work is ongoing and in collaboration with several other academic and non-academic laboratories. These results are not the focus of this dissertation but instead provide an example which demonstrate some of the successes of this selection method.

Figure 2.9. Chemical structure of the three whole cell active compounds which resistant mutants were selected against and mutations in Rv0206 were identified. The corresponding amino acid change is shown.
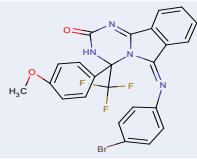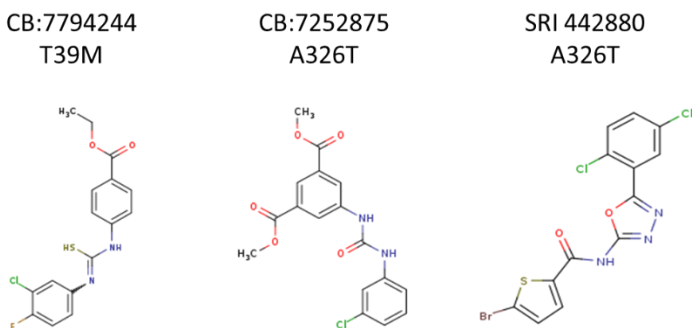

Examination of the Identified Target(s): Rv2857

As described earlier, *mmpL3* seems to be highly mutagenic, and susceptible to mutations spanning the entire gene. This data makes it difficult to reconcile MmpL3 as a potential drug target given the diversity observed between pharmacophores and the varying location of mutations. This led to the hypothesis that MmpL3 may be acting as a facilitator for transporting the drug in or out of the cell. If this is the case, mutations in

MmpL3 may be masking the identity of the true intracellular target. In order to discern the actual gene(s) which gave rise to the resistant phenotype, additional mutations besides the ones discovered in MSMEG_0250 were examined. MSMEG_2598, orthologous to Rv2857c in H37Rv, was identified as a potential candidate. Its gene product is annotated as a hypothetical protein with no assigned function and an A24V amino acid substitution in the resistant mutant. However, further validation of MSMEG_2598/ Rv2857c as the target of 7704244 was unsuccessful via recombineering and as such was eliminated from further rounds of characterization(s).

Figure 2.10. Chemical structures of several whole cell active molecules which resistant isolates have been selected against in *M. tuberculosis* which have identified mutations in Rv0206.
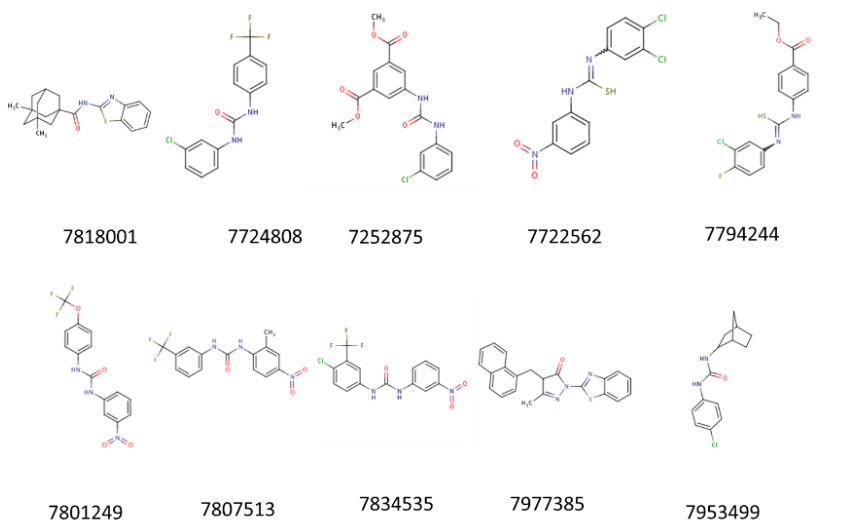
Examination of the Identified Target(s): Rv0272

A mutation in MSMEG_0605 was identified as the potential mechanism of resistance towards EN:T0509-9548 [Figure 2.12]. Initially, the mutation was overlooked because traSH data eluded to it being non-essential *in vitro*. However, after examination of the SNPs in each of the 3 isolates resistant to EN:T0509-9548, no essential genes which could describe the mechanism of resistance were identified. Therefore, all SNPs, regardless of essentiality, were re-evaluated. After a thorough analysis of all mutations leading to non-synonymous base changes, one particular gene stood out, MSMEG_0605.

However, MSMEG_0605 was originally declared non-essential and its causation for resistance was questioned. Therefore, a manual examination of the traSH data was initialized, and after careful consideration it was discerned that all the insertions in MSMEG_0605 were at the termini of the gene under every growth condition except one. What this suggests is that the gene is essential for survival under *in vitro* conditions because mutations at the C-terminus or N-terminus of genes many times do not affect the function of the resulting gene product. Only when the culture was grown using glycerol as the sole carbon source, MSMEG_0605 became dispensable for growth.

The identified codon mutation leads to a S333F amino acid substitution and MSMEG_0605 has an orthologue in *M. tuberculosis,* Rv0272. Rv0272c is predicted to encode for a hypothetical hydrolase of unknown function and does not map to any known biochemical pathway. This information combined with newly analyzed traSH data, presented a unique scenario to describe a possible drug target as well as annotate a protein

of unknown, but essential function. Given these criteria, Rv0272 was selected for further

characterization.

Figure 2.11. Cross resistance of one isolated mutant with an identified SNP in Rv0206.
The top plate is wild type *M. smegmatis* and the bottom plate is *M. smegmatis* with a
mutation in Rv0206 which leads to an A326T change. A 17-fold increase in MIC is
shown for the parent compound (7252875) used in selection (black box) against the
mutant strain. Each column is a dilution series of compounds which resistance has been
generated against and mutations in Rv0206 identified. The mutant strain demonstrates a
high level of resistance to four of the nine compounds compared to wild type. The top
row has a drug concentration of 112µM and each subsequent well in the column is a
two-fold dilution series down to 0.875µM. Pink wells represent respiring bacteria and
blue wells represent non-respiring bacteria.
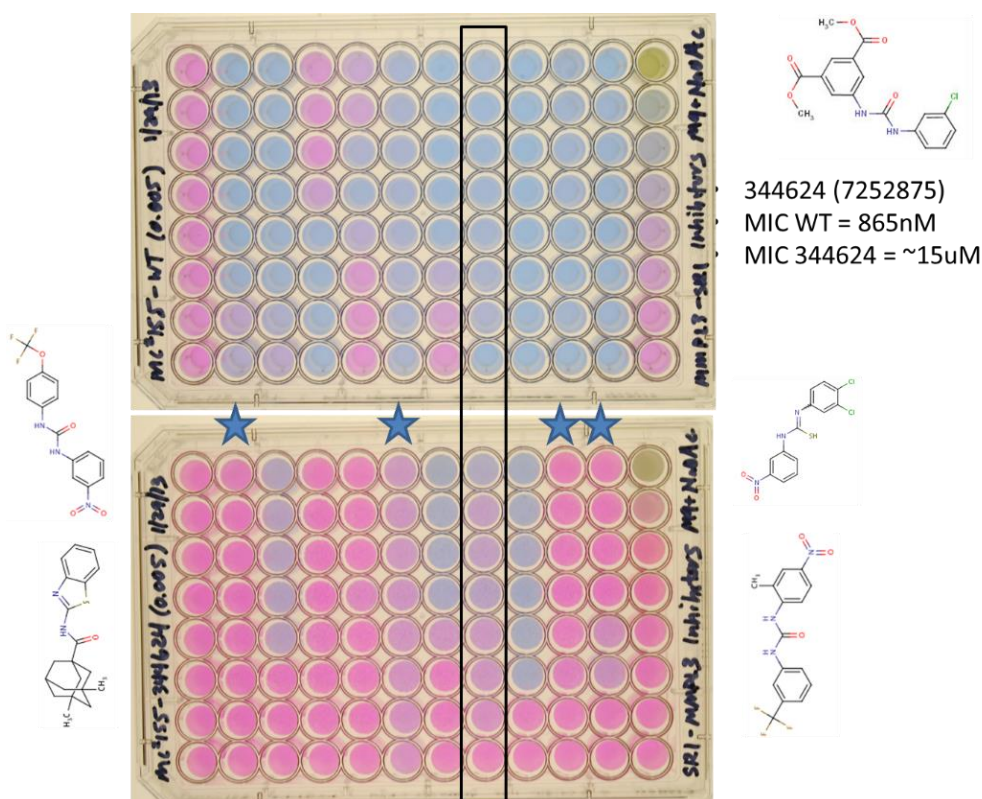
Figure 2.12. Chemical structure of EN:T0509-9548.
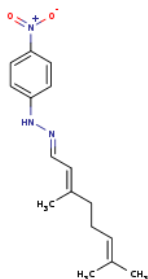
DISCUSSION

Classification of Small Molecule Growth Inhibitors

1255 hits were found in Sac1 to be active against MC^{2}7000 when grown on NaOAc as the primary carbon source and 542 compounds from Sac2 when grown on both NaOAc and dextrose. In an attempt to define specific classes of molecules, a structure based clustering analysis was performed using Chemmine on the hits from the Sac2 library. 354 clustered together when the similarity threshold was set to 0.4 or greater. The other 183 compounds failed to cluster, which is not surprising given that the software uses Tanimoto scores as its main determinant to characterize similarity. The Sac1 and Sac2 libraries were designed using Tanimoto scores less than 0.7 as a selection criteria. When the similarity threshold was increased to 0.5, none of the compounds clustered successfully. Therefore, in order to attempt to identify chemical classes of molecules, hierarchical and

multidimensional clustering were used. This method differs slightly by computing similarity using Tanimoto scores against item-item distances and compares them across the entire input family to establish any linkage. However, this method failed to yield any significant clustering of compounds in terms of specific chemical classes. This gives merit to the chemical diversity present in the compound libraries and allows the screen to probe a broad range of biological targets.

Cross Species Comparison of Small Molecule Growth Inhibitors

The 880 hits which were active against MC^27000 at 10µM grown on NaOAc were cross referenced against our HTS on Lymphoma 2631 cells. 827 of the 880 hits were not active against Lymphoma 2631 cells, which indicates low cytotoxicity against human cells. The active molecules are likely promiscuous inhibitors containing nitro or multi-halogenated R groups. It is also possible that some of these cytotoxic molecules target homologous proteins in the lymphoma cell line. The 880 hits found from the Sac1 library were compared to the hits which were found on a similar screen with the primary carbon source being dextrose instead. 198 compounds were active on both NaOAc alone and dextrose alone. This result suggests that these compounds may inhibit intracellular targets which are not involved in metabolism, or are required for both glycogenesis and gluconeogenesis. It also suggests that these active compounds may have more than one target. In addition, at 2.5 µM, 284 compounds were specific to growth on NaOAc alone and 21 were specific to growth on dextrose alone. These compounds are most likely

specific inhibitors for proteins that are involved in gluconeogenesis (NaOAc) and glycolysis (Dextrose) respectively.

Candidate(s) Targets of Whole Cell Active Small Molecules

Utilizing a selection method in a liquid medium and EMS combined with sequencing of poly-clonal isolates allowed a high-throughput selection of 140 resistant mutants across multiples NTMs and the identification of 18 possible genes responsible for resistance. From this study, 3 potential targets were selected and subjected to validation as viable drug targets for further characterization; Rv0206, Rv2857, and Rv0272, with emphasis on the hypothetical genes, Rv0272 and Rv2857. However, further validation of Rv2857 and Rv0206 were unsuccessful which led to their removal from future consideration. Therefore, Rv0272 became the sole candidate for biochemical target validation and functional characterization.

There were several limitations to this methodology, especially related to the technology available at the time of the experiments. The amount of sample coverage, complete coverage of whole genome sequencing data for some of the NTMs, the multiplexing capabilities of the Illumina, and the proprietary software used to identify mutations were all in stages of infancy. The technology and the methodology for selection and sequencing were being pioneered at the time of these experiments. The algorithms used to identify single base changes were still in the early stages of development and the feedback gathered as a result of these findings were used to develop more sophisticated

and accurate software revisions. If the sequencing were to be repeated today, the amount of correctly identified SNPs would be estimated to increase 10 fold.

CONCLUSION

Although *M. tuberculosis* is the causative agent of the world's deadliest disease, discovering inhibitors of additional pathogenic mycobacteria is also paramount. The nontuberculous mycobacteria (NTMs) are closely related to *M. tuberculosis* but do not cause tuberculosis or leprosy. They can produce chronic pulmonary infection and little is known about optimal treatment and long term outcomes. These include but are not limited to *M. abscessus* and *M. fortuitum*, which are responsible for thousands of deaths a year in the United States (194). While the primary object of this screen was to find novel inhibitors of *M. tuberculosis*, secondary goals were successful in identifying inhibitors of other potentially pathogenic, closely related mycobacteria. Additionally, *M. smegmatis,* while non-pathogenic, shares more than 70% genome sequence homology with *M. tuberculosis,* has a rapid doubling time, and lends itself to genetic manipulation. Given these traits, *M. smegmatis,* is arguably a great model organism for the identification and development of *M. tuberculosis* therapeutics, and as such was included as part of the screen.

The discovery of new small molecule hits against *M. tuberculosis* is the first step required when developing anti-mycobacterial therapeutics. What this HTS accomplished was not only the identification of whole cell active compounds against several mycobacterial strains, but also the validation of non-cytotoxic and *M. tuberculosis* specific

compounds. These can be further evaluated as potential drug candidates through target identification and characterization.

Sequencing DNA of resistant mutants from a liquid culture treated with EMS provides several challenges. For one, the population is not clonal and therefore the mutations which occur will be a mixture of genetic populations across all reads of the sequencing run. Secondly, when exposing a culture to a mutagen, the amount of mutations increases as well as the rate of resistance. Identifying a single gene among the potential hundreds of SNPs and heterogeneous sites of conversion, is quite labor intensive and many times futile. Most often the data is broken down into a subset of mutated genes for each isolate that may be responsible for resistance. Only after these genes are subjected to secondary genetic and biochemical assays do we get a more precise understanding behind the mechanism of resistance.

CHAPTER III

CHARACTERIZATON OF RV0272: A POTENTIAL DRUG TARGET OF
UNKNOWN FUNCTION IN *MYCOBACTERIUM TUBERCULOSIS*

BACKGROUND

Sequenced Based Characterization

BLAST programs are widely used tools for identifying protein and DNA sequence similarities. A PSI-BLAST is a modified matrix which takes into account position specific sequence hits which are more sensitive to weak but biologically relevant sequence similarities (195). A PSI-BLAST search often reveals conserved functional domains which may give insight into an enzyme's biology. A DELTA-BLAST is an updated BLAST algorithm which is more sensitive than a traditional BLAST (196).

Rv0272 is 377 amino acid protein with no predicted function. A DELTA-BLAST was performed on Rv0272 against all known organisms. The results identified two conserved domains, YvaK and Abhydrolase_6. Residues 300-343 corresponded to the YvaK domain which is known to be a conserved region among certain esterases and lipases involved in secondary metabolite biosynthesis, transport and catabolism. Residues 219-370 corresponded to the Abhydrolase_6 domain, which represents a family of α/β hydrolase enzymes of diverse specificity. Further sequence analysis revealed a 30-98% sequence identity with other proteins of unknown function with an Abhydrolase_6 domain. A detailed investigation of the BLAST results identified only three enzymes of predicted function. A 4-carboxymuconolcatone decarboxylase from *Streptomyces* with

11% sequence identity, a 3-oxoadipate enol-lactonase from *Steptomyces* with 12% sequence identity, and a pimeloyl-ACP methyl ester carboxylesterase with 16% sequence identity from *Chelatococcus sambhunathii*.

Genetics Based Enzyme Characterization

Analysis of a gene's location on a chromosome along with the upstream and downstream genes can lead to inferences about its particular role in the organism's biology. Rv0272 does not appear in a previously annotated operon. The upstream and downstream genes are annotated as hypothetical or regulatory proteins (Rv0273c, Rv0274, Rv0275c, Rv0276). However, there are two genes downstream with proposed functions based on sequence similarity. FadD2 and FadE6 are annotated as a possible fatty-acid-CoA ligase and an acyl-CoA dehydrogenase, respectively [Figure 4.1].

Figure 3.1. Proposed operon of Rv0272. Genes with no previously described function are depicted in red. Genes depicted in black are involved in lipid metabolism and genes. Genes depicted in blue encode for regulatory proteins.
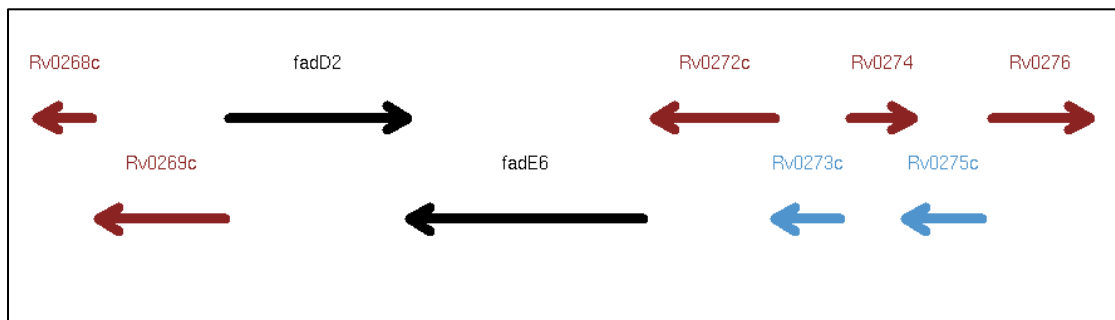
AIM OF THE STUDY

The main goal of the project was to attempt to completely characterize potentially important enzymes that are indispensable for *M. tuberculosis* survival. Ultimately, characterization would be comprised of assigning one primary biology function for each individual enzyme as well as identifying where in an established biological pathway that function has a defined role. Secondary objectives included assessing identified enzymes for their relevance as a chemotherapeutic target. This included identifying small molecules which could perturb the enzyme's function leading to the limitation or elimination of the organism's ability to survive *in vitro*.

MATERIALS AND METHODS

Cloning, Expression, and Purification

The gene Rv0272 from *M. tuberculosis* was amplified by PCR using primers Rv0272-For-**NdeI** (5'-**CATATG**TTGACTGGTCGTGCTGC-3') and Rv0272-Rev-**HindIII** (5'-**AAGCTT**TCAGCGCCACCGCTTG-3'). The gene was cloned downstream of the Lac promoter, 6x Histidine and TEV cleavage coding sequence in a modified vector Pet28b. The gene was transformed into BL21(DE3) (EMD Millipore) chemically competent *E. coli* cells suitable for protein expression. The gene was verified via sequencing. (Eaton Biosciences)

E. coli BL3(DE3) transformed with Rv20272c-Pet28b was grown in LB medium containing 50µg/ml of Kanamycin at 37°C with shaking at 180rpm. Once the culture reached an OD_{600} of 0.8, the cultures were chilled on ice for 15 min, 0.5mM of isopropyl-

β-D-thiogalactopyranosidase (IPTG) was added and the cultures were grown overnight at 18°C. The cells were pelleted by centrifugation at 4,500 rpm for 30 minutes and re-suspended in 40mM 4-(2-hydroxyethyl)-1-piperazineethanesulfonic acid (HEPES) buffer, pH 7.4, 300mM sodium chloride (NaCl), and 10mM imidazole. Cells were lysed by three passes through a French press at 20,000 psi and cell lysates were separated by centrifugation at 17,000 rpm for 30min at 4°C. Cell lysates were loaded onto a Nickel-chelate resin for high capacity immobilized metal affinity chromatography (IMAC) (Roche) according to manufacturer's instructions. The column was washed with the same buffer used during lysis. Three consecutive washes of 10 column volumes were performed and the enzyme was eluted with 300mM Imidazole in HEPES buffer pH 7.4, 150mM NaCl. The eluted enzyme was dialyzed against 30mM HEPES 7.4, 100mM NaCl for 4 hours at 4°C in the presence of 0.5-1.0mg of tobacco etch protease (TEV) in order to cleave the 6x HIS tag. After dialysis, the tag-less enzyme was passed over the same IMAC Nickel column to separate Rv0272 from TEV and other potentially contaminating proteins. The purified enzyme was concentrated using vivaspin-30kD (Sartorius) and loaded onto a size exclusion gel filtration column. The resulting protein was analyzed for molecular weight and purity by sodium dodecyl sulfate-polyacrylamide gel electrophoresis, purified fractions pool together, concentrated to 5-10mg/ml, and used immediately for crystallization trials, biochemical assays, or frozen in liquid nitrogen and stored at -80°C for future use.

Crystallization

Initial crystallization trials were done in 96-well sitting drop intelli-plates by the sitting drop vapor diffusion method. (Art Robbins Institute) 50uL of crystallization condition was aliquoted into each well for a total of 96 different conditions per plate. A total 768 different screening conditions aliquoted into eight plates were utilized; Index, Peg/Ion, Salt, Crystal (Hampton Research), Wizard (Rigaku), Lab, Adventure Hike and Adventure Dive (Sacchettini). Each trial consisted of 0.5uL of screening condition and 0.5uL of purified protein dispensed per well with a Mosquito LCP Robot (TTP Labtech). The wells were sealed and incubated at 16°C until crystal formation was observed. Conditions which were conducive to crystal formation were identified and optimized for hanging drop vapor diffusion experiments. Rv0272 yielded large hexagonal pyramidal crystals after 5 days in 3% Tacsmiate pH 5.0 and 22% PEG 3350 (Hampton Research) [Figure 4.2] Crystals reached full maturation after 20 days and were flash frozen in liquid nitrogen before data collection.

Structure Determination

Data were collected at Advance Photon Source (APS) at Argonne National Laboratory and utilizing a home source X-ray generator equipped with a copper rotating anode (CuKα, λ = 1.54 Å) (Bruker). Initial structure determination attempts began using crystals which were soaked in 1mM KAu(CN)$_2$ overnight in an attempt to covalently bind gold to the crystallized enzyme. Diffraction data were collected from a single crystal with one degree oscillation widths for a total range of at least 160° at the gold edge of λ = 1.0Å.

Data were indexed, integrated, and scaled using HKL2000. Heavy atom positions and initial phases were obtained by Single Anomalous Diffraction (SAD) using HYSS and PHASER (Phenix). The resulting difference electron density maps were inspected and used to hand build the initial model in coot. Alternating rounds of refinements in Phenix combined with manual building in coot resulted in the final model of Rv0272. Data collection and refinement statistics are shown [Table 4.1].

Apo and ligand bound structures, excluding malonic acid bound structures, were obtained by first back soaking crystals formed in 3-5% Tacsminate pH 5.0 (1.8305 M Malonic acid, 0.25 M Ammonium citrate tribasic, 0.12 M Succinic acid, 0.3 M DL-Malic acid, 0.4 M Sodium acetate trihydrate, 0.5 M Sodium formate, and 0.16 M Ammonium tartrate dibasic), 22% PEG3350 into a condition consisting of 100mM Tris(hydroxymethyl)aminomethane (Tris) pH 7.4, 100mM NaCl for 30 minutes. Crystals were then soaked in 1-10mM ligand in the same buffer condition for a minimum of 2 hours and flash frozen in liquid nitrogen prior to data collection. Ligand models and their geometric restraints were created in ELBOW (Phenix). The previously built model of Rv0272 was used to obtain the phases by molecular replacement for all inhibitor and ligand bound structures.

Table 3.1. Data Statistics for Rv0272

Wavelength (Å)	
Resolution range (Å)	50 - 1.42 (1.44 - 1.42)
Space group	P 21 21 21
Unit cell	63.587 86.256 122.365 90 90 90
Total reflections	708774
Unique reflections	106548
Multiplicity	6.6 (4.4)
Completeness (%)	83.61 (37.47)
Mean I/sigma(I)	19.95 (2.24)
Wilson B-factor	17.17
R-merge	0.086 (0.857)
R-meas	
CC1/2	
CC*	
R-work	0.2357 (0.2390)
R-free	0.2519 (0.3022)
CC(work)	
CC(free)	
Number of atoms	6045
macromolecules	5595
ligands	14
water	432
Protein residues	733
RMS(bonds)	0.006
RMS(angles)	1.07
Ramachandran favored (%)	97
Ramachandran outliers (%)	0
Clashscore	0.53
Average B-factor	19.1
macromolecules	18.3
ligands	20
solvent	30

Identification of Small Molecule Binders

10µM enzyme was incubated with 1-10mM of ligand in 50mM HEPES, and 7x Sypro orange in 96 well UV clear PCR plates. A Stratagene Mx3000P QPCR System was used to determine melting temperatures of Rv2072 in the presence and absence of biologically relevant molecules. The samples were subject to a protocol of incremental temperature increases of 1°C per minute from 25°C to 95°C. The melting temperatures were quantified by taking the first derivative of the fluorescent intensities versus temperature (MxPro-Mx3005P from Stratagene). Any molecule which increased the thermal stability of the enzyme by more than 3°C compared to control was qualified as binding to the enzyme.

Figure 3.2. Crystals of Rv0272 formed from hanging drop vapor diffusion method.
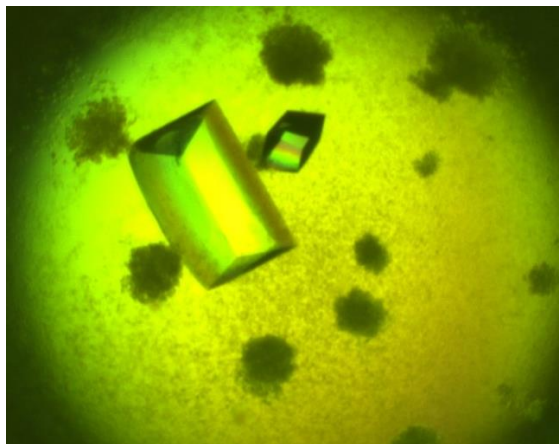
The 542 Compounds which were shown to be whole cell active growth inhibitors of *M. tuberculosis* were initially screened for binding. A fragment library consisting of 1152 small molecules with a molecular weight less than 350g/mol were also screened (Enamine) for binding. In addition, Hampton Research's Additive Screen, composed of 96 compounds ranging from alcohols, metals, detergents to sugars, and enzyme co-factors were evaluated as potential binders. A hand-picked substrate plate made up of 80 biological relevant molecules derived from dicarboxylic acids was screened (Sigma, Fluka). Hits were chosen based on their effect on enzyme thermal stability. These hits were used for secondary binding assays, enzyme assays, and crystallization trials on Rv0272.

Enzymatic Assays: D-Ala-D-Ala Carboxypeptidase

Di-peptide hydrolysis was determined by measuring the release of free of amino acids using the cadmium-ninhydrin method (197). 10-100µg of purified enzyme was incubated with substrate for 30 minutes at 25°C or 37°C in 50mM HEPES pH 7.4. Then 7X reaction volumes of cadmium-ninhydrin solution were added and the sample(s) were incubated at 100°C for 5 minutes to induce color development. The optical density at 505 nm of each sample was determined using a Cary 100 UV/VIS spectrophotometer. Standards were read using 0.1, 0.5, 1.0, 5.0, and 10mM D-Alanine and D-Glycine. Negative controls consisted of substrate and buffer alone.

Enzymatic Assays: Beta-Lactamase

β-Lactamase activity was determined by the hydrolysis of the chromogenic cephalosporin, Nitrocefin (Caymen Chemicals). The resulting product is colored and has an optical density of 490 nm, which is directly proportional to the amount of β-Lactamase activity. In order to determine if Rv0272 demonstrated β-Lactamase activity, 0.1-1.0mM of Nitrocefin was added to 10-100 µg of purified enzyme in 50mM HEPES pH 7.4 and the reaction monitored at 490 nm using a Cary 100 UV/VIS Spectrophotometer at 25°C. The results were compared against samples without enzyme and samples with a known β-Lactamase, BlaC (198).

Enzymatic Assays: Esterase and Phosphatase

Esterase activity was determined by monitoring the product formation of 4-nitrophenoxide via the hydrolysis of 4-nitrophenyl esters which have an absorbance at 410 nm. 4-nitrophenyl-formate, 4-nitrophenyl-acetate, 4-nitrophenyl-butyrate, 4-nitrophenyl-dodecanoate, 4-nitrophenyl-palmitate (Sigma) were tested for activity. 0.1-1.0 mM substrate was added to 10 µg purified enzyme in 50mM HEPES pH 7.4. The hydrolysis was monitored at 410 nm using a Cary 100 UV/VIS Spectrophotometer at 25°C. Phosphatase activity was measured in the same manner except using 4-nitrophenyl phosphate (sigma) as the substrate. All reactions were compared against a negative control reaction without enzyme.

Enzymatic Assays: Thioesterase

Thioesterase activity was determined by monitoring the product formation of mixed sulfides of 5, 5-dithio-bis-(2-nitrobenzoic acid) (DTNB) and Coenzyme A at 412 nm. Acetyl-CoA, propionyl-CoA, buturyl-CoA, succinyl-CoA, benzoyl-CoA, malonyl-Coa, methylmalonyl-CoA, glutaryl-CoA, and hydroxybutyryl-CoA (Sigma) were tested as possible substrates. Substrate was incubated in 50 mM HEPES pH 7.4 and 0.5 mM DTNB and the reaction was initiated with the addition of 10 µg purified enzyme. Substrate hydrolysis was monitored at 412 nm using a Cary 100 UV/VIS Spectrophotometer at 25°C. Samples without substrate and without enzyme were used as negative controls.

RESULTS

Three-Dimensional Structure of Rv0272

Crystals of Rv0272 belong to the space group $P2_12_12_1$ and diffract to a resolution of 1.4 Å. The asymmetric unit contains a physiological homo dimer, with each monomer made up of two domains. The first domain consists of a canonical α/β hydrolase catalytic domain which has 7 parallel and 1 antiparallel β-strands forming a mostly parallel β-sheet. The β-sheet demonstrates a left-handed super helical twist with the first and last strand nearly perpendicular to each other. This is flanked on either side by 6 α-helices [Figure 4.3]. The second domain extends from the 6th β-strand and spans residues 161-315 ending at the 7th β-strand. This "foot" domain is comprised primarily of short loops and a long 31 amino acid α-helix [Figure 4.3].

Catalytic Site

Electrostatic surface maps and comparisons with canonical α/β hydrolase enzymes helped identify an active site pocket located between the two domains. Upon further investigation, the conserved Serine-Histidine-Aspartate catalytic triad was discovered. Serine-118 is positioned directly after β-strand 5 on what is called the "nucleophile elbow". This elbow is identified by an X-X-N-X-X consensus sequence with the flanking residues on either side usually small amino acids. G-G-S-N-G is the sequence in Rv0272 which agrees with the conserved sequence. Histidine-353 is located after the last β-strand, which is absolutely conserved in α/β hydrolases. Aspartate-324 is found after β-strand 7 [Figure 4.4]. These locations are consistent with previous descriptions of the α/β hydrolase catalytic triad.

Figure 3.3. Overall structure of Rv0272. Blue colored ribbon is the "cap" domain while pink colored ribbon is the "α/β hydrolase" domain.
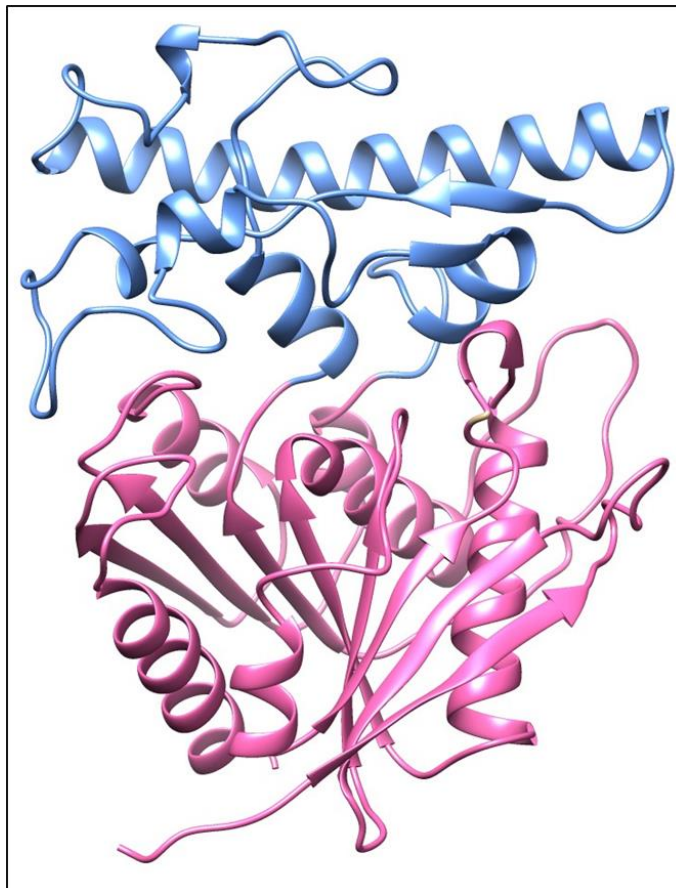
After refinement and structure building, the final maps shows good electron density for the entire polypeptide chain except for the first 8 residues. Unknown electron density was found in the catalytic site of the α/β hydrolase domain which appeared to correspond to malonate, which is a component of Tacsimate from the original crystallization condition [Figure 4.5].

Figure 3.4. Active site of Rv0272 showing the catalytic triad of Asp324, His353, and Ser118 depicted in cyan.
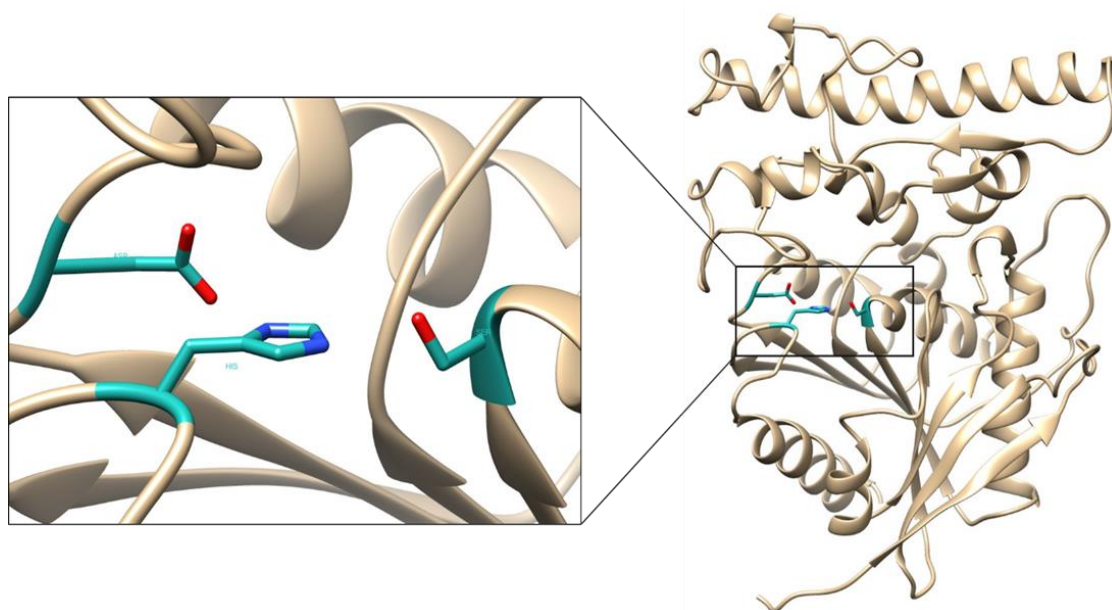
Figure 3.5. Electron density corresponding to malonate bound in the active site coordinated by Arg166 and Ser119. Chemical structure of malonate is also shown.
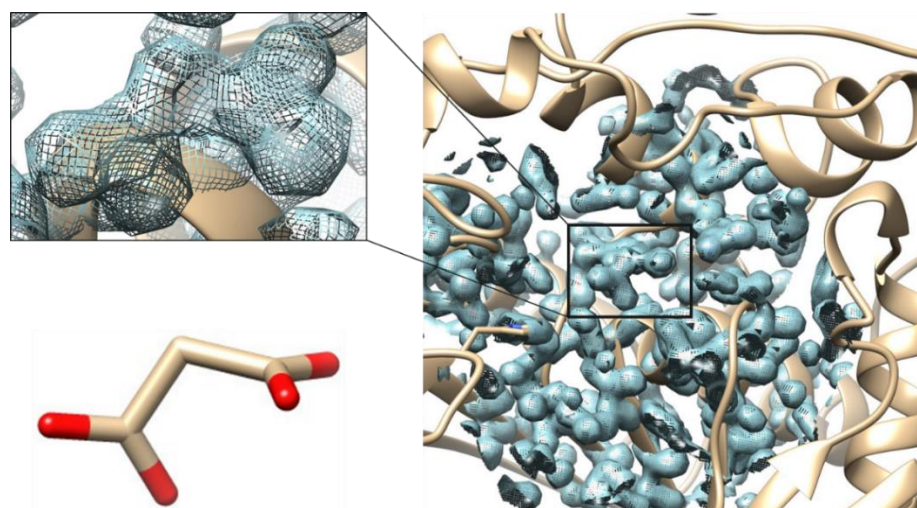
Characterization of Rv0272

In order to establish a function for an enzyme which displays very little sequence homology and has no predicted biological relevance, a "shot gun" approach is a likely scenario. Molecule libraries which are usually reserved for drug discovery become useful tools to probe for scaffolds which may be recognized by the enzyme. In addition, many enzymes have certain requirements for functionality such as co-factors (NAD, CoA, FAD, PEP, etc), metals, other proteins, specific environmental conditions (reducing, acidic), post-translational modifications, and specific substrate concentrations. It is very difficult to probe for enzymatic activity when there is no pre-existing data on what the enzyme requires for proper function. Therefore, all the proceeding methods have a high rate of failure and mostly fall under the purview of "guess and check". Furthermore, enzymes with no prescribed functionality are often somewhat promiscuous and may moonlight as the proprietor of many intercellular activities. However, after rigorous "guessing and checking" using the shotgun approach, it has been demonstrated that Rv0272 can perform multiple functions *in vitro*, with the most convincing evidence suggesting that Rv0272 recognizes a variety of short chain esters and phthalated-molecules and can enzymatically cleave the esters into the corresponding alcohol and acid as well as the cleave the phthalated molecules into phthalate and its counterpart. Finally, the proceeding evidence will show that Rv0272 is a short chain esterase/ thioesterase, recognizing small dicarboxylic acyl chains as biological substrates and is also capable of cleaving phthalated compounds *in vitro*.

Identification of Small Molecule Binders

Based on the observation that Rv0272 co-crystallized with a small biologically relevant molecule, it became a priority to expand upon that evidence and identify other small molecules that bind and may offer insight into the enzyme's function. Hampton Research developed a library of reagents that can affect the solubility and crystallization of large macromolecules. The library composition contains a diverse set of 96 molecules from 18 different classifications. DSF was used to identify ligands which stabilized the enzyme against thermal denaturation. Several molecules were found to increase the melting temperature (ΔT_m) by more than 3^oC. 50mM Sodium Malonate pH =7.0 demonstrated the highest ΔT_m of 10^oC. 5mM Zinc chloride ($\Delta T_m = 4^oC$) and 50mM Sodium citrate tribasic dihydrate ($\Delta T_m = 5^oC$), also imparted thermal stability to the enzyme. These results suggest and agree with the ligand bound structure that dicarboxylic acids and possibly metal ions, such as zinc, could play a role in the enzyme's biology.

In order to expand the search and further validate Rv0272's ligand specificity, a custom substrate screening plate was developed. This consisted of 24 small carboxylic acids, co-factors, and metabolites. Nine ligands were identified which increased the thermal stability of the enzyme by 2^oC or more at a 5mM concentration [Table 4.2]. Notably malonate only shows a ΔT_m of $5.0\,^oC$ compared to the $10\,^oC$ recorded previously. This can be attributed to the large difference in final concentration of substrate used (50mM vs 5mM). The ΔT_m of citrate also decreased by 2 fold ($5.0\,^oC$ vs $2.5\,^oC$). The panel of molecules all contain one carboxylic acid and are metabolites mainly found in the citric acid cycle. Most notably is the $8.0\,^oC$ shift demonstrated by methylmalonate, an increase

of 3°C compared to malonate. Methylmalonate's biological role is largely uncharacterized but is believed to be a product in three interconnected pathways; pyrimidine metabolism, valine, leucine, isoleucine degradation, and propionate metabolism (KEGG).

A thorough investigation of the three pathways where methylmalonate has a predicted metabolic role revealed two possible methylmalonate utilizing enzymes which have yet to be described in *M. tuberculosis.* A predicted methylmalonyl-CoA hydrolase theoretically catalyzes the formation of CoA and methylmalonate and acts in the methylmalonate pathway as part of propionate metabolism and in the degradation of valine, leucine, and isoleucine [Figure 4.6]. Methylmalonate has also been shown to be the product of an ureidomalonase, an enzyme which normally converts 3-oxo-ureidopropanoate into malonate and urea but can also utilize 3-oxo-3-ureidoisobutyrate as substrate to generate methylmalonate and urea [Figure 4.6]. This is a critical step in pyrimidine metabolism which feeds methylmalonate into the two other methylmalonate utilizing pathways.

Table 3.2. Ligands which when added to Rv0272 in solution show a positive change in melting temperature compared to protein alone.

Ligand (5mM)	Melting Temperature (T_m)	Change in Melting Temperature (ΔT_m)
Control	53.5 °C	0.0 °C
Malonate	58.5 °C	5.0 °C
Citrate	56.0 °C	2.5 °C
Propionate	56.0 °C	2.5 °C
Fumarate	55.5 °C	2.0 °C
Oxalosuccinate	57.0 °C	3.5 °C
Maleic Acid	60.0 °C	6.5 °C
Methylmalonate	61.5 °C	8.0 °C
Succinate	59.5 °C	6.0 °C
Methylmalonyl-CoA	62.0 °C	8.5 °C

Careful interrogation of the other metabolites which demonstrated binding revealed previously characterized enzymes in *M. tuberculosis* which utilize each small molecule as a substrate(s) and/or a product(s). Only one predicted orphan metabolite, maleic acid, was found to be a substrate for a maleamate amidohydrolase, currently not annotated in *M. tuberculosis.* This enzyme is required in the nicotinate degradation pathway, which ultimately generates fumarate to feed into the alanine, aspartate, and glutamate metabolic pathways (199, 200).

Figure 3.6. Methylmalonyl-CoA hydrolase (top); Ureidomalonase (bottom).
Methylmalonyl-CoA hydrolase catalyzes a water mediated thioester cleavage of
malonyl-CoA to form malonate and CoA. Ureidomalonase catalyzes a water mediated
ester cleavage to form malonate and urea.
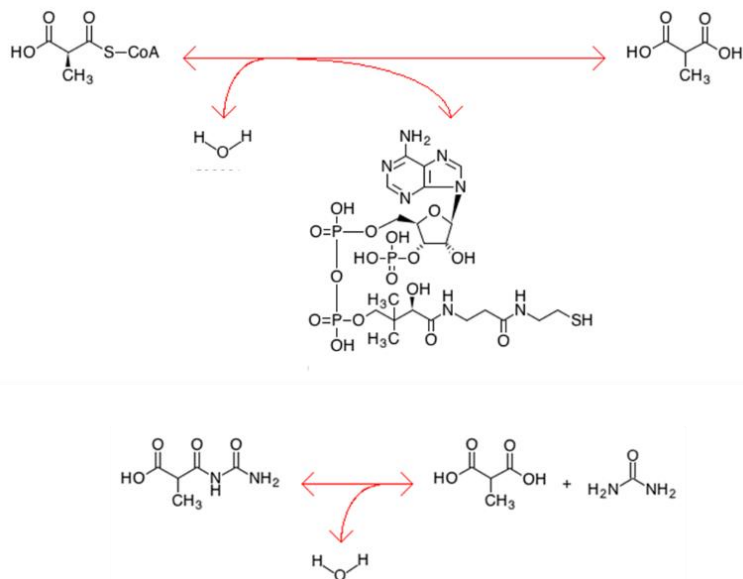
Methylmalonate Pathway

In *M. tuberculosis,* catabolism of odd chain fatty acids proceeds through two
distinct pathways, the Vitamin B12-dependent pathway (methylmalonate pathway) and
the vitamin B12-independent pathway (methylcitrate cycle). At least one pathway is
required for survival to remove the toxicity associated with propionyl-CoA derivatives
(201, 202). In the mathylmalonate pathway, propionyl-CoA is converted to (S)-
Methylmalonyl-CoA via propionyl-CoA carboxylase. Methylmalonyl-CoA can then be
converted to succinyl-CoA by methylmalonyl-CoA epimerase and the B12-dependent
methylmalonyl-CoA mutase or decarboxylated to form methylmalonate and CoA via

methylmalonyl-CoA hydrolase [Figure 4.7]. The purpose of converting methylmalonyl-CoA to CoA and methylmalonate is widely unknown. There may be an unknown cellular function for methylmalonate, but presumably, hydrolysis of methylmalonyl-CoA would be to generate free CoA. This may be advantageous when vitamin B12 is limiting and propionyl-CoA can be regenerated in order to be catabolized through the vitamin B12 independent methyl citrate cycle. Methylmalonate semialdehyde dehydrogenase utilizes CoA, NAD, and methylmalonate semi-aldehyde to form propionyl-CoA.

Thioesterase Enzymatic Activity Assay

Based on the data observed from DSF binding, Rv0272 was probed for thioesterase activity. Several acyl-CoAs were tested as possible substrates in a coupled DNTB reaction including acetyl-CoA, propionyl-CoA, malonyl-CoA, methylmalonyl-CoA, benzoyl-CoA, glutaryl-CoA, succinyl-CoA, butyryl-CoA, and acetoacetyl-CoA. Initially, Rv0272 displayed activity for propionyl-CoA, malonyl-CoA, and methylmalonyl-CoA. However, results were not repeatable and specific enzyme activity was never determined.

Alternative Activity Assay(s)

Due to the several short comings of a DTNB coupled assay, an alternative mass spectrometry based method of measuring enzyme activity was explored. The enzyme was incubated with methylmalonyl-CoA at several concentrations (0.1mM, 0.2mM, 0.5mM) for different intervals of time (10min, 30min, 1hour, 12hours). Potential turnover was monitored via liquid chromatography mass spectrometry (LCMS) to determine the

amount of CoA, methylmalonate, and methylmalonyl-CoA left in the reaction. The data showed no clearly identifiable enzyme activity and after extensive analysis it was concluded that methylmalonyl-CoA hydrolysis did not occur under these experimental conditions.

Figure 3.7. Methylmalonate pathway in *M. tuberculosis*. Annotated enzymes in *M. tuberculosis* are depicted as empty boxes overlaid on top of arrows, while metabolites are depicted as empty circles. Relevant substrate(s)/ Product(s) are labeled adjacent to the empty circles. Methylmalonyl-CoA hydrolase is colored blue.
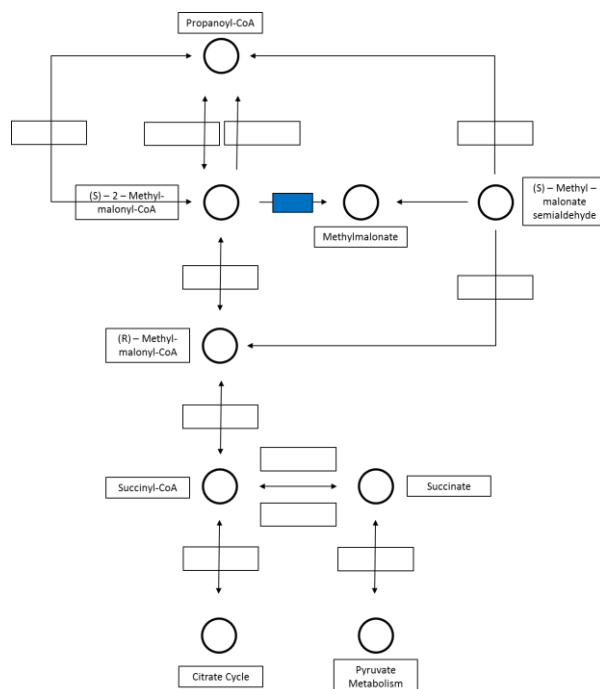
Previous studies have shown that methylmalonyl-CoA hydrolase is specific for the R racemic form. Therefore, a mixture of R and S methylmalonyl-CoA may be inhibiting the enzymatic reaction. In an attempt to determine if that is the case, a hypothetical protein, Rv1322a, in *M. tuberculosis* was identified as a potential methylmalonyl-CoA epimerase based on sequence similarity to other homologous methylmalonyl-CoA epimerases. The X-ray crystal structure of Rv1322a was determined and through three-dimensional structural comparisons, confirmed as a methylmalonyl-CoA epimerase [Figure 4.8]. The purified epimerase was added to the DNTB coupled reaction with Rv0272 and methylmalonyl-CoA. However, enzyme dependent hydrolysis of methylmalonyl-CoA was not observed. Methylmalonyl-CoA has been characterized as a metal dependent enzyme with a preference for cobalt or manganese. The reaction was again initiated in the presence of either Mn or Co. Neither metal had an observable effect on activity. However, this coupled assay does not eliminate the possibility of DNTB binding to the enzyme and interfering with hydrolysis.

Figure 3.8. Structure of Rv1322a; methylmalonate epimerase. Dimeric protein in the ASU with each monomer colored (blue and pink)
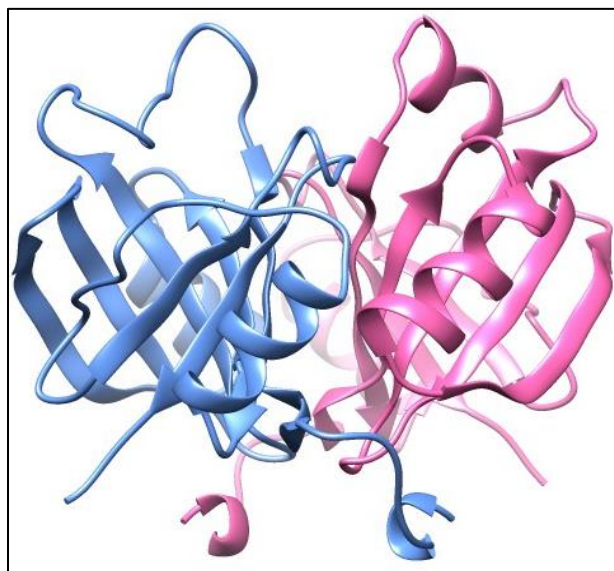
In order to move away from a DTNB coupled assay, a novel coupled reaction was proposed involving Rv0272 and Rv0753c, a predicted methylmalonate semi-aldehyde dehydrogenase. In this scheme, the free CoA generated from the hydrolysis of methylmalonyl-CoA would be utilized by Rv0753 and converted to propionyl-CoA in the presence of NAD^+ and methylmalonate semi-aldehyde. The change in absorbance at 340 nm due to the reduction of NAD^+ to NADH could be monitored and enzymatic turnover by Rv0272 determined. The X-ray crystal structure of Rv0753 was determined and through three-deminsional structural comparisons, confirmed as a methmalonate semi-

aldehyde dehydrogenase [Figure 4.9]. The coupled enzyme reaction was attempted both with and without the purified methylmalonyl-CoA epimerase. The addition of either enzyme did not seem to have an effect and no activity could be observed. This may be explained by the instability of the methylmalonate semi-aldehyde substrate as well as its unconfirmed identity after synthesis.

There are a couple possibilities which may explain the absence of activity. The enzyme may require a co-factor such as a metal or additional small molecule for hydrolysis to occur. DSF results seem to suggest Zn may bind to the enzyme and could play a role in its activity. The addition of 0.1mM to 2mM $ZnCl_2$ to the DTNB coupled assay did not significantly affect the results. Another possibility is that the enzyme is sensitive to oxidation and a reducing environment is a requirement for activity. In order to address this possibility, a reducing agent such as tris(2-carboxyethyl)phosphine (TCEP) was added during purification and slowly dialyzed away before proceeding with the enzyme reaction. Since TCEP will reduce DTNB to NTB, reducing agent is not conducive for this type of assay. The addition of TCEP during purification did not have an effect on the observed activity. In addition, it is possible that DTNB interacts with the enzyme and competes with the acyl-CoA for binding in the active site. This is a valid assumption given the overall structure of DTNB which contains two carboxyl groups and two nitro groups, both which could be coordinated into the active site by Arg166 [Figure 4.10]. DTNB could also be interacting with surface exposed cysteines on the enzyme, which could interfere with substrate binding and subsequent turnover.

Figure 3.9. Structure of methylmalonate semi-aldehyde dehydrogenase. Dimeric protein in the ASU with each monomer colored (blue and pink)
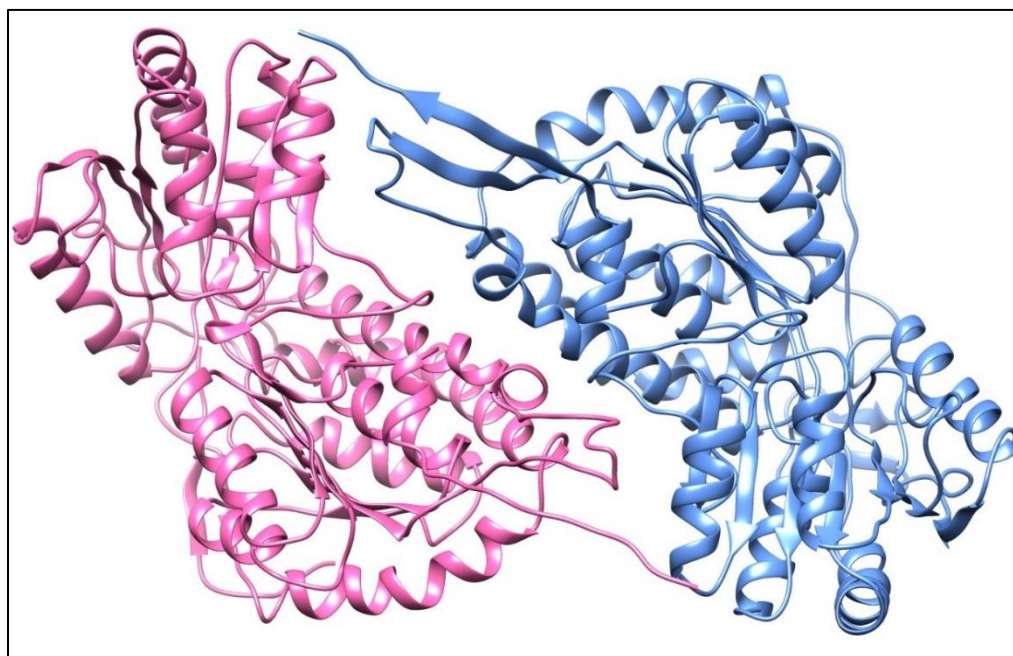
In an attempt to overcome these possible deficiencies, several rounds of optimization were tried. DSF experiments revealed enzyme stability was greatest at pH = 6.0 with the addition of 100mM NaCl. This buffer composition was used in further assay experiments but failed to influence the outcome. Pre-incubation of enzyme with substrate before the addition of DTNB was also performed. In these trials initial activity was observed but remained consistent regardless of protein or substrate concentration and failed to hydrolyze more than 25µM of acyl-CoA substrate over 30 minutes. This is further evidence that DTNB, the acyl-group, or CoA could all be competing for binding, thus inhibiting the reaction and preventing a proper kinetic analysis.

Figure 3.10. DTNB reaction which reacts with free thiols to form a yellow colored TNB bound to thiol ligand product.
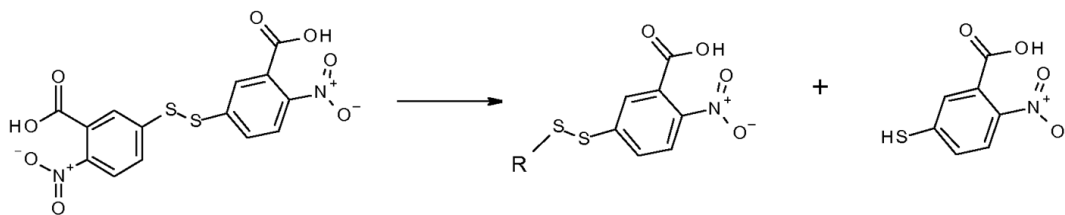
In order to address the possibility that an additional co-factor may be required, 96 different small molecules from the Hampton additive screen and the custom substrate plate were added in combination with the acyl-CoA substrate. Activity did not appear to be influenced with the addition of any tested small molecule. This does not preclude the possibility that the enzyme may require some un-recognized co-factor in order for the reaction to efficiently proceed.

Identification of Additional Small Molecule Binders

The pool of metabolites was increased to encompass even more biologically relevant molecules specific to Rv0272. From this set, 3 new compounds emerged which displayed an ability to increase the thermal stability of the enzyme when screen at 5mM. Phthalic acid ($\Delta T_m = 11\ ^oC$), anthranilic acid ($\Delta T_m = 3\ ^oC$), and quinolinic acid ($\Delta T_m = 5\ ^oC$) compared to malonate ($\Delta T_m = 6\ ^oC$) Comparing the three, it is interesting to note the subtle differences which lead to drastic changes in binding capacity [Figure 4.10]. Phthalic

acid is an aromatic dicarboxylic acid, while anthranilic acid is an aminobenzoic acid, swapping an amino group for a carboxylate group. However, the difference in melting temperature is 8°C between the two, suggesting that the second carboxylate is required for tight binding. Interestingly, if that amino group is replaced with a nitro group, the resulting nitrobenzoic acid molecule demonstrates no change in thermal stability compared to protein alone. If the benzene ring is replaced with a pyridine ring, the resulting quinolinic acid demonstrates only a 5°C change in thermal stability as compared to 11°C seen with phthalic acid.

Figure 3.11. Comparison of benzoic acid derivatives and the differences in Rv0272 melting temperatures observed in the presence of ligand.

Phthalic Acid
$\Delta T_m = 11\,°C$

Quinolinic Acid
$\Delta T_m = 5\,°C$

Anthranilic Acid
$\Delta T_m = 3\,°C$

Nitrobenzoic Acid
$\Delta T_m = 0\,°C$
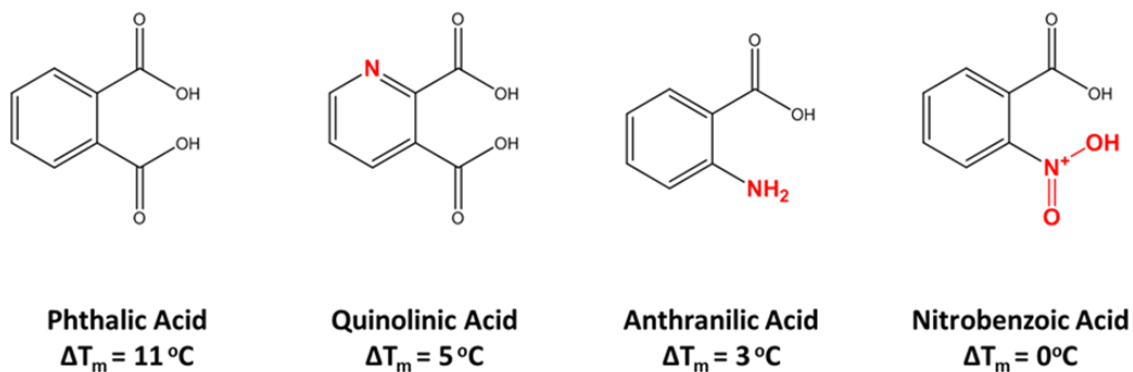
The relevance of phthalic acid to mycobacterium biology is unknown and does not belong to any known metabolic pathway. However, previous studies have identified a phthalyl amidase from *Xanthobacter agilis* which exhibits a broad substrate specificity for *o*-phthalylated amides. Phthalylating metabolites may serve as a novel route of protecting amino acids from premature degradation. In addition, the structural similarities shared between phthalic acid and maleic acid show that both would bind in a similar manner in the active site, which may implicate the more biologically relevant maleic acid in determining the function of Rv0272.

NMR Based Metabolomics

In order to effectively expand the metabolite pool and have an additional measurement for binding, NMR-based metabolomics was employed. In collaboration with John Markley at the University of Wisconson-Madison, an NMR based ligand affinity screen was performed on Rv0272. The protein was screened against 500-metabolite-like compounds and binding was assessed based on the change in 1-D NMR spectra of the test molecule(s) upon addition of enzyme [Figure 4.11]. The screen for Rv0272 identified 33 hits which could be classified into a few structurally similar compounds. Cholic acids are well represented as well as small acids such as α-ketoisovaleric acid, oxaloacetic acid, and fumaric acid [Figure 4.12]. Interestingly, D-alanyl-D-alanine was identified as a hit and also was shown to be enzymatically converted into D-alanine in the presence of Rv0272 [Figure 4.13]. This activity represents a different class of enzyme, D-Ala-D-Ala carboxypeptidases, which hydrolyze peptides during bacterial cell wall biosynthesis. This

type of enzyme is a primary target of β-lactam antibiotics, which was also identified in this screen in the form of phenoxymethylpenicillinic acid (PMPA).

This study agrees with previous data showing a preference for short chain acids and thiol groups but also introduces a new small peptide candidate in D-Alanyl-D-Alanine. Interrogation of the additional hits shows that amino acid groups are additionally represented in glycocholic acid, glycodeoxycholic acid, N-(3-indolylacetyl)-DL-aspartic acid, N-acetyl-L-alanine, acetyl-L-cysteine, and DL-homocysteine.

Figure 3.12. NMR metabolomics: example of signal flattening which is an indication of binding. The result below is an example using oxaloacetic acid alone (top) compared to Oxaloacetic acid and Rv0272 (bottom) is considered a positive hit for ligand binding.
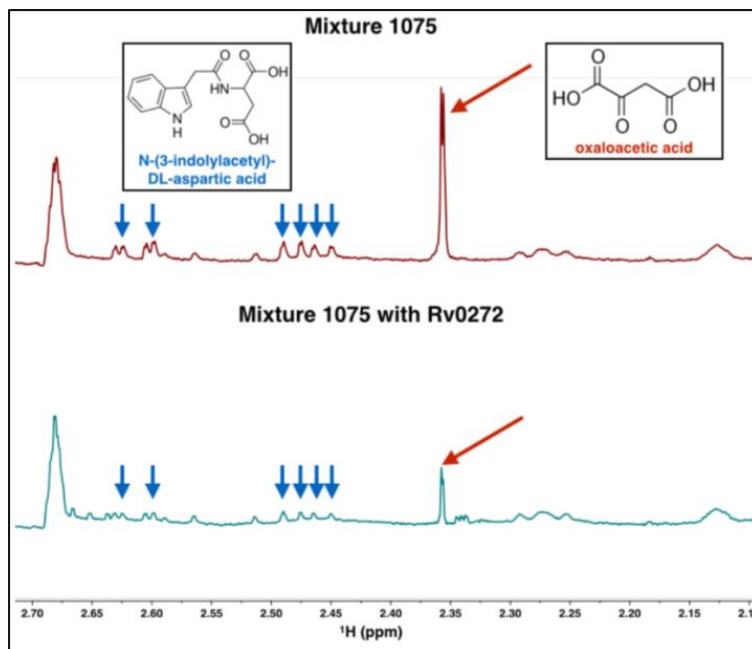
Figure 3.13. Small molecule "hits" from the NMR metabolomics screen

5-methoxy-3-indoleacetic acid   D-Pinitol   2,4,5-trichlorophenoxyacetic acid   N-(3-indolylacetyl)-DL-aspartic acid

oxaloacetic acid   3,3',5,5'-tetrabromobisphenol A   glycocholic acid   cholic Acid

fumaric acid   octanoic acid   glycodeoxycholic acid   apocholic acid

myristic acid   11-ketoetiocholanolone   deoxycholic acid, sodium salt   adenosine 3'-monophosphate

bisphenol C   indole-3-pyruvic acid   4-methylcatechol   2,2-bis(4-hydroxy-3-methylphenyl)propane

taurocholic acid sodium salt hydrate   alpha-ketoisovaleric acid

Figure 3.13 Continued

Cytidine   D-alanyl-D-alanine   ADP   DL-homocysteine

acetyl-L-cysteine   N-acetyl-L-alanine   phenoxymethylpenicillinic acid   dioctyl sulfosuccinate

α-D-glucose-1-phosphate   8-anilino-1-naphthalene-sulfonic acid   khellin

Enzyme Dependent Peptide Hydrolysis

In order to ascertain Rv0272's ability to recognize di-peptides or other amino acid derivatives, two separate assays were employed. The first was a Cadmium-Ninhydrin based amino acid detection method while the other was a coupled enzymatic reaction. Ninhydrin reacts with primary amines and is a useful method for determining free amino acid concentration. In concordance with the NMR metabolomics, D-alanyl-D-alanine, taurocholate, deoxytaurocholate, glycocholate, and deoxyglycocholate were tested as

potential substrates and compared against a glycine or an alanine standard. However, the experiment failed to demonstrate activity for any of the four metabolites. A secondary assay was developed which coupled Rv0272 to D-Alanine oxidase, catalase, and lactate dehydrogrenase. The resulting reduction of NAD^+ to NADH was monitored at 340 nm to determine conversion of D-alanyl-D-alanine to D-alanine. Enzyme activity for Rv0272 using D-alanyl-D-alanine as a substrate was not observed using this method. It should be noted that D-alanyl-D-alanine, taurocholate, deoxytaurocholate, glycocholate, and deoxyglycocholate also failed to demonstrate a change in thermal stability using DSF.

Figure 3.14. Results of NMR Metabolomics: The top figure in red depicts D-Ala-D-Ala alone. The bottom figure depicts the change in NMR spectrum which Rv0272 is added to D-Ala-D-Ala. The resulting peak is indicative of enzymatic conversion of D-Ala-D-Ala to D-Ala.
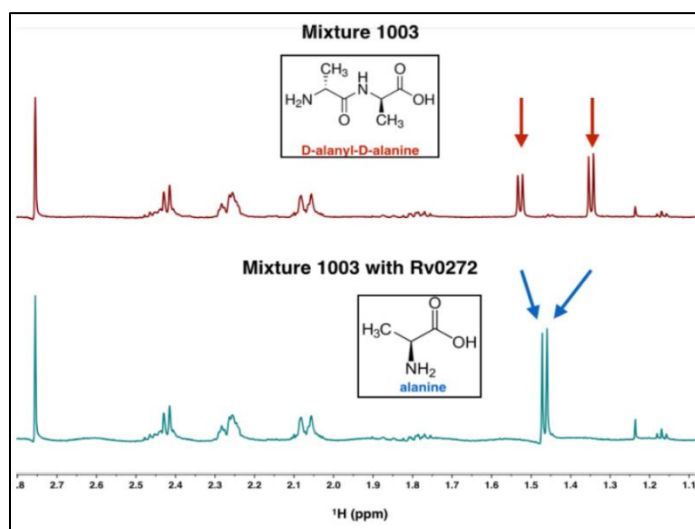
Rv0272 Recognizes β-Lactam Antibiotics

Bocillin is a fluorescent penicillin which covalently binds to the active site serine of penicillin-binding proteins (PBPs). Rv0272 was incubated with Bocillin and analyzed via SDS-PAGE and a gel dock imaging system for penicillin binding. The results indicate that Bocillin does bind Rv0272 and may be a target for β-lactam antibiotics. In order to test whether or not Rv0272 hydrolyzes β-lactams, a chromogenic cephalosporin substrate, nitrocefin, was utilized. Upon hydrolysis of the lactam ring, the compound color changes from yellow to red which gives a measurable absorbance at 486 nm. The results show that Rv0272 has activity for nitrocefin with a turnover rate of 3μM nitrocefin/min/1μg enzyme. Although the result demonstrates activity, the reaction is almost 100 times slower than previously reported β-lactamase enzymes.

Several β-lactam antibiotics were tested using DSF to determine their ability to bind Rv0272. Cloxacillin, Oxacillin, Amoxicillin, Ampicillin, Carbenicillin, Cephalexin, Cephalosporin, Cefixime, Cefpirome, Nitrocefin, and Bocillin were tested and all failed to yield a change in melting temperature. The enzyme catalyzed reaction of Nitrocefin may be somewhat non-specific and the observed activity might not represent the primary function of Rv0272. The enzyme may recognize certain structurally features of the β-lactam including the amide and carboxylate groups without fully accommodating the entire molecule as a substrate. This may account for the Nitrocefin activity that was observed.

Esterase Activity of Rv0272

In general, esterases catalyze the hydrolysis of aliphatic and aromatic esters and function in a variety of metabolic functions. Based on previous results that Rv0272 may recognize thioester and amide moieties, its ability to recognize esters was also tested. 4-nitrophenyl esters are ideal substrates for detecting esterase activity. Once the ester is hydrolyzed, the resulting 4-nitrophenol has an absorbance at 400 nm which can be measured to directly determine the amount of hydrolyzed ester. 4-nitrophenyl acetate, butyrate, octanoate, decanoate, phosphate, and palmitate were all tested as possible substrates. Only the short chain esters (acetate and butyrate) could function as potential substrates. 4-nitrophenyl acetate had a calculated K_m of 600µM and a specific activity of $1.7x105$µM substrate/mg protein/min using 1µg of protein at 25°C. 4-nitrophenyl butyrate was a slightly worse substrate with a Km of 800µM and a specific activity of $3.8x10^4$µM substrate/mg protein/min using 1µg of protein at 25°C. No activity was observed for any 4-nitro phenyl ester longer than four carbons.

Using Fragment and Whole Cell Active Inhibitors as Molecular Probes for the Identification of Chemical Scaffolds Which May Represent Potential Biological Substrates

In order to expand the search for molecules that bind to Rv0272 which may infer function, a library of 823 small molecular weight compounds were screened using DSF. There were 31 identified molecule which demonstrated a ΔT_m of a least 3°C compared to control at a concentration of 5mM [Table 4.3]. There were 6 fragments which showed a

ΔT_m greater than the $\Delta T_m = 5.0^\circ C$ of malonic acid. Five of the six fragments contain 6-membered rings with a carboxylate group and at least one amide bond [Figure 4.14].

Figure 3.15. Fragments which showed a positive change in melting temperature of Rv0272 as determined by DSF.

EN:T0501-0213
$\Delta T_m = 8.0^\circ C$

EN:T5764482
$\Delta T_m = 6.0^\circ C$

EN:EN300-12792
$\Delta T_m = 6.0^\circ C$

EN103318-06
$\Delta T_m = 6.0^\circ C$

EN:EN300-49784
$\Delta T_m = 13.0^\circ C$

EN:T6307026
$\Delta T_m = 9.0^\circ C$
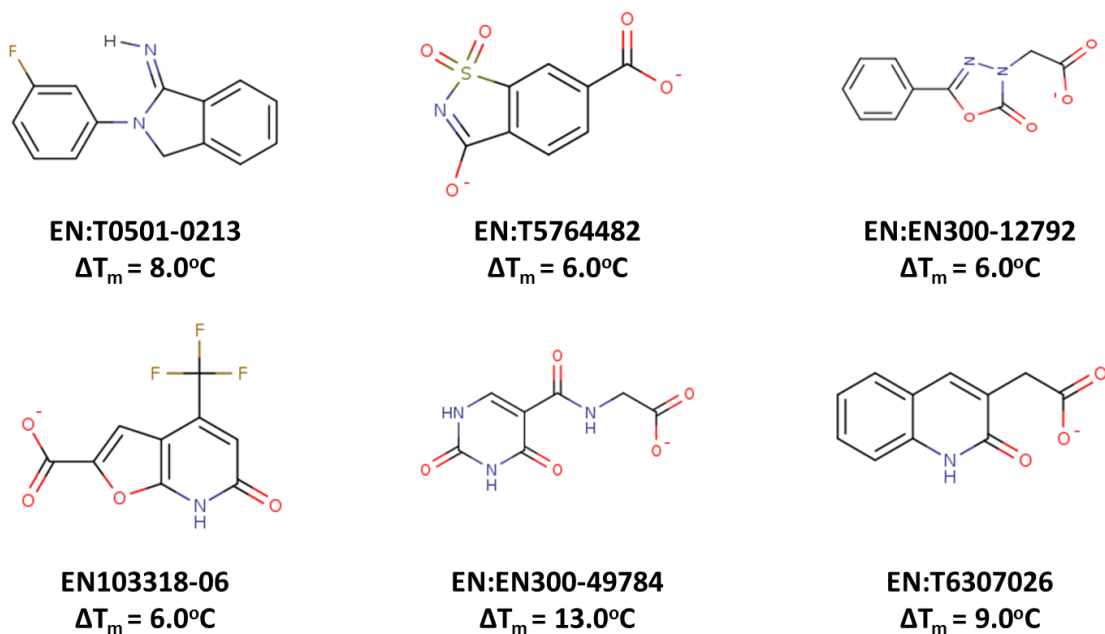
An extended search for biologically relevant moieties included screening the library of whole cell active inhibitors against *M. tuberculosis* for binding to Rv0272 using

DSF. 542 compounds were tested at 0.5mM and binding was determined to occur when the thermal stability increased by 2°C or more compared to control. There were 27 compounds identified and 5 which demonstrated significant protection against heat denaturation [Figure 4.15].

Figure 3.16. Whole cell active molecules which showed a positive change in melting temperature of Rv0272 determined using DSF.
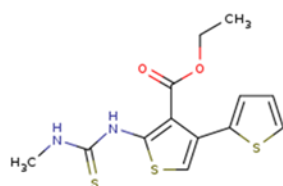
EN:T5521370
MIC50 = 2.5μM
ΔT_m = 4.0°C
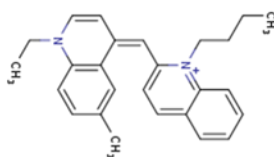
AS:BAS04197408
MIC50 = 2.5μM
ΔT_m = 4.0°C
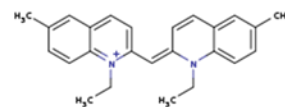
AS:BAS03302219
MIC50 = 1.25μM
ΔT_m = 5.0°C
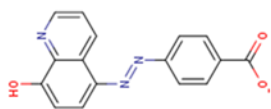
AS:BAS02226747
MIC50 = 10μM
ΔT_m = 7.0°C
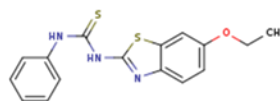
AS:BAS00444145
MIC50 = 1.25μM
ΔT_m = 4.0°C

Structural Comparison(s) of Small Molecules Bound to Rv0272

Three dimensional structures of the molecules which demonstrated a positive shift in melting temperature were obtained bound to the enzyme. Through comparisons of their binding interactions and binding locations within Rv0272, potential substrate preferences can be inferred. Detailed investigation of the individual hydrogen bonding atoms between substrate(s) and the active site residues revealed subtle differences which may attempt to explain the discrepancies in the change in enzyme thermal stability upon small molecule binding [Figure 4.16]. Binary structures of Rv0211172 were initially obtained with the following ligands bound: citrate, malonate, methylmalonate, and maleate. There are five amino acid residues in the active site which directly coordinate ligand binding, His52, Ser118, His153, Arg166, and His353. Interestingly, citrate, which had the lowest ΔT_m of only 5°C of the four molecules, but displayed the most amount of potential hydrogen bonds with 13. Citrate also makes the closest interaction in the active site with Oβ1 of the ligand binding to Oγ of Ser118 at 2.11 Å distance.

Further interrogation of the differences in binding distance between ligands suggests that the overall thermal stability is determined by the amount of atomic interactions and distances between those interactions of the ligand and Arg166. Methylmalonate, which has a ΔT_m of 8°C, greater than the other three, makes four distinct hydrogen bounds with Arg166. Oγ1 of methylmalonate is 2.99 Å away from Nϵ of Arg166 and 3.37 Å away from NH1 of Arg166. Oγ2 of methylmalonate is 2.25 Å from NH1 of Arg166 and 3.37 Å from Nϵ of Arg166. Binding affinity may also be affected in some part by the distance of His52 from the bound ligand. However, it is still far from conclusive

which specific interactions dictate the observed differences in thermal stability between

ligands [Table 4.4].

Figure 3.17. Comparison of metabolite(s) binding in the catalytic site of Rv0272. Top
Left -methylmalonate. Top Right - maleate. Bottom Left - citrate. Bottom Right –
malonate.
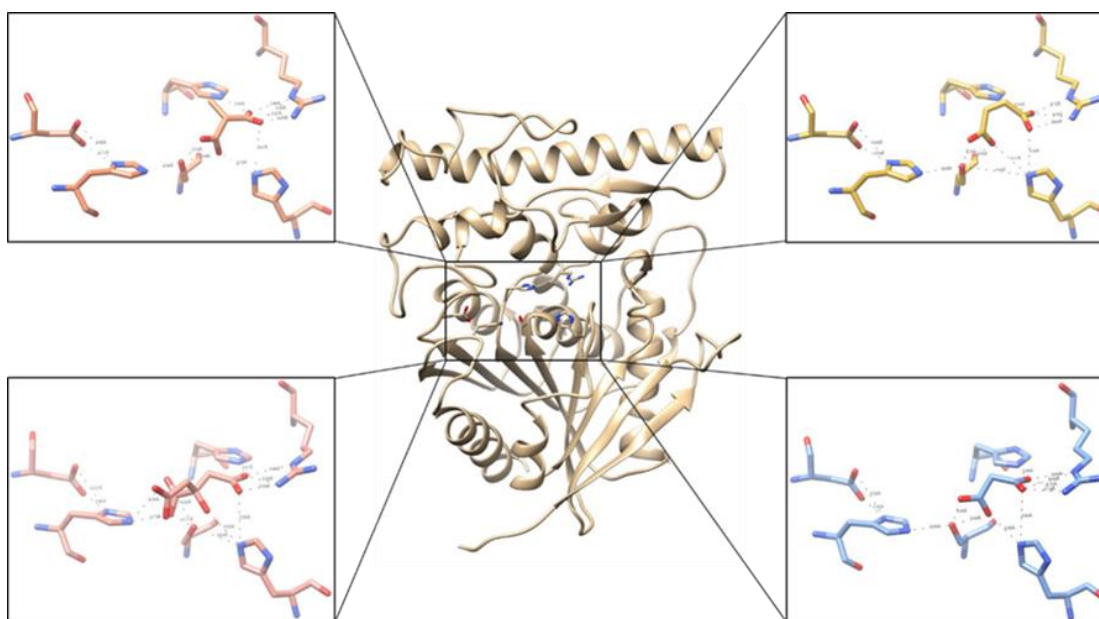
Table 3.3. Possible bonding distances between active site residues and ligand

	Maleate	Malonate	Methylmalonate	Citrate
Asp324				
Asp324 (OD1) – His353 (ND1)	3.39	3.56	3.60	3.57
Asp324 (OD2) – His353 (ND1)	2.54	2.68	2.71	2.80
His353				
His353 (NE2) – Lig (OB2)	4.02			3.56
His353 (NE2) – Lig (OB1)				2.73
His353 (NE2) – Ser118 (OG)	3.08	2.86	2.92	4.02
Ser118				
Ser118 (OG) – Lig (OB1)	2.53	2.88	2.64	2.11
Ser118 (OG) – Lig (OB2)	2.78	3.08	3.15	3.55
Ser118 (OG) – Lig (OHB)				2.92
Ser118 (OG) – His52 (NE2)				3.64
His52				
His52 (NE2) – Lig (OHB)				3.05
His52 (NE2) – Lig (OB1)	3.17	2.85	2.73	
His52 (NE2) – Lig (OG2)	3.34	3.64	3.57	3.50
His163				
His163 (NE2) – Lig (OG1)	3.34	2.88	2.95	2.97
Arg166				
Arg166 (NE) – Lig (OG1)	2.72	3.09	2.99	3.08
Arg166 (NH1) – Lig (OG1)	3.05	3.72	3.37	3.05
Arg166 (NH1) – Lig (OG2)	2.94	2.73	2.25	2.51
Arg166 (NE) – Lig (OG2)		3.58	3.37	

Inconsistent with the results from DSF is the fact that CoA also binds in the active site. CoA differs from the previous four ligands in that a phosphate group of adenosine interacts with the active site amino acids and not a hydroxyl or a carboxyl group [Figure 4.17]. The three available phosphate oxygen atoms form an extensive network of hydrogen bonds with the active site with Ser118, His52, His163 and Arg166. Notably, O9α from the phosphorylated adenosine, forms a hydrogen bond with the Oγ of Ser118 at a distance of

2.17 Å. Distinct from the other ligands, phosphate is coordinated into place through the dynamics of two residues, Arg166 and His163. The guanidinium group of arg166 moves 3.77 Å towards His163 which in turn causes His163 to swing 4.13 Å away [Figure 4.18]. This movement positions NH1 of Arg166 into hydrogen bonding distance with O8α of the ligand at a distance of 2.89 Å as well as Nε2 of His163 with O7α at a distance of 2.55 Å with the ligand. Yet, CoA fails to give a positive shift in thermal stability except when the acyl chain is composed of a molecule which is known to bind on its own.

Methylmalonyl-CoA was soaked into Rv0272 crystals which resulted in the appearance of two distinctly different electron densities in the active site. In one form, clear density is observed for methylmalonate in the same orientation as seen in previous methylmalonate soaks. This result indicates that the enzyme may be participating in the thioester cleavage of methylmalonyl-CoA. Additionally, methylmalonyl-CoA was incubated for 48 hours in the same crystallization condition, and analyzed via mass spectrometry to show the intact compound had not undergone enzyme independent hydrolysis. However, the second trial had an unusual outcome, resulting in electron density which was not easily discernable. Each active site displayed different and unique electron densities. In crystal chain A, density stems out from Arg166 at the γC, δC, and NE positions and extends past the γO of Ser118. Attempts to build any ligand product from methylmalonyl-CoA has been unsuccessful. In crystal chain B, density appears similar to what was observed with CoA alone, with the only major difference seen at the active site phosphate group [Figure 4.19]. The electron density does not correspond to

phosphate and all attempts to build in the CoA ligand have failed. The movement of

residue His163 was also observed, however the Arg166 residue remained static.

Figure 3.18. CoA binding in the active site of Rv0272. The sugar phosphate is located in the active site coordinated by Arg166 and His163.

Figure 3.19. Dynamics of active site residues upon CoA binding. Arg166 moves 3.77 Å while His163 moves 4.13 Å. Teal residues represent the active site of Rv0272 with CoA bound while yellow represents Apo Rv0272.

Figure 3.20. Comparison of active site density after crystals were soaked with methylmalonyl-CoA. Top - monomer one of two from the dimeric protein found in the ASU. Bottom = monomer two of two from the dimeric protein found in the ASU. The molecule(s) which are represented by the observed electron densities have yet to be conclusively identified.
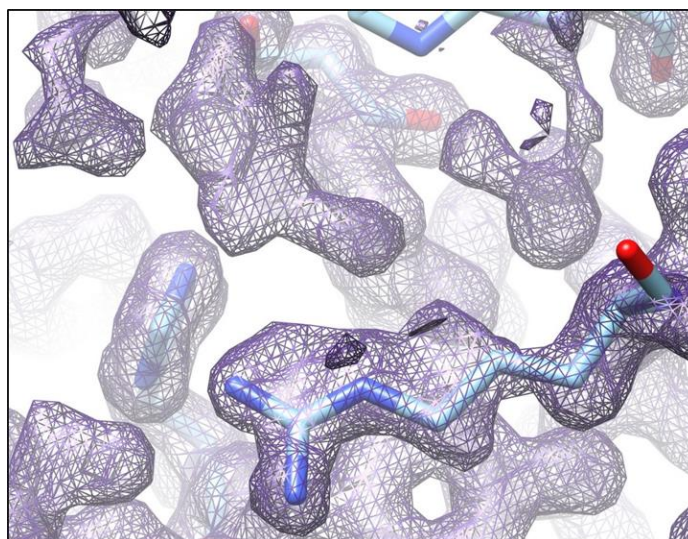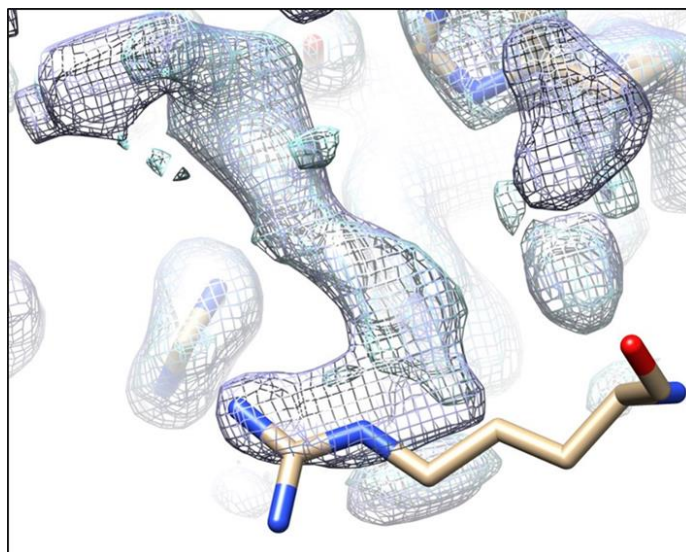
Structural Comparison(s) of Fragment and Whole Cell Active Inhibitors Bound to Rv0272

The results from the binding studies revealed that a wide range of molecular compounds demonstrated binding to Rv0272. This presented an opportunity to use fragments and whole cell active molecules in a unique way. Instead of characterizing the small molecules as enzymatic inhibitors, the molecules were used to probe the chemical space required for recognition by Rv0272. These experiments were primarily carried out by soaking the aforementioned molecules into Rv0272 crystals and observing the resulting electron density in the active site. These experiments gave insight into the size and type of small molecules which bind and allowed inferences to be made on the types of potential substrates the enzyme could recognize. Additionally, the molecules that have an affinity for Rv0272 could be compared to known metabolites found within the KEGG database and possible functions for the enzyme could be postulated.

EN:T6574300

Molecule EN:T6574300 showed a ΔT_m of 4ºC and the structure of ligand bound enzyme was successfully determined. Initial investigation of the molecule revealed some slight similarities with the metabolite methylmalonate. A search of the KEGG database using a similarity cut off of 75% identified one structurally similar molecule, benzyl 2-methyl-3-oxobutanoate. This metabolite is a highly specific substrate for a NADP dependent dehydrogenase found in baker's yeast (203). In order to expand the pool of similar metabolites, an additional search of the KEGG database was performed without the benzyl group. One additional metabolite, 3-hydroxyisobutyrate, was identified. 3-

hydroxyisobutyrate is found in the "valine, leucine, and isoleucine degradation pathway" and is utilized in two different enzymatic reactions. It is a product of a 3-hydroxy-isobutyryl-CoA hydrolase and subsequently a substrate of the next enzyme in the pathway, a 3-hydroxy-isobutyrate dehydrogenase. This enzyme converts 3-hydroxy-isobutyrate into methylmalonate semialdehyde utilizing NAD as a cofactor. The isobutyryl-CoA hydrolase has yet to be annotated in *M. tuberculosis* and is two steps away from a potential methylmalonanyl-CoA hydrolase.

Comparison of the active site residue interactions with EN:T6574300 and methylmalonate demonstrate similar recognition, especially at Arg166 [Figure 4.20]. One major difference is the chirality of EN:T6574300 could not be determined from the structure. Both (R) and (S) chiral forms were properly built into electron density and refined. However, in methylmalonate structures, obtained from soaking Rv0272 crystals with methylmalonate, all appear bound in the (S) chiral form. In the (S) form of methylmalonate, the methyl group points away from the active site serine interacting with Trp173, Ile283, and Val169.

Figure 3.21. Structure of EN:T6574300 bound in the active site. Bottom - Overlay of EN:T6574300 and methylmalonate.
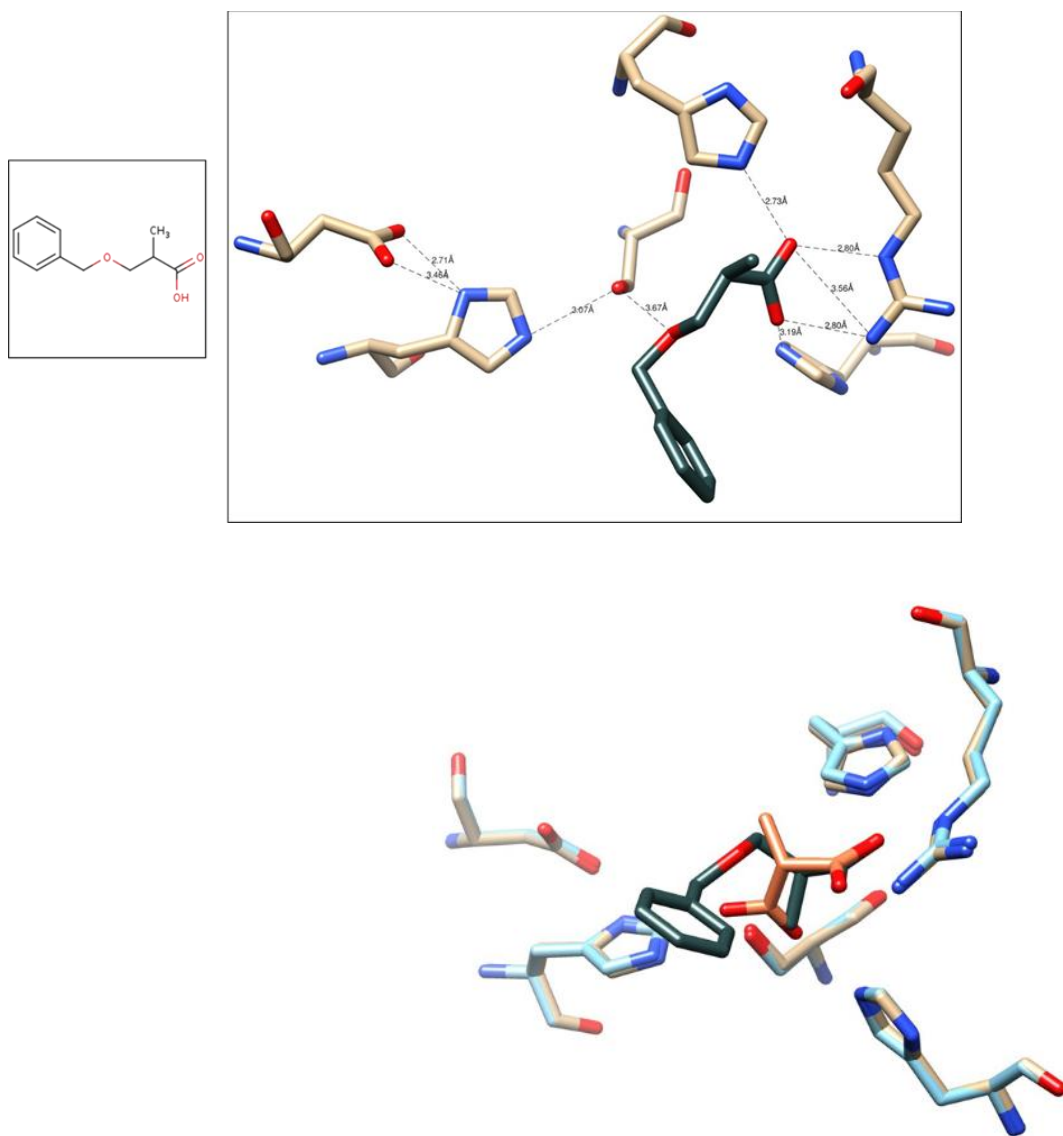
EN:EN300-25711

Molecule EN:EN300-25711 showed a ΔT_m of 4°C and a co-crystal structure was successful obtained bound to Rv0272. Upon initial investigation of the binding interactions in the catalytic site with the ligand, several differences stand out. The ligand carboxylate tail is rotated out of plane from Arg166, replacing the usual hydrogen bond of carboxylate oxygen to Nϵ of Arg166 with the backbone nitrogen of Gly119. In addition, the catalytic Ser118 is flipped away from the ligand, now making interactions Nϵ2 of His353 and a water molecule. His163 is also dynamic, demonstrating partial occupancy between two positions in the active site. In one position it is interacting with Ile327, while in the other, it is potentially hydrogen bond with the ligand carboxylate. What appears to be occurring is that the nitrogen rich 5-membered ring is interacting with Gln54 and possibly Arg166, likely through electrostatic repulsion, which is moving the carboxylate tail deeper into the active site cavity. As a result, His163 is pulled closer to Ser118, possibly resulting in Ser118's movement away from the active site. Interestingly, the sulfur atom does not appear to be interacting with any atoms in the active site. However, sulfur does have a Van Der Walls radius of 1.8 Å, therefore it be interacting Trp173 which is 3.83 Å away [Figure 4.21]. Not surprisingly, a similarity search of the KEGG database returned no biologicals which are at least 60% similar in structure.

Figure 3.22. Structure of EN:EN300-25711 bound in the active site. Bottom - Overlay of EN:EN300-25711 and methylmalonate
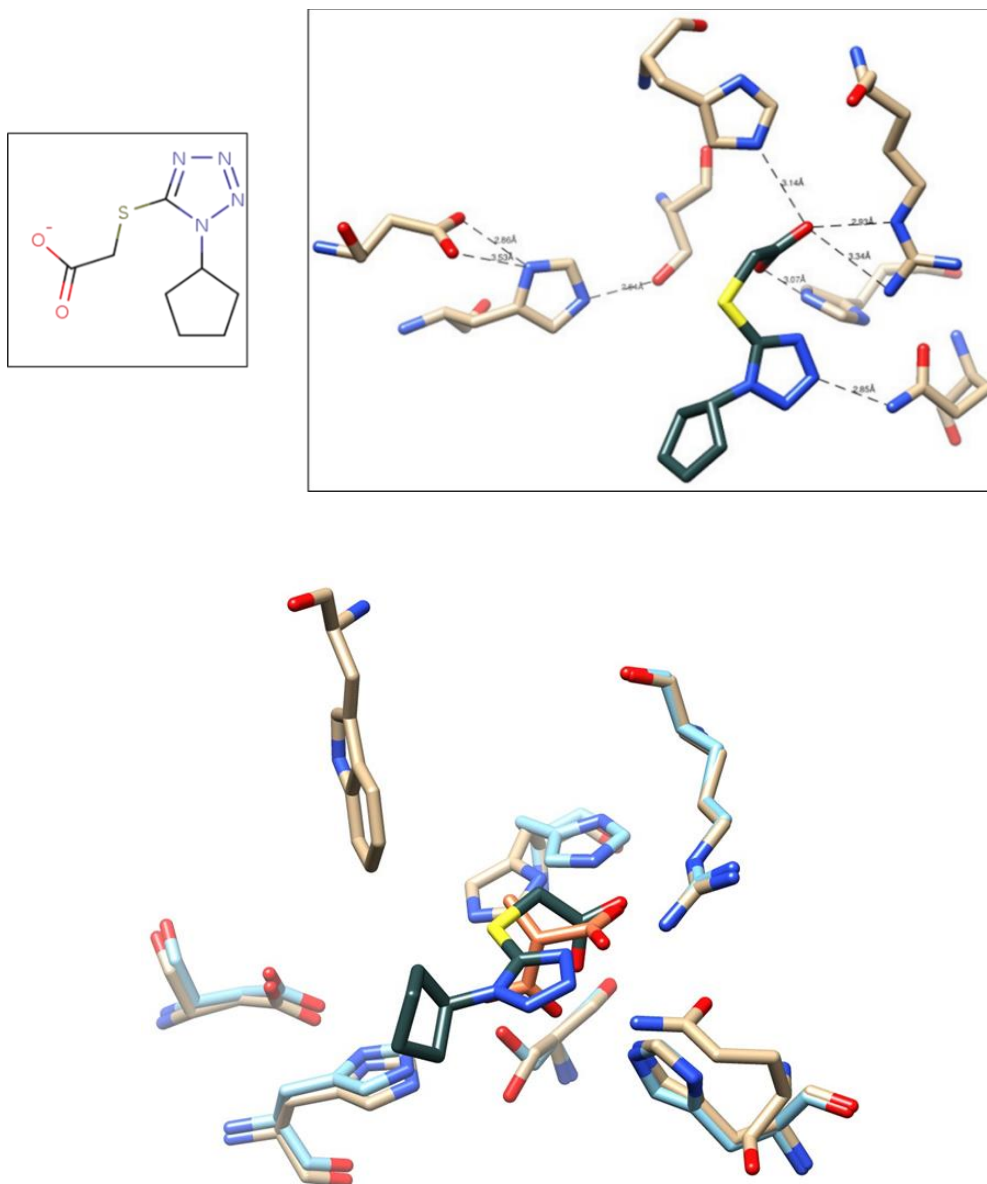
EN:T6531385

Molecule EN:T6531385 showed a ΔT_m of 4°C and a co-crystal structure was obtained with Rv0272 [Figure 4.22]. Investigation of the interactions between the ligand and active site residues again demonstrated the dynamics of His163. The ligand methyl group points towards His163 and may be responsible for its movement out of the pocket and towards Ser118. However, in this case Ser118 remains unaffected and still is within hydrogen bonding distance of one of the nitrogen groups in the ligand ring. The chlorine atom may have Van Der Walls interactions with the hydroxyl group from Tyr354. A similarity search identified one molecule in the KEGG database that displayed a 60% structural similarity to EN:T6531385, N-methyl-L-alanine. N-methyl-L-alanine is described as a substrate involved in the reaction of N-methyl-L-alanine to form pyruvate and methylamine, using NADP as a cofactor. However, this enzyme can carry out the reverse reaction as well forming N-methyl-L-alanine, although the function of this metabolite *in vivo* has not been established (204).

Figure 3.23. Structure of EN:T6531385 bound in the active site. Bottom - Overlay of EN:T6531385 and methylmalonate
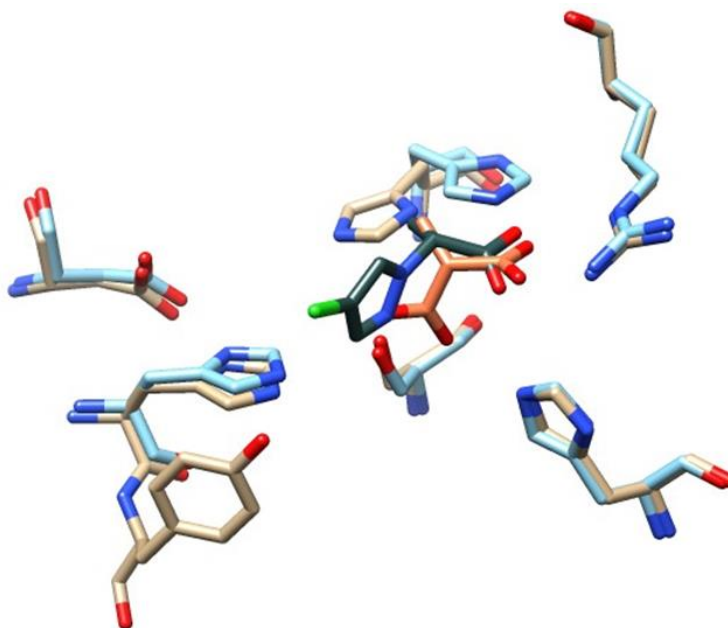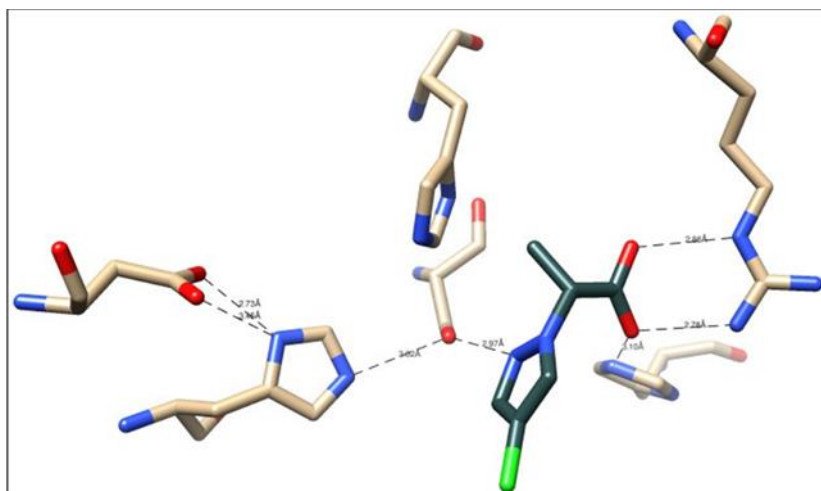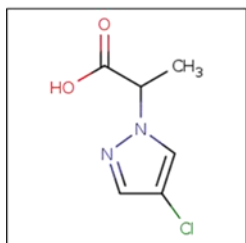
EN:EN300-49784

Molecule EN:EN300-49784 showed a ΔT_m of 13°C and a co-crystal structure was determined with Rv0272 [Figure 4.23]. This compound gave the largest ΔT_m of all the fragments and upon inspection of the active site it becomes a little more clear as to why. The carboxylate of the ligand interacts with Arg166 in a similar manner as previous ligand bound structures. However, EN:EN300-49784 has several potential hydrogen bonding atoms in its ring moiety as well as its carboxylate tail linker. It has both an oxygen and nitrogen atom available to hydrogen bond with the Oδ of Ser118 as well as the backbone nitrogen from Gly119. A nitrogen and an oxygen atom are both within hydrogen bonding distance of the hydroxyl oxygen from Tyr354. In addition, the 6-membered ring of the ligand composed of 2 nitrogen atoms, 2 carbon atoms, and 2 oxygen atoms, form an entire network of hydrophobic and Van Der Walls interactions with residues in the surrounding environment (Ile55, Tyr269, Trp173, Ile283, Trp248).

A similarity search identified 3 metabolites which display at least a 65% structurally similarity to EN:EN300-49784. Uracil 5-carboxylate, thymine, and 5-hydroxymethyluracil were all identified. Uracil 5-carboxylate is the product of an oxidoreductase reaction converting uracil 5-carbaldehyde and 2-oxoglutarate into uracil 5-carboxylate and succinate. Succinate was a metabolite which also showed binding with a ΔT_m of 6°C. Uracil 5-carboxylate is also the substrate for a decarboxylase which removes the carboxyl group to form uracil. This enzyme does not require a cofactor and is an intermediate in the conversion of pyrimidines to uracil (205, 206). Thymine can function as a substrate and/or product in several enzymatic reactions involved in pyrimidine

metabolism. It is the product of a dihydropyridime dehydrogenase, an iron-sulfur flavo-enzyme which converts 5,6-dihydrothymine to thymine using NAD as a cofactor. Thymine is the product of a 5-methylcytosine aminohydrolase which converts 5-methylcytosine to thymine and ammonia. Thymine can be the product of a thymidine phosphorylase, which catalyzes the formation of thymine and 2-deoxy-D-ribose-1-phosphate from thymidine and phosphate.

Thymine is also the substrate of a thymine dehydrogenase which converts thymine to 5-methylbarbiturate found in the oxidative pyrimidine-degrading pathway (207). Interestingly, this pathway is responsible for converting uracil or thymine into malonate or methymalonate with the help of 3 zinc dependent enzymes, 2 of which are hydrolases [Figure 4.24]. These function(s) are significant given the propensity of Rv0272 to bind EN:EN300-49784, malonate, and methylmalonate with high apparent affinities. Alternatively, these enzymes can also convert atrazine into carboxybiuret which then spontaneously decarboxylates to biuret and seem to be found almost exclusively in bacteria (208).

Figure 3.24. Structure of EN:EN300-49784 bound in the active site. Bottom - Overlay of EN:EN300-49784 and methylmalonate
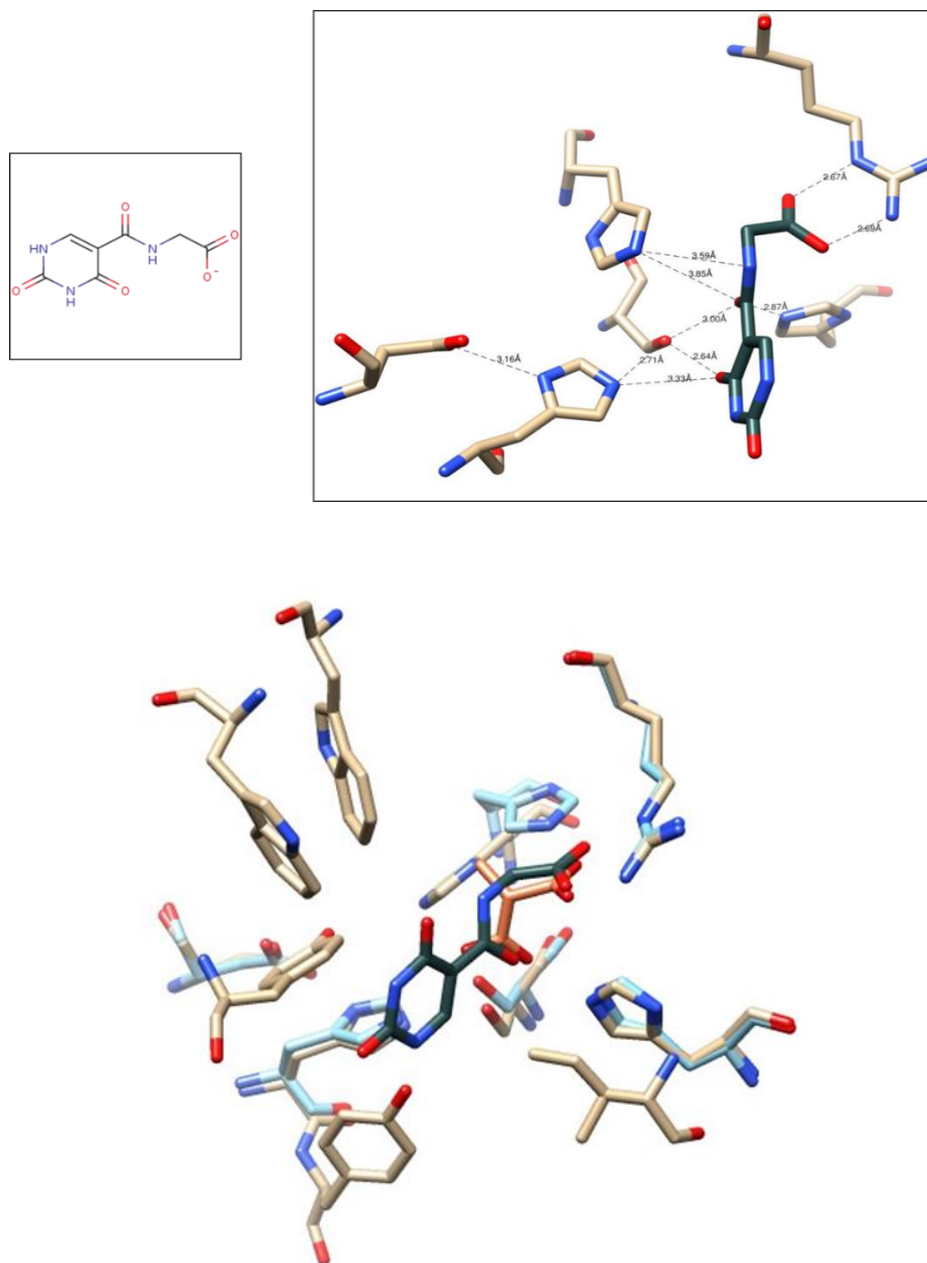
Figure 3.25. Oxidative pyrimidine degradation pathway. Uracil is oxidized by uracil dehydrogenase to form barbitaric acid which then is converted into ureidomalonic acid by barbiturase. Finally ureidomalonase converts ureidomalonic acid into malonic acid and urea.
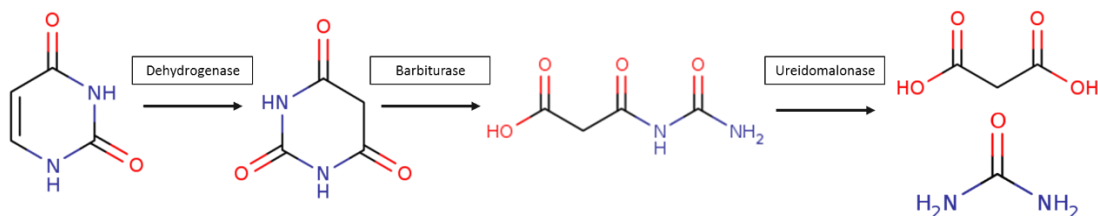
EN:T6307026

Molecule EN:T6307026 showed a ΔT_m of 9°C and a co-crystal structure was determined with Rv0272 [Figure 4.25]. Inspection of the active site residues involved in binding with the ligand revealed that Arg166 coordinates the carboxylate of the ligand. In this case Ser118 is within hydrogen bonding distance of the hydroxyl group of the ligand. The ligand hydroxyl is also interacting with the backbone nitrogen of Gly119 and Nε of His52. Additionally, the ring nitrogen of the ligand is within hydrogen bonding distance of both Ser118 and what originally appeared to be a water molecule. However, upon subsequent rounds of refinement, the electron density did not correspond to water, but to metal. Although the identity of the metal is not known, Zn refined perfectly into the density map. This is the first structure that electron density corresponding to a metal has been observed in the active site. However, this metal was only observed in one monomer of the

dimer in the ASU. The other active site had electron density which corresponded to a water

molecule.

Figure 3.26. Structure of EN:T6307026 bound in the active site. Bottom - Overlay of EN:T6307026 and methylmalonate. Zinc is shown in gray.
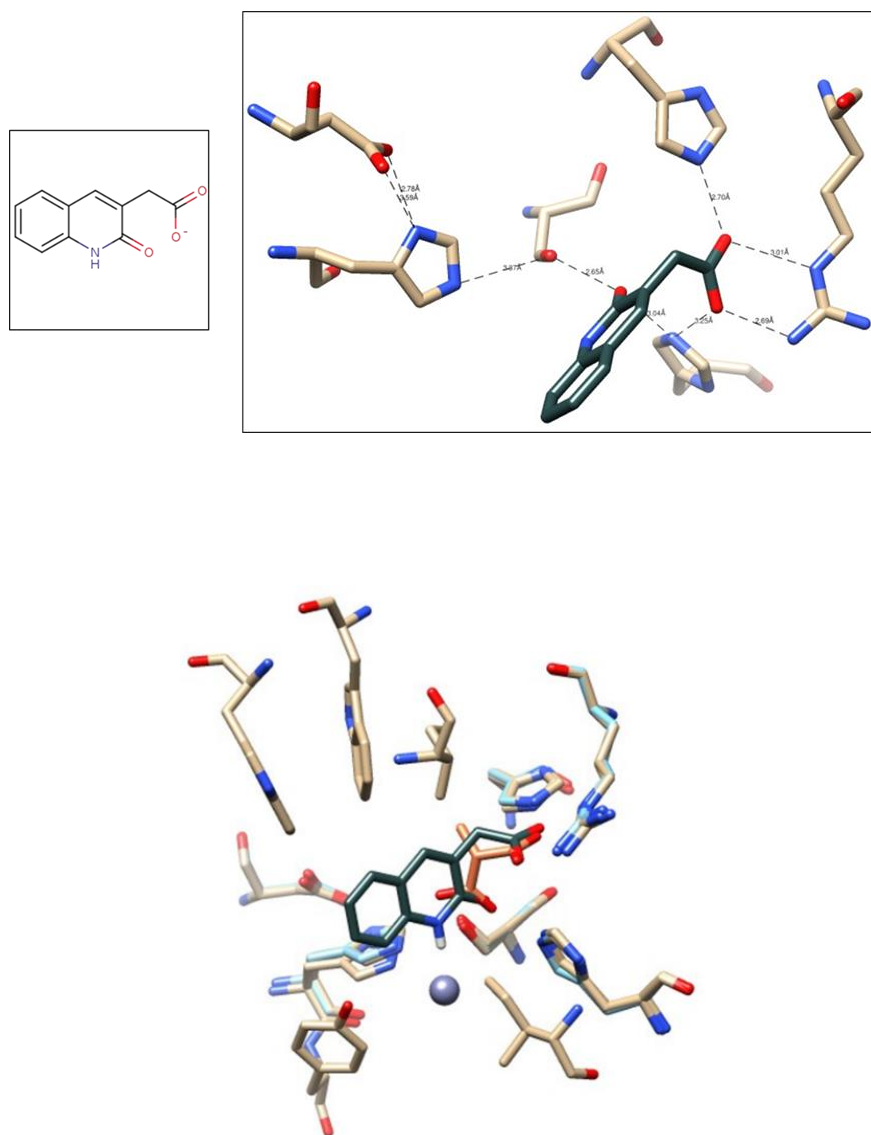
A similarity search of the KEGG database found one metabolite which is at least 65% similar in structure to EN:T6307026, 2,4-dihydroxyquinolone (DHQ) [Figure 4.26]. DHQ is an extracellular metabolite produce by *Pseudomonas aeruginosa* that is required for virulence and in quorum sensing. Its role has never been described in *M. tuberculosis* and it's not well understood how it is regulated in *Pseudomomas aeruginosa.* It has been shown to be important in the process of biofilm production as well. DHQ is made through 4 separate reactions using 2 enzymes, beginning with anthranilate as a substrate, a molecule which binds to Rv0272. The reaction process utilizes two different CoA molecules, malonyl-CoA and 3-(2-aminophenyl)-3-oxopropanoyl-CoA.

Figure 3.27. Chemical structure of 2, 4-dihydroxyquinolone (DHQ).
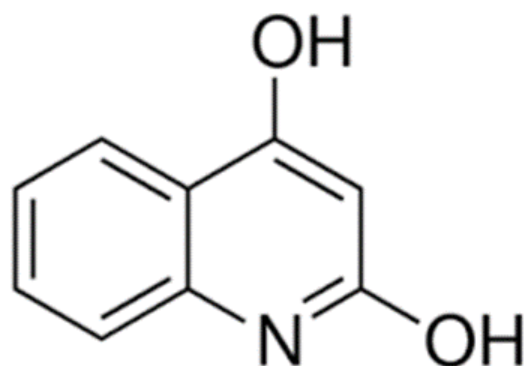
EN:T5810855, EN:T5764482 & EN:T0518-6321

EN:T5810855, EN:T5764482 and EN:T0518-6321 gave positive shifts in ΔT_m of 4ºC, 6ºC, and 4ºC respectively. However, attempts at obtaining a co-crystal structure with Rv0272 have failed. Although each molecule contains a carboxylate R group, electron density consistent corresponding to the three molecules was never seen. The only commonality between each molecule is a sulfur atom that may be inferring with binding in the crystal/ crystallization condition [Figure 4.27].

Figure 3.28. EN:T5810855, EN:T5764482 & EN:T0518-6321. Three compounds which demonstrated a positive shift in melting temperature for Rv0272.
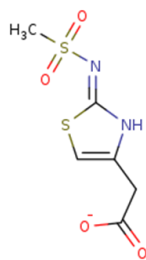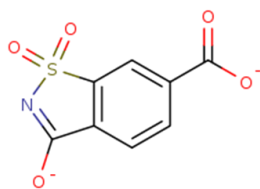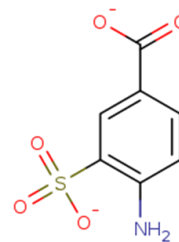
EN:T5810855   EN:T5764482   EN:T0518-6321

EN:T5970989

Molecule EN:T5970989 showed a ΔT_m of $6^{\circ}C$ and a co-crystal structure was attempted with Rv0272 [Figure 4.28]. The resulting structure had significant electron density in the active site which appeared to represent part(s) of the fragment. However, the entire molecule was not able to fit into the resulting density. The electron density did correspond to the carboxylate tail and parts of the bicyclic core, yet the tri-fluoro group could not be identified and neither could the molecule in its entirety. EN:T5970989 most likely underwent a cleavage event, either spontaneous or enzymatic, which altered the final product found in the crystal structure. To date, the fragment product has not been identified but future experiments will be aimed at determining its identity through a combination of mass spectrometry and reverse phase liquid chromatography. Attempts to identify metabolites in the KEGG database which showed at least 60% structural similarity failed to give a single positive hit.

Figure 3.29. Electron density in the active site of Rv0272 observed after soaking Rv0272 crystals with EN:T5970989, also shown.
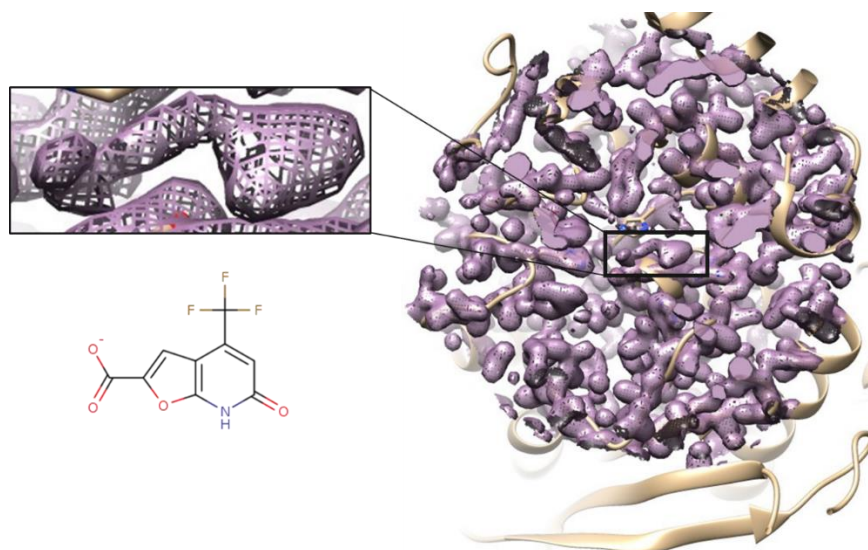
EN:T6178680 & EN:T0501-0213

Molecules EN:T6178680 and EN:T0501-0213 showed a ΔT_m of 5°C and ΔT_m of 6°C respectively, and co-crystal structure(s) were attempted with Rv0272. The results were similar to what was observed EN:T5970989 except in this case the fragment product could be determined from the electron density. Surprisingly, the density did not correspond to either molecule, yet both displayed identical density maps [Figure 4.29]. The resulting structures were collected at less than 1.8 Å resolution each and demonstrated clear electron density for a bi-substituted 6-membered ring. The substitutions occurred at adjacent positions and were clearly defined as either nitro or carboxyl groups and mimicked exactly what was seen earlier in the case of phthalate, nitrobenzoate, and

quinolinate. All 3 molecules could be successfully built into the model and refined without arguments. However, no previously defined enzymatic mechanism could predict any of the three possible products from either starting fragment. Each fragment was analyzed via mass spectrometry and the resulting mass matched the expected mass of each parent fragment. The soaks were repeated a total of 3 times, each time the same result was observed in the crystal structure.

In an attempt to rationalize this product formation enzymatically, the KEGG database was searched for any metabolite that had at least 60% structurally similarity between the fragment(s). The search returned no positive hits. Therefore, the KEGG database was investigated manually for any similar chemical scaffolds that may be found in biological pathways which phthate, anthranilate, or quinolinate are utilized. In tryptophan metabolism, a hydrolase enzyme was found to convert L-kynurenine into anthranilate and L-alanine [Figure 4.30]. L-Kynurenine shares a similar scaffold to EN:T6178680, but nothing could be identified for EN:T0501-0213. Attempts were made to soak L-Kynurenine into crystals of Rv0272, but electron density was never observed for the expected molecule, either Anthranilate or L-alanine. This reaction has been previously described as a pyridoxal-phosphate (PLP) dependent protein in *Neurospora crassa* (209). However, PLP was not used in the original attempts for obtaining a co-crystal of the reaction product.

Figure 3.30. Observed electron density in the active site of Rv0272 after crystals had been soaked with EN:T6178680 (top left) and EN:T0501-0213 (bottom left). Bottom – Chemical structure of phthlate, quinolinate, nitrobenzoate, respectively. The electron density appears to correspond to pthlate.
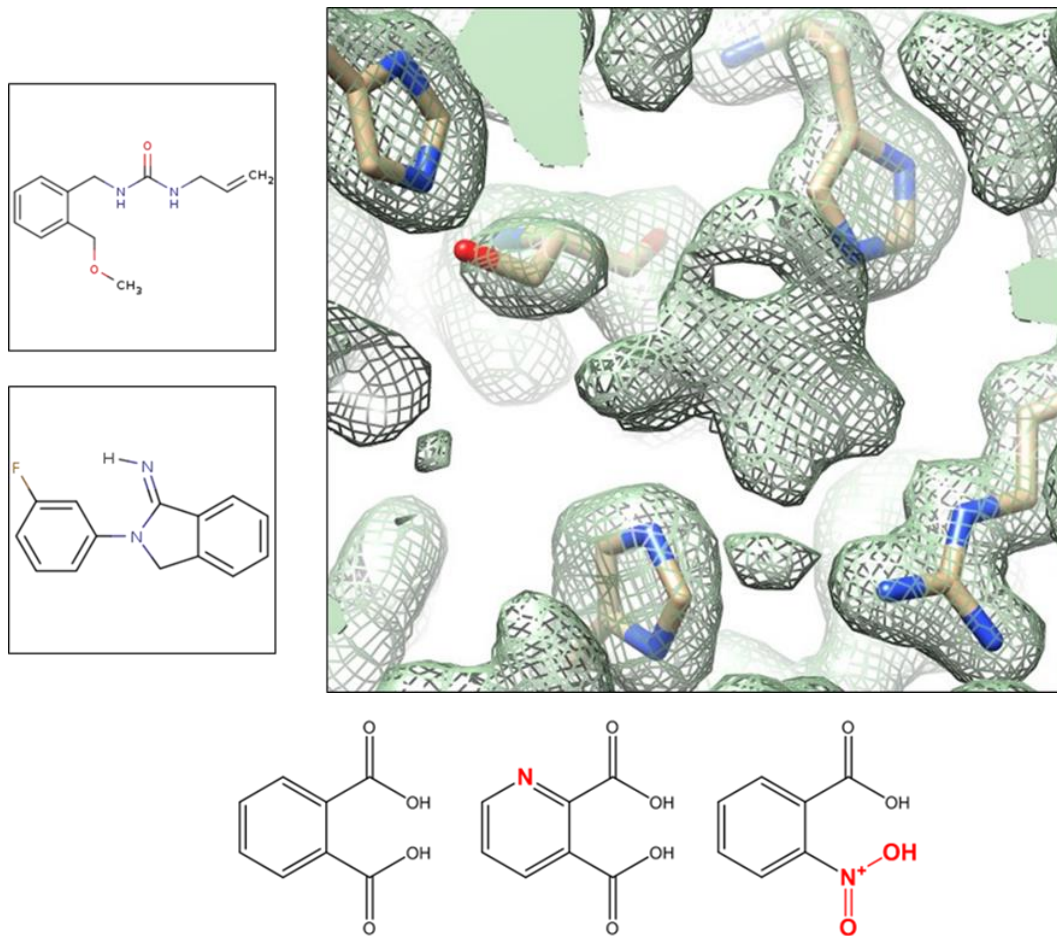
Figure 3.31. Top: L-kynurenine hydrolase which catalyzes the cleavage of L-kynurenine into anthranilic acid and L-alanine, using PLP as a co-factor. Bottom: Comparison of EN:T617860, which when soaked into Rv0272 crystals resulted in an electron density which may correspond to anthranilic acid. Kynurenine is shown adjacent for comparison of the two chemical scaffolds.

EN:T617860   Kynurenine
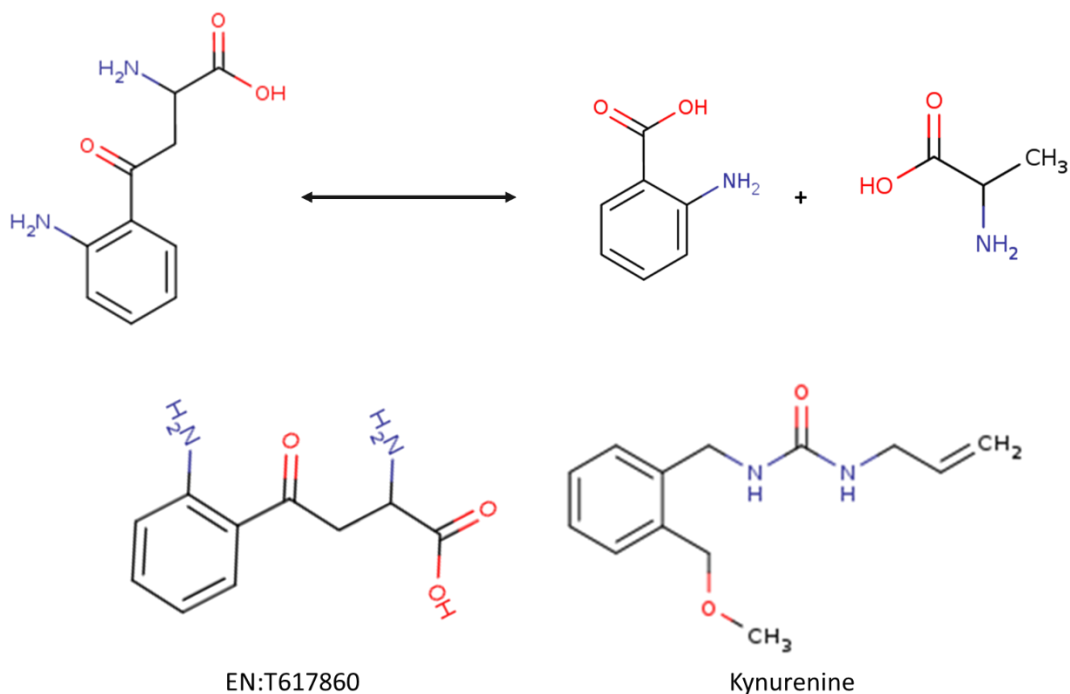
Rv0272 Demonstrates Phthalyl Amidase Activity in Crystals

In order to ascertain whether nor not the conversion of these fragments to a benzoic acid derivative is specific to Rv0272 some assumptions were made based on DSF binding data. It was shown that phthalate had the highest change in thermal stability out of all the molecules tested. Therefore the compound libraries were probed for molecules, regardless

of whole cell activity, which contained a phthalyl moiety. Three compounds were initially identified and selected for testing, CB:9117573, CB:5105142, and CB:9156115 [Figure 4.31]. They were first tested for binding DSF and compared against phthlalic acid. Two of the three molecules demonstrated the same ΔT_m as phthlalic acid ($\Delta T_m = 11^oC$) while one molecule, CB:5105142, was slightly less effective but still showed binding with a ΔT_m of 9^oC. The molecule identity of each compound was confirmed by analyzing the mass of each via liquid chromatography mass spectrometry. All three compounds were subjected to crystallization trials in order to obtain co-crystal structures by soaking crystals of Rv0272 for 2 hours with 1mM of compound. Ligand bound structures were obtained for each molecule and in all three cases density was observed which corresponded to phthalic acid. Phthalic acid was built into the electron density and refined into the active site [Figure 4.32]. In all three cases, the molecule is bound in the same location, interacting with the same active site residues, with no observable orphan density which could represent the rest of the compound.

Electron density differences between phthalate and other similar molecules such as anthranilate, quinolinate, and nitrobenzoate, may be hard to distinguish. A reference of electron density was obtained for each via co-crystallization of all four metabolites. Nitrobenzoate had very low occupancy, anthranilate was distinguishable from the others based on weaker electron density around the nitrogen atom compared to the two oxygen atoms of quinolinate and phthalate. However, based on electron density, quinolinate and phthalate were indistinguishable. This is some-what unexpected given the difference in melting temperatures from DSF between the two. The local environment of the active site

also remained unchanged between the two. As such, determining the location of the nitrogen atom on quinolinate was not possible.

Identification of a phthalyl amidase activity was unexpected and not a enzymatic function previously described in *M. tuberculosis.* However, *Xanthobacter agilis* has been shown to phthalate amino acids in order to protect them from degradation pathways. They contain an enzyme which is specific for phthalated substrates such as amino acids, but also demonstrate a broad activity on multiple phthalated substrates, including phthlated β-lactams. It has been hypothesized that this enzyme would serve as a mechanism for deprotecting amino acids (210).

Figure 3.32. Three phthalyl containing compounds identified from the Sac1 and Sac2 chemical libraries selected to test for activity.

CB:9117573   CB:5105142   CB:9156115
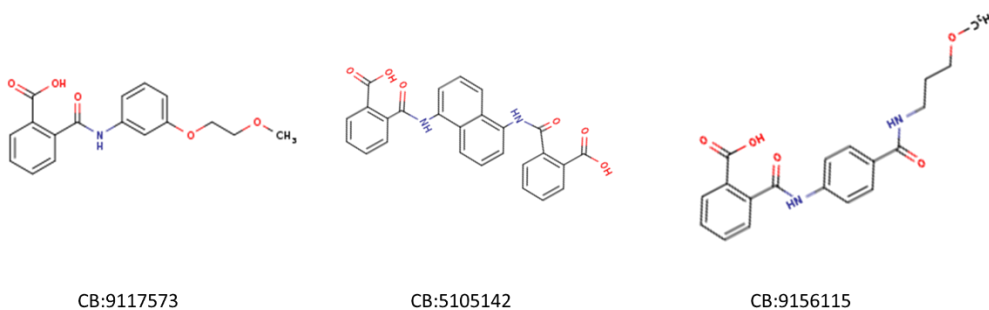
Figure 3.33. Phthalic acid bound in the active site to Rv0272.
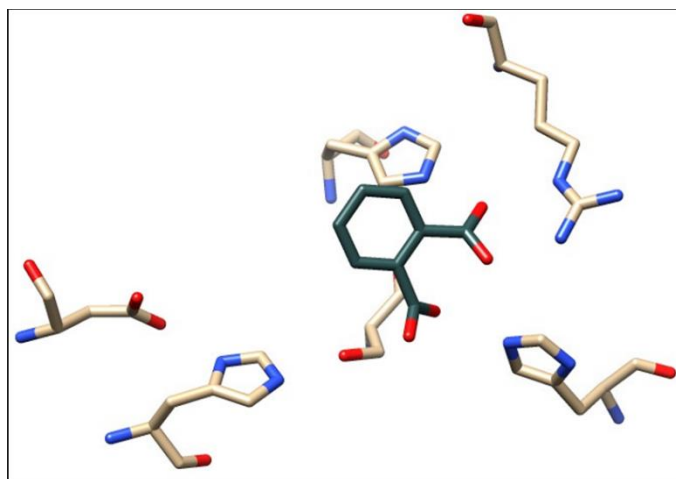
Rv0272 Binds Folic Acid

Although folate metabolism is very well described in *M. tuberculosis*, folic acid gave a 4°C from DSF when screening against possible metabolites and cofactors that have amide bonds and are structurally similar to molecules which have previously demonstrated binding. A co-crystal structure of folic acid was obtained [Figure 4.33].

Figure 3.34. Structure of folic acid bound in the active site of Rv0272.
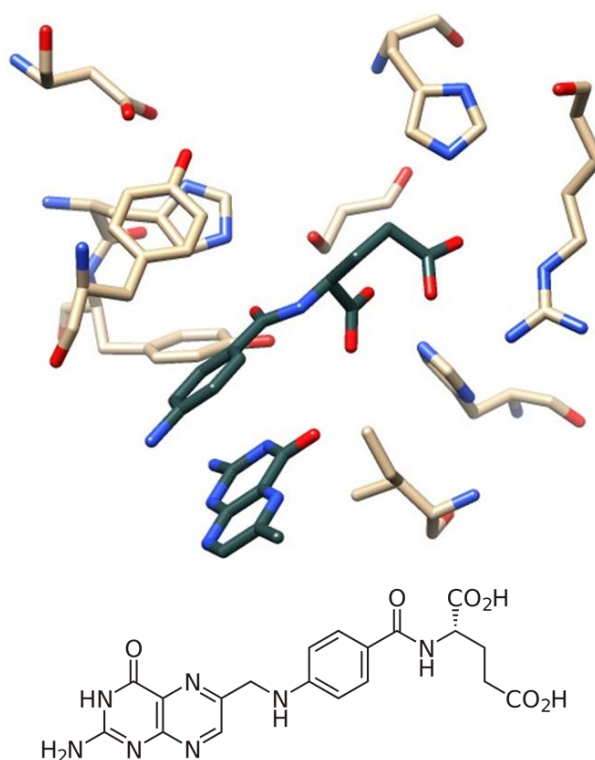
DISCUSSION

Rv0272 is an indispensable gene in *M. tuberculosis* in all conditions with the exception of *in vitro* growth on glycerol as a sole carbon source. Rv0272 demonstrates an incredible elasticity in its catalytic site with the ability to bind a broad spectrum of molecules. The binding of methylmalonate was able to increase the thermal stability of the enzyme by up to 10°C more than enzyme alone. Through crystallographic analysis of Rv0272 bound with ligand, CoA was also shown to bind to the enzyme but did not

demonstrate a shift in melting temperature. Interrogating the possible biological functions of an enzyme with a binding affinity for CoA and methymalonate lead to the hypothesis that Rv0272 is a methylmalonyl-CoA hydrolase.

In vitro attempts to support this hypothesize by demonstrating enzymatic turnover of methylmalonyl CoA were unsuccessful. Although initial attempts did show promise, the DNTB coupled reaction did not yield consistent and repeatable activity. Several factors could have influenced the failed outcomes, including the possible requirement of certain conditions for the reaction to occur *in vitro* (pH, salts, cofactors, metals), post-translational modifications, reduction/oxidizing environment, and inhibition by the DTNB reagent, either through modification of a surface exposed cysteine or by binding to the active site directly. In addition, the substrate chirality may play a role in preventing the reaction from occurring.

In contrast, it was demonstrated that Methylmalonyl-CoA was modified enzymatically when soaked into a crystal of Rv0272. The extent of the modification and the specific reaction which is being catalyzed is still uncertain. Unexpectedly, in an attempt to co-crystallize Rv0272 with acetyl-CoA, the resulting structure was bound with CoA, yet soaks with malonyl-CoA yielded a malonate bound structure.

In an attempt to further elucidate the function of Rv0272, several small molecule fragments, whole cell active inhibitors, and other potential metabolites were identified by their ability to bind to the enzyme. An in depth structurally comparison of the identified binders led to the exploration of other possible enzymatic functions. Maleate demonstrated binding to Rv0272 which prompted the hypothesis that the enzyme was functioning as a

maleamate amidase, converting maleate to maleamate in the nicotinic acid degradation pathway. Although an enzymatic assay has yet to be employed to pursue this possibility, co-crystallization attempts with the substrate maleamate did not yield the product, maleate, bound to the enzyme.

The identification of a benzoic acid derivative bound to the crystallized enzyme when soaked with a structurally unrelated molecule led to the exploration of an additional activity. Based on the observed reaction, a kynurenine hydrolase function was proposed. Kynurenine did not demonstrate binding using DSF. However, PLP is not amenable for use in DSF and it may be that kynurenine requires PLP to bind first before it binds. Attempts to soak PLP and kynurenine into Rv0272 crystals abolished x-ray diffraction. This activity is still being considered as a possible function. Consistent with the binding of the benzoic acids and the previous observation of activity within Rv0272 crystals, a phthalyl amidase function was proposed. Several phthlated compounds were confirmed to bind using DSF and hydrolysis of the phthalyl group was observed upon soaking into enzyme crystals. An enzymatic assay is currently being developed to recapitulate these findings. NMR metabolomics demonstrated convincing results that Rv0272 is able to hydrolyze D-Ala-D-Ala peptides. However, this activity could not be confirmed via enzymatic assays or crystallization trials. The possibility that Rv0272 was functioning as a PBP, carboxypeptidase, serine protease, and/or β-lactamase were all considered but none yielded convincing evidence to support such a hypothesis.

CONCLUSION

Rv0272 has demonstrated incredible substrate plasticity and the possibility exists that it may have multiple, essential biological functions. Evidence supports the notion that the enzyme recognizes a carboxylate group by coordinating the two carboxyl oxygens into the active site with Arg166. The catalytic triad of Ser, His, and Arg may recognize esters, thioesters, and amides, with specificity determined by the distance between the carboxylate tail and the site recognized by the catalytic serine. To date, two possible functions stand above the rest; a methylmalonyl-CoA hydrolase and a phthalyl amidase.

CHAPTER IV

CONCLUSIONS AND FUTURE WORK

Through careful consideration of host environmental conditions faced by mycobacteria, two separate screening protocols were created. One screen was performed using NaOAc as the sole carbon source. The rationale being that during persistent infections, fatty acids are most likely used as the primary carbon source. Although enzymes involved directly in fatty acid degradation may be dispensable for growth on acetate, the downstream pathways, specifically β-oxidation and the glyoxylate cycle are required. These pathways contain several enzymes which are essential for bacterial infection and persistence, notably malate synthase and isocitrate lysase (211, 212). The HTS was carried out against several NTMs for two reasons. First, modern diagnostics have revealed that NTM pathogenesis is much more pronounced that originally believed. Historically, NTMs have been treated with antibiotics developed for the treatment of *M. tuberculosis*. However, NTMs commonly display intrinsic resistance to known anti-tubercular drugs and as such new hits for drug development specific to NTMs is required. Second, given NTMs genome similarity to each other and *M. tuberculosis*, they could be used as a model organism for *M. tuberculosis* drug target identification and resistant mutant selection. NTMs are more amenable to manipulate *in vitro* given their fast doubling time and low rate of pathogenicity in humans.

The HTS carried out with NaOAc as the sole carbon source was successful in identifying almost 1,000 molecules which could inhibit bacterial cell growth at 10μM.

Hits specific for *M. tuberculosis, M. smegmatis, M. abscessus, and M. fortuitum* could be compared and molecules could be separated based on their activity, either specific or broad spectrum. Over 20% of the compounds from the NaOAc HTS were shown to demonstrate broad anti-bacterial properties and were active against all the NTMs and *M. tuberculosis.* In addition these hits could be compared against hits obtained from a previous screen carried out on dextrose as the sole carbon source.

A second HTS was carried out using a mixed carbon source of dextrose and NaOac. The rationale of this method was to attempt to identify molecules which may target enzymes which are indispensable for growth on either carbon source. In a cross-validation study, it was shown that less than 10% of compounds were lost when screening on a mixed carbon source versus two separate screens on individual carbon sources. These data compiled from the HTS served as hit libraries for potential enzymatic inhibitors which were also potent inhibitors of bacterial growth.

The hits identified from the HTS were the focus of resistant mutant selection in order to determine mechanism of resistance and in turn identify the inhibited target responsible for whole cell growth inhibition. Several enzymes were found which could be promising therapeutic targets. Rv0272 was the primary focus of this body of work, but two other enzymes were also partially characterized, Rv2857c and Rv0206c.

Rv0272 has demonstrated an ability to bind a broad range of molecules from short chain dicarboxylic acids such as methylmalonate to comparatively large, unrelated metabolites such as folic acid. Deciphering the identity of the most preferred substrate for Rv0272 has been a challenge. NMR based metabolomics demonstrated significant and

177

reproducible evidence of a D-Ala-D-Ala carboxypeptidase activity. *In vitro* activity assays have been inconsistent and have failed thus far to recapitulate a specific enzyme activity with any degree of certainty. The most promising avenue has been the observation(s) of the product of an enzyme driven reaction through co-crystallization and structure determination of hypothesized substrates. These experiments have demonstrated enzyme dependent reactions occurring within the crystal when using acyl-CoA's and phthalated compounds as substrates. Although the data suggest a phthalyl amidase activity, the biological significance of such a function is still unclear. However, the data suggesting a methylmalonyl-CoA thioesterase activity is a little less convincing, but the biological significance is pronounced and in need of annotation in *M. tuberculosis*.

Future work involved in characterizing Rv0272 will focus on developing a colorimetric enzyme assay for a phthalyl amidase activity using a 4-nitrophenyl R group which when hydrolyzed could potentially have an absorbance at 400 nm. If the activity of Rv0272 becomes more defined, a structure and activity relationship study of this enzyme with potential whole cell active inhibitors would be ideal given its ability to form robust, highly diffracting crystals, which are amenable to ligand soaks, while maintaining enzymatic function in a crystalline state.

There exist 4,019 protein encoding genes in the *M. tuberculosis* genome and 1096 of those genes are annotated as hypothetical, conferring little to no functional information and fairly weak associations with enzymes of known function (213). Bioinformatics approaches can infer possible functions through homology and orthology based approaches. However, many of these "hypothetical" protein encoding genes only share

significant sequence homology with "hypothetical" protein encoding genes in other organisms. In fact, of the approximately 20,000,000 protein sequences from around 400 completely sequenced genomes found in the NCBI protein database, one in three proteins had no assigned function and one in ten proteins was annotated as "hypothetical". Even in the most well studied organism, *E. coli* K-12, almost half of its entire genome has yet to be experimentally characterized (214). This knowledge gap in the proteomic/ genomic database is a significant road block in understanding the biological complexity that exists not only in the host-pathogen relationship in *M. tuberculosis* infections but also in many other closely related human pathogens. Although biochemically characterizing poorly annotated proteins is often time consuming and costly, the potential evidence garnered could be applicable across multiple homologous species which could reveal previously unknown biological pathways and enzymatic functions necessary for survival and pathogenicity. In addition, these proteins could potentially be attractive drug targets that once properly elucidated could be paramount in guiding future drug discovery efforts.

Tropism of pathogenic bacteria dictates the ability of the microbe to infect its host. A multitude of factors play a role in determining the range of host environments as well as the success rate at which a microbial pathogens can sustain an infection. The molecular and genetic mechanisms which determine host specificity are often times not understood and are comprised of many poorly characterized surface receptor proteins, excreted proteins, and virulence factors that are essential for nutrient acquisition and host immune evasion (215). Tuberculosis is without question the most dangerous and adaptive of all human pathogenic bacteria, but many other human pathogens have evolved similar

mechanisms and cellular machinery to infect and persist within their host environment. A few of these include but are not limited to the species and antibiotic-resistant species from the genera of *Streptococcus, Treponema,* and *Staphylococcus,* which the CDC estimates are responsible for more than 700,000 deaths world-wide per year. Similar to *E. coli,* and *M. tuberculosis,* more than half of all their protein encoding genes have yet to be characterized biochemically.

It becomes clear that identifying and characterizing "hypothetical" proteins, which may also include the factors involved in host specificity and pathogenicity, can provide potential clues to aid in the design of new strategies and antimicrobials for the control and elimination of microbial diseases. Therefore, significant efforts will be put towards identifying and characterizing proteins in *M. tuberculosis* which are poorly or incompletely annotated. In turn, the goal would be to establish useful information on molecular mechanisms responsible for *M. tuberculosis* infection and persistence that could potentially be applicable to drug development against a wide range of human pathogenic bacteria.

REFERENCES

1.   Manchester K. Tuberculosis and leprosy in antiquity: an interpretation. Med Hist. 1984;28(2):162-73. PubMed PMID: 6387342; PMCID: PMC1139422.

2.   Ryan F. Tuberculosis: The Greatest Story Never Told: Swift Publishers; 1992. 446 p.

3.   Wells C. Two Mediaeval Cases of Malignant Disease. Br Med J. 1964;1(5398):1611-2. PubMed PMID: 14134489; PMCID: PMC1814753.

4.   Morse D, Brothwell DR, Ucko PJ. Tuberculosis in Ancient Egypt. Am Rev Respir Dis. 1964;90:524-41. doi: 10.1164/arrd.1964.90.4.524. PubMed PMID: 14221665.

5.   Ortner DJ. Disease and mortality in the Early Bronze Age people of Bab edh-Dhra, Jordan. Am J Phys Anthropol. 1979;51(4):589-97. doi: 10.1002/ajpa.1330510411. PubMed PMID: 391058.

6.   Formicola V, Milanesi Q, Scarsini C. Evidence of spinal tuberculosis at the beginning of the fourth millennium BC from Arene Candide cave (Liguria, Italy). Am J Phys Anthropol. 1987;72(1):1-6. doi: 10.1002/ajpa.1330720102. PubMed PMID: 3826326.

7.   Stirland A. The late Sir Thomas Reynes: a medieval identification. J Forensic Sci Soc. 1990;30(1):39-43. PubMed PMID: 2181055.

8.   Rogers J, Watt I, Dieppe P. Palaeopathology of spinal osteophytosis, vertebral ankylosis, ankylosing spondylitis, and vertebral hyperostosis. Ann Rheum Dis. 1985;44(2):113-20. PubMed PMID: 3883915; PMCID: PMC1001584.

9.   Clark GA, Kelley MA, Grange JM, Hill MC. The evolution of mycobacterial disease in human populations: a reevaluation. Curr Anthropol. 1987;28(1):45-62. PubMed PMID: 11618572.

10.   Behnisch R. Pharmacological Methods, Receptors and Chemotherapy. Discoveries in Pharmacology1986. p. 256.

11.   Sotgiu G, D'Ambrosio L, Centis R, Mura I, Castiglia P, et al. The multidrug-resistant tuberculosis threat: old problems and new solutions. J Thorac Dis. 2015;7(9):E354-60.   doi: 10.3978/j.issn.2072-1439.2015.09.21.   PubMed   PMID: 26543630; PMCID: PMC4598488.

12.   Organization WH. Treatment of Tuberculosis Guidelines for National Programmes. 4th ed. Geneva2010 2010.

13.   Ebina T, Motomiya M, Munakata K, Kobuya G. [Effect of isoniazid on fatty acids in Mycobacterium]. C R Seances Soc Biol Fil. 1961;155:1176-8. PubMed PMID: 13889034.

14.   Barclay WR, Ebert RH, Kochweser D. Mode of action of isoniazid. Am Rev Tuberc. 1953;67(4):490-6. PubMed PMID: 13031065.

15.   Russe HP, Barclay WR. The effect of isoniazid on lipids of the tubercle bacillus. Am Rev Tuberc. 1955;72(6):713-7. PubMed PMID: 13268845.

16.   Winder FG, Collins PB. Inhibition by isoniazid of synthesis of mycolic acids in Mycobacterium tuberculosis. J Gen Microbiol. 1970;63(1):41-8. doi: 10.1099/00221287-63-1-41. PubMed PMID: 5500025.

17.   Takayama K, Wang L, David HL. Effect of isoniazid on the in vivo mycolic acid synthesis, cell growth, and viability of Mycobacterium tuberculosis. Antimicrob Agents Chemother. 1972;2(1):29-35. PubMed PMID: 4208567; PMCID: PMC444261.

18.   Takayama K, Schnoes HK, Armstrong EL, Boyle RW. Site of inhibitory action of isoniazid in the synthesis of mycolic acids in Mycobacterium tuberculosis. J Lipid Res. 1975;16(4):308-17. PubMed PMID: 806645.

19.   Davidson LA, Takayama K. Isoniazid inhibition of the synthesis of monounsaturated long-chain fatty acids in Mycobacterium tuberculosis H37Ra. Antimicrob Agents Chemother. 1979;16(1):104-5. PubMed PMID: 112917; PMCID: PMC352798.

20.   Zhang Y, Heym B, Allen B, Young D, Cole S. The catalase-peroxidase gene and isoniazid resistance of Mycobacterium tuberculosis. Nature. 1992;358(6387):591-3. doi: 10.1038/358591a0. PubMed PMID: 1501713.

21.   Mdluli K, Slayden RA, Zhu Y, Ramaswamy S, Pan X, et al. Inhibition of a Mycobacterium tuberculosis beta-ketoacyl ACP synthase by isoniazid. Science. 1998;280(5369):1607-10. PubMed PMID: 9616124.

22.   Slayden RA, Barry CE, 3rd. The role of KasA and KasB in the biosynthesis of meromycolic acids and isoniazid resistance in Mycobacterium tuberculosis. Tuberculosis (Edinb). 2002;82(4-5):149-60. PubMed PMID: 12464486.

23.   Sun YJ, Lee AS, Wong SY, Paton NI. Analysis of the role of Mycobacterium tuberculosis kasA gene mutations in isoniazid resistance. Clin Microbiol Infect. 2007;13(8):833-5. doi: 10.1111/j.1469-0691.2007.01752.x. PubMed PMID: 17501974.

24.   Hazbon MH, Brimacombe M, Bobadilla del Valle M, Cavatore M, Guerrero MI, et al. Population genetics study of isoniazid resistance mutations and evolution of multidrug-resistant Mycobacterium tuberculosis. Antimicrob Agents Chemother. 2006;50(8):2640-9. doi: 10.1128/AAC.00112-06. PubMed PMID: 16870753; PMCID: PMC1538650.

25.   Marrakchi H, Laneelle G, Quemard A. InhA, a target of the antituberculous drug isoniazid, is involved in a mycobacterial fatty acid elongation system, FAS-II. Microbiology. 2000;146 (Pt 2):289-96. doi: 10.1099/00221287-146-2-289. PubMed PMID: 10708367.

26.   Vilcheze C, Wang F, Arai M, Hazbon MH, Colangeli R, et al. Transfer of a point mutation in Mycobacterium tuberculosis inhA resolves the target of isoniazid. Nat Med. 2006;12(9):1027-9. doi: 10.1038/nm1466. PubMed PMID: 16906155.

27.   Muller B, Streicher EM, Hoek KG, Tait M, Trollip A, et al. inhA promoter mutations: a gateway to extensively drug-resistant tuberculosis in South Africa? Int J Tuberc Lung Dis. 2011;15(3):344-51. PubMed PMID: 21333101.

28.   Miesel L, Weisbrod TR, Marcinkeviciene JA, Bittman R, Jacobs WR, Jr. NADH dehydrogenase defects confer isoniazid resistance and conditional lethality in

Mycobacterium smegmatis. J Bacteriol. 1998;180(9):2459-67. PubMed PMID: 9573199; PMCID: PMC107189.

29.   Vilcheze C, Av-Gay Y, Attarian R, Liu Z, Hazbon MH, et al. Mycothiol biosynthesis is essential for ethionamide susceptibility in Mycobacterium tuberculosis. Mol Microbiol. 2008;69(5):1316-29. doi: 10.1111/j.1365-2958.2008.06365.x. PubMed PMID: 18651841; PMCID: PMC2628429.

30.   Mokrousov I, Narvskaya O, Otten T, Limeschenko E, Steklova L, et al. High prevalence of KatG Ser315Thr substitution among isoniazid-resistant Mycobacterium tuberculosis clinical isolates from northwestern Russia, 1996 to 2001. Antimicrob Agents Chemother. 2002;46(5):1417-24. PubMed PMID: 11959577; PMCID: PMC127151.

31.   Wengenack NL, Uhl JR, St Amand AL, Tomlinson AJ, Benson LM, et al. Recombinant Mycobacterium tuberculosis KatG(S315T) is a competent catalase-peroxidase with reduced activity toward isoniazid. J Infect Dis. 1997;176(3):722-7. PubMed PMID: 9291321.

32.   Saint-Joanis B, Souchon H, Wilming M, Johnsson K, Alzari PM, et al. Use of site-directed mutagenesis to probe the structure, function and isoniazid activation of the catalase/peroxidase, KatG, from Mycobacterium tuberculosis. Biochem J. 1999;338 (Pt 3):753-60. PubMed PMID: 10051449; PMCID: PMC1220113.

33.   Upton AM, Mushtaq A, Victor TC, Sampson SL, Sandy J, et al. Arylamine N-acetyltransferase of Mycobacterium tuberculosis is a polymorphic enzyme and a site of isoniazid metabolism. Mol Microbiol. 2001;42(2):309-17. PubMed PMID: 11703656.

34.   Payton M, Auty R, Delgoda R, Everett M, Sim E. Cloning and characterization of arylamine N-acetyltransferase genes from Mycobacterium smegmatis and Mycobacterium tuberculosis: increased expression results in isoniazid resistance. J Bacteriol. 1999;181(4):1343-7. PubMed PMID: 9973365; PMCID: PMC93516.

35.   Ducasse-Cabanot S, Cohen-Gonsaud M, Marrakchi H, Nguyen M, Zerbib D, et al. In vitro inhibition of the Mycobacterium tuberculosis beta-ketoacyl-acyl carrier protein reductase MabA by isoniazid. Antimicrob Agents Chemother. 2004;48(1):242-9. PubMed PMID: 14693546; PMCID: PMC310174.

36.   Chen P, Bishai WR. Novel selection for isoniazid (INH) resistance genes supports a role for NAD+-binding proteins in mycobacterial INH resistance. Infect Immun. 1998;66(11):5099-106. PubMed PMID: 9784509; PMCID: PMC108635.

37.   Place VA, Thomas JP. Clinical pharmacology of ethambutol. Am Rev Respir Dis. 1963;87:901-4. doi: 10.1164/arrd.1963.87.6.901. PubMed PMID: 13943910.

38.   Peets EA, Sweeney WM, Place VA, Buyske DA. The Absorption, Excretion, and Metabolic Fate of Ethambutol in Man. Am Rev Respir Dis. 1965;91:51-8. doi: 10.1164/arrd.1965.91.1.51. PubMed PMID: 14260000.

39.   Pilheu JA, Maglio F, Cetrangolo R, Pleus AD. Concentrations of ethambutol in the cerebrospinal fluid after oral administration. Tubercle. 1971;52(2):117-22. PubMed PMID: 5560732.

40.   Diermeier HF, Kaiser JA, Yuda N. Safety evaluation of ethambutol. Ann N Y Acad Sci. 1966;135(2):732-46. PubMed PMID: 5296041.

41.   Bobrowitz ID. Ethambutol in the retreatment of pulmonary tuberculosis. Ann N Y Acad Sci. 1966;135(2):796-822. PubMed PMID: 5220240.

42.   Donomae I, Yamamoto K. Clinical evaluation of ethambutol in pulmonary tuberculosis. Ann N Y Acad Sci. 1966;135(2):849-81. PubMed PMID: 5328006.

43.   Carr DT, Karlson AG. Optimal regimens of antituberculous drugs. Am Rev Respir Dis. 1961;84:90-2. doi: 10.1164/arrd.1961.84.1.90. PubMed PMID: 13690990.

44.   Tacquet A, Tison F. [Invitro and in vivo activity of dextro-2,2'-bis-(ethylenediimino)-1-butanol (Ethambutol) used alone or in combination on atypical mycobacteria]. Rev Tuberc Pneumol (Paris). 1963;27:431-43. PubMed PMID: 13980127.

45.   Thomas JP, Baughn CO, Wilkinson RG, Shepherd RG. A new synthetic compound with antituberculous activity in mice: ethambutol (dextro-2,2'-(ethylenediimino)-di-l-butanol). Am Rev Respir Dis. 1961;83:891-3. doi: 10.1164/arrd.1961.83.6.891. PubMed PMID: 13776497.

46.	Shepherd RG, Wilkinson RG. Antituberculous Agents. Ii. N,N'-Diisopropylethylenediamine and Analogs. J Med Pharm Chem. 1962;91:823-35. PubMed PMID: 14056415.

47.	Takayama K, Kilburn JO. Inhibition of synthesis of arabinogalactan by ethambutol in Mycobacterium smegmatis. Antimicrob Agents Chemother. 1989;33(9):1493-9. PubMed PMID: 2817850; PMCID: PMC172689.

48.	Silve G, Valero-Guillen P, Quemard A, Dupont MA, Daffe M, et al. Ethambutol inhibition of glucose metabolism in mycobacteria: a possible target of the drug. Antimicrob Agents Chemother. 1993;37(7):1536-8. PubMed PMID: 8363387; PMCID: PMC188008.

49.	Kilburn JO, Takayama K. Effects of ethambutol on accumulation and secretion of trehalose mycolates and free mycolic acid in Mycobacterium smegmatis. Antimicrob Agents Chemother. 1981;20(3):401-4. PubMed PMID: 7305326; PMCID: PMC181709.

50.	Telenti A, Philipp WJ, Sreevatsan S, Bernasconi C, Stockbauer KE, et al. The emb operon, a gene cluster of Mycobacterium tuberculosis involved in resistance to ethambutol. Nat Med. 1997;3(5):567-70. PubMed PMID: 9142129.

51.	Forbes M, Kuck NA, Peets EA. Effect of Ethambutol on Nucleic Acid Metabolism in Mycobacterium Smegmatis and Its Reversal by Polyamines and Divalent Cations. J Bacteriol. 1965;89:1299-305. PubMed PMID: 14293001; PMCID: PMC277643.

52.	Takayama K, Armstrong EL, Kunugi KA, Kilburn JO. Inhibition by ethambutol of mycolic acid transfer into the cell wall of Mycobacterium smegmatis. Antimicrob Agents Chemother. 1979;16(2):240-2. PubMed PMID: 485133; PMCID: PMC352831.

53.	Cheema S, Khuller GK. Metabolism of phospholipids in Mycobacterium smegmatis ATCC 607 in the presence of ethambutol. Indian J Med Res. 1985;82:207-13. PubMed PMID: 4077161.

54.	Paulin LG, Brander EE, Poso HJ. Specific inhibition of spermidine synthesis in Mycobacteria spp. by the dextro isomer of ethambutol. Antimicrob Agents Chemother. 1985;28(1):157-9. PubMed PMID: 4037776; PMCID: PMC176332.

55.   Tsukamura M. Resistance pattern of Mycobacterium tuberculosis and Mycobacterium bovis to ethambutol. Acta Tuberc Pneumol Scand. 1965;46(2):88-92. PubMed PMID: 4964850.

56.   Gupta SK, Mathur IS. Stability of Ethambutol [d-2,2'-(ethylenediimino)-di-I-butanol] resistant mycobacteria grown in the absence of Ethambutol. Indian J Exp Biol. 1965;3(3):176-7. PubMed PMID: 5320364.

57.   Escuyer VE, Lety MA, Torrelles JB, Khoo KH, Tang JB, et al. The role of the embA and embB gene products in the biosynthesis of the terminal hexaarabinofuranosyl motif of Mycobacterium smegmatis arabinogalactan. J Biol Chem. 2001;276(52):48854-62. doi: 10.1074/jbc.M102272200. PubMed PMID: 11677227.

58.   Zhang N, Torrelles JB, McNeil MR, Escuyer VE, Khoo KH, et al. The Emb proteins of mycobacteria direct arabinosylation of lipoarabinomannan and arabinogalactan via an N-terminal recognition region and a C-terminal synthetic region. Mol Microbiol. 2003;50(1):69-76. PubMed PMID: 14507364.

59.   Belanger AE, Besra GS, Ford ME, Mikusova K, Belisle JT, et al. The embAB genes of Mycobacterium avium encode an arabinosyl transferase involved in cell wall arabinan biosynthesis that is the target for the antimycobacterial drug ethambutol. Proc Natl Acad Sci U S A. 1996;93(21):11919-24. PubMed PMID: 8876238; PMCID: PMC38159.

60.   Sreevatsan S, Stockbauer KE, Pan X, Kreiswirth BN, Moghazeh SL, et al. Ethambutol resistance in Mycobacterium tuberculosis: critical role of embB mutations. Antimicrob Agents Chemother. 1997;41(8):1677-81. PubMed PMID: 9257740; PMCID: PMC163984.

61.   Mokrousov I, Otten T, Vyshnevskiy B, Narvskaya O. Detection of embB306 mutations in ethambutol-susceptible clinical isolates of Mycobacterium tuberculosis from Northwestern Russia: implications for genotypic resistance testing. J Clin Microbiol. 2002;40(10):3810-3. PubMed PMID: 12354887; PMCID: PMC130875.

62.   Jarallah JS, Elias AK, al Hajjaj MS, Bukhari MS, al Shareef AH, et al. High rate of rifampicin resistance of Mycobacterium tuberculosis in the Taif region of Saudi Arabia. Tuber Lung Dis. 1992;73(2):113-5. doi: 10.1016/0962-8479(92)90065-R. PubMed PMID: 1643296.

63.   Wade MM, Zhang Y. Mechanisms of drug resistance in Mycobacterium tuberculosis. Front Biosci. 2004;9:975-94. PubMed PMID: 14766424.

64.   Hartmann G, Honikel KO, Knusel F, Nuesch J. The specific inhibition of the DNA-directed RNA synthesis by rifamycin. Biochim Biophys Acta. 1967;145(3):843-4. PubMed PMID: 4863911.

65.   Archambault J, Friesen JD. Genetics of eukaryotic RNA polymerases I, II, and III. Microbiol Rev. 1993;57(3):703-24. PubMed PMID: 8246845; PMCID: PMC372932.

66.   Campbell EA, Korzheva N, Mustaev A, Murakami K, Nair S, et al. Structural mechanism for rifampicin inhibition of bacterial rna polymerase. Cell. 2001;104(6):901-12. PubMed PMID: 11290327.

67.   Sat B, Hazan R, Fisher T, Khaner H, Glaser G, et al. Programmed cell death in Escherichia coli: some antibiotics can trigger mazEF lethality. J Bacteriol. 2001;183(6):2041-5. doi: 10.1128/JB.183.6.2041-2045.2001. PubMed PMID: 11222603; PMCID: PMC95100.

68.   Zhu L, Zhang Y, Teh JS, Zhang J, Connell N, et al. Characterization of mRNA interferases from Mycobacterium tuberculosis. J Biol Chem. 2006;281(27):18638-43. doi: 10.1074/jbc.M512693200. PubMed PMID: 16611633.

69.   Jin DJ, Gross CA. Mapping and sequencing of mutations in the Escherichia coli rpoB gene that lead to rifampicin resistance. J Mol Biol. 1988;202(1):45-58. PubMed PMID: 3050121.

70.   Lisitsyn NA, Sverdlov ED, Moiseyeva EP, Danilevskaya ON, Nikiforov VG. Mutation to rifampicin resistance at the beginning of the RNA polymerase beta subunit gene in Escherichia coli. Mol Gen Genet. 1984;196(1):173-4. PubMed PMID: 6384726.

71.   Telenti A, Imboden P, Marchesi F, Lowrie D, Cole S, et al. Detection of rifampicin-resistance mutations in Mycobacterium tuberculosis. Lancet. 1993;341(8846):647-50. PubMed PMID: 8095569.

72.   Musser JM. Antimicrobial agent resistance in mycobacteria: molecular genetic insights. Clin Microbiol Rev. 1995;8(4):496-514. PubMed PMID: 8665467; PMCID: PMC172873.

73.   Kapur V, Li LL, Iordanescu S, Hamrick MR, Wanger A, et al. Characterization by automated DNA sequencing of mutations in the gene (rpoB) encoding the RNA polymerase beta subunit in rifampin-resistant Mycobacterium tuberculosis strains from New York City and Texas. J Clin Microbiol. 1994;32(4):1095-8. PubMed PMID: 8027320; PMCID: PMC267194.

74.   Williams DL, Waguespack C, Eisenach K, Crawford JT, Portaels F, et al. Characterization of rifampin-resistance in pathogenic mycobacteria. Antimicrob Agents Chemother. 1994;38(10):2380-6. PubMed PMID: 7840574; PMCID: PMC284748.

75.   Bodmer T, Zurcher G, Imboden P, Telenti A. Mutation position and type of substitution in the beta-subunit of the RNA polymerase influence in-vitro activity of rifamycins in rifampicin-resistant Mycobacterium tuberculosis. J Antimicrob Chemother. 1995;35(2):345-8. PubMed PMID: 7759399.

76.   Moghazeh SL, Pan X, Arain T, Stover CK, Musser JM, et al. Comparative antimycobacterial activities of rifampin, rifapentine, and KRM-1648 against a collection of rifampin-resistant Mycobacterium tuberculosis isolates with known rpoB mutations. Antimicrob Agents Chemother. 1996;40(11):2655-7. PubMed PMID: 8913484; PMCID: PMC163595.

77.   Dabbs ER, Yazawa K, Mikami Y, Miyaji M, Morisaki N, et al. Ribosylation by mycobacterial strains as a new mechanism of rifampin inactivation. Antimicrob Agents Chemother. 1995;39(4):1007-9. PubMed PMID: 7785970; PMCID: PMC162673.

78.   Salfinger M, Heifets LB. Determination of pyrazinamide MICs for Mycobacterium tuberculosis at different pHs by the radiometric method. Antimicrob Agents Chemother. 1988;32(7):1002-4. PubMed PMID: 3142340; PMCID: PMC172333.

79.   Zhang Y, Mitchison D. The curious characteristics of pyrazinamide: a review. Int J Tuberc Lung Dis. 2003;7(1):6-21. PubMed PMID: 12701830.

80.   Zimhony O, Vilcheze C, Arai M, Welch JT, Jacobs WR, Jr. Pyrazinoic acid and its n-propyl ester inhibit fatty acid synthase type I in replicating tubercle bacilli.

Antimicrob Agents Chemother. 2007;51(2):752-4. doi: 10.1128/AAC.01369-06. PubMed PMID: 17101678; PMCID: PMC1797748.

81.   Zhang Y, Wade MM, Scorpio A, Zhang H, Sun Z. Mode of action of pyrazinamide: disruption of Mycobacterium tuberculosis membrane transport and energetics by pyrazinoic acid. J Antimicrob Chemother. 2003;52(5):790-5. doi: 10.1093/jac/dkg446. PubMed PMID: 14563891.

82.   Vandal OH, Pierini LM, Schnappinger D, Nathan CF, Ehrt S. A membrane protein preserves intrabacterial pH in intraphagosomal Mycobacterium tuberculosis. Nat Med. 2008;14(8):849-54. doi: 10.1038/nm.1795. PubMed PMID: 18641659; PMCID: PMC2538620.

83.   Zhang T, Li SY, Nuermberger EL. Autoluminescent Mycobacterium tuberculosis for rapid, real-time, non-invasive assessment of drug and vaccine efficacy. PLoS One. 2012;7(1):e29774. doi: 10.1371/journal.pone.0029774. PubMed PMID: 22253776; PMCID: PMC3256174.

84.   Zhang Y, Scorpio A, Nikaido H, Sun Z. Role of acid pH and deficient efflux of pyrazinoic acid in unique susceptibility of Mycobacterium tuberculosis to pyrazinamide. J Bacteriol. 1999;181(7):2044-9. PubMed PMID: 10094680; PMCID: PMC93615.

85.   Kim H, Shibayama K, Rimbara E, Mori S. Biochemical characterization of quinolinic acid phosphoribosyltransferase from Mycobacterium tuberculosis H37Rv and inhibition of its activity by pyrazinamide. PLoS One. 2014;9(6):e100062. doi: 10.1371/journal.pone.0100062. PubMed PMID: 24949952; PMCID: PMC4065032.

86.   Shi W, Zhang X, Jiang X, Yuan H, Lee JS, et al. Pyrazinamide inhibits trans-translation in Mycobacterium tuberculosis. Science. 2011;333(6049):1630-2. doi: 10.1126/science.1208813. PubMed PMID: 21835980; PMCID: PMC3502614.

87.   Simons SO, Mulder A, van Ingen J, Boeree MJ, van Soolingen D. Role of rpsA gene sequencing in diagnosis of pyrazinamide resistance. J Clin Microbiol. 2013;51(1):382. doi: 10.1128/JCM.02739-12. PubMed PMID: 23269981; PMCID: PMC3536190.

88.   Zhang S, Chen J, Shi W, Liu W, Zhang W, et al. Mutations in panD encoding aspartate decarboxylase are associated with pyrazinamide resistance in Mycobacterium

tuberculosis. Emerg Microbes Infect. 2013;2(6):e34. doi: 10.1038/emi.2013.38. PubMed PMID: 26038471; PMCID: PMC3697303.

89.   Shi W, Chen J, Feng J, Cui P, Zhang S, et al. Aspartate decarboxylase (PanD) as a new target of pyrazinamide in Mycobacterium tuberculosis. Emerg Microbes Infect. 2014;3(8):e58. doi: 10.1038/emi.2014.61. PubMed PMID: 26038753; PMCID: PMC4150287.

90.   Dillon NA, Peterson ND, Rosen BC, Baughn AD. Pantothenate and pantetheine antagonize the antitubercular activity of pyrazinamide. Antimicrob Agents Chemother. 2014;58(12):7258-63. doi: 10.1128/AAC.04028-14. PubMed PMID: 25246400; PMCID: PMC4249577.

91.   Jureen P, Werngren J, Toro JC, Hoffner S. Pyrazinamide resistance and pncA gene mutations in Mycobacterium tuberculosis. Antimicrob Agents Chemother. 2008;52(5):1852-4. doi: 10.1128/AAC.00110-08. PubMed PMID: 18316515; PMCID: PMC2346646.

92.   Koser CU, Comas I, Feuerriegel S, Niemann S, Gagneux S, et al. Genetic diversity within Mycobacterium tuberculosis complex impacts on the accuracy of genotypic pyrazinamide drug-susceptibility assay. Tuberculosis (Edinb). 2014;94(4):451-3. doi: 10.1016/j.tube.2014.04.002. PubMed PMID: 24870943; PMCID: PMC4075347.

93.   Scorpio A, Lindholm-Levy P, Heifets L, Gilman R, Siddiqi S, et al. Characterization of pncA mutations in pyrazinamide-resistant Mycobacterium tuberculosis. Antimicrob Agents Chemother. 1997;41(3):540-3. PubMed PMID: 9055989; PMCID: PMC163747.

94.   Raynaud C, Laneelle MA, Senaratne RH, Draper P, Laneelle G, et al. Mechanisms of pyrazinamide resistance in mycobacteria: importance of lack of uptake in addition to lack of pyrazinamidase activity. Microbiology. 1999;145 (Pt 6):1359-67. doi: 10.1099/13500872-145-6-1359. PubMed PMID: 10411262.

95.   Aono A, Chikamatsu K, Yamada H, Kato T, Mitarai S. Association between pncA gene mutations, pyrazinamidase activity, and pyrazinamide susceptibility testing in Mycobacterium tuberculosis. Antimicrob Agents Chemother. 2014;58(8):4928-30. doi: 10.1128/AAC.02394-14. PubMed PMID: 24867972; PMCID: PMC4136016.

96.   Springer B, Kidan YG, Prammananan T, Ellrott K, Bottger EC, et al. Mechanisms of streptomycin resistance: selection of mutations in the 16S rRNA gene conferring resistance.   Antimicrob   Agents   Chemother.   2001;45(10):2877-84.   doi: 10.1128/AAC.45.10.2877-2884.2001. PubMed PMID: 11557484; PMCID: PMC90746.

97.   Heifets LB, Lindholm-Levy PJ, Flory M. Comparison of bacteriostatic and bactericidal activity of isoniazid and ethionamide against Mycobacterium avium and Mycobacterium   tuberculosis.   Am   Rev   Respir   Dis.   1991;143(2):268-70.   doi: 10.1164/ajrccm/143.2.268. PubMed PMID: 1899326.

98.   Grumbach F, Rist N, Libermann D, Moyeux M, Cals S, et al. [Experimental antituberculous activity of certain isonicotinic thioamides substituted on the nucleus]. C R Hebd Seances Acad Sci. 1956;242(17):2187-9. PubMed PMID: 13330249.

99.   Baulard AR, Betts JC, Engohang-Ndong J, Quan S, McAdam RA, et al. Activation of   the   pro-drug   ethionamide   is   regulated   in   mycobacteria.   J   Biol   Chem. 2000;275(36):28326-31. doi: 10.1074/jbc.M003744200. PubMed PMID: 10869356.

100.   Fraaije MW, Kamerbeek NM, Heidekamp AJ, Fortin R, Janssen DB. The prodrug activator EtaA from Mycobacterium tuberculosis is a Baeyer-Villiger monooxygenase. J Biol   Chem.   2004;279(5):3354-60.   doi: 10.1074/jbc.M307770200.   PubMed   PMID: 14610090.

101.   Wang   F,   Langley   R,   Gulten   G,   Dover   LG,   Besra   GS,   et   al.   Mechanism   of thioamide drug action against tuberculosis and leprosy. J Exp Med. 2007;204(1):73-8. doi: 10.1084/jem.20062100. PubMed PMID: 17227913; PMCID: PMC2118422.

102.   Vannelli TA, Dykman A, Ortiz de Montellano PR. The antituberculosis drug ethionamide   is   activated   by   a   flavoprotein   monooxygenase.   J   Biol   Chem. 2002;277(15):12824-9. doi: 10.1074/jbc.M110751200. PubMed PMID: 11823459.

103.   Morlock GP, Metchock B, Sikes D, Crawford JT, Cooksey RC. ethA, inhA, and katG loci of ethionamide-resistant clinical Mycobacterium tuberculosis isolates. Antimicrob Agents Chemother. 2003;47(12):3799-805. PubMed PMID: 14638486; PMCID: PMC296216.

104.   Brossier F, Veziris N, Truffot-Pernot C, Jarlier V, Sougakoff W. Molecular investigation of resistance to the antituberculous drug ethionamide in multidrug-resistant

clinical isolates of Mycobacterium tuberculosis. Antimicrob Agents Chemother. 2011;55(1):355-60. doi: 10.1128/AAC.01030-10. PubMed PMID: 20974869; PMCID: PMC3019671.

105.   Lehmann J. Para-aminosalicylic acid in the treatment of tuberculosis. Lancet. 1946;1(6384):15. PubMed PMID: 21008766.

106.   Ratledge C, Brown KA. Inhibition of mycobactin formation in Mycobacterium smegmatis by p-aminosalicylate. A new proposal for the mode of action of p-aminosalicylate.   Am   Rev   Respir   Dis.   1972;106(5):774-6.   doi: 10.1164/arrd.1972.106.5.774. PubMed PMID: 5078877.

107.   Zheng J, Rubin EJ, Bifani P, Mathys V, Lim V, et al. para-Aminosalicylic acid is a prodrug targeting dihydrofolate reductase in Mycobacterium tuberculosis. J Biol Chem. 2013;288(32):23447-56. doi: 10.1074/jbc.M113.475798. PubMed PMID: 23779105.

108.   Chakraborty S, Gruber T, Barry CE, 3rd, Boshoff HI, Rhee KY. Para-aminosalicylic acid acts as an alternative substrate of folate metabolism in Mycobacterium tuberculosis.   Science.   2013;339(6115):88-91.   doi: 10.1126/science.1228980.   PubMed PMID: 23118010; PMCID: PMC3792487.

109.   Cheng YS, Sacchettini JC. Structural Insights into Mycobacterium tuberculosis Rv2671 Protein as a Dihydrofolate Reductase Functional Analogue Contributing to para-Aminosalicylic   Acid   Resistance.   Biochemistry.   2016;55(7):1107-19.   doi: 10.1021/acs.biochem.5b00993. PubMed PMID: 26848874.

110.   Mathys V, Wintjens R, Lefevre P, Bertout J, Singhal A, et al. Molecular genetics of para-aminosalicylic acid resistance in clinical isolates and spontaneous mutants of Mycobacterium tuberculosis. Antimicrob Agents Chemother. 2009;53(5):2100-9. doi: 10.1128/AAC.01197-08. PubMed PMID: 19237648; PMCID: PMC2681553.

111.   Ginsburg AS, Grosset JH, Bishai WR. Fluoroquinolones, tuberculosis, and resistance. Lancet Infect Dis. 2003;3(7):432-42. PubMed PMID: 12837348.

112.   Ball P, Mandell L, Niki Y, Tillotson G. Comparative tolerability of the newer fluoroquinolone antibacterials. Drug Saf. 1999;21(5):407-21. PubMed PMID: 10554054.

113. Yew WW, Wong CF, Wong PC, Lee J, Chau CH. Adverse neurological reactions in patients with multidrug-resistant pulmonary tuberculosis after coadministration of cycloserine and ofloxacin. Clin Infect Dis. 1993;17(2):288-9. PubMed PMID: 8399888.

114. Lesher GY, Froelich EJ, Gruett MD, Bailey JH, Brundage RP. 1,8-Naphthyridine Derivatives. A New Class of Chemotherapeutic Agents. J Med Pharm Chem. 1962;91:1063-5. PubMed PMID: 14056431.

115. Drlica K, Malik M. Fluoroquinolones: action and resistance. Curr Top Med Chem. 2003;3(3):249-82. PubMed PMID: 12570763.

116. Alangaden GJ, Manavathu EK, Vakulenko SB, Zvonok NM, Lerner SA. Characterization of fluoroquinolone-resistant mutant strains of Mycobacterium tuberculosis selected in the laboratory and isolated from patients. Antimicrob Agents Chemother. 1995;39(8):1700-3. PubMed PMID: 7486904; PMCID: PMC162811.

117. Takiff HE, Salazar L, Guerrero C, Philipp W, Huang WM, et al. Cloning and nucleotide sequence of Mycobacterium tuberculosis gyrA and gyrB genes and detection of quinolone resistance mutations. Antimicrob Agents Chemother. 1994;38(4):773-80. PubMed PMID: 8031045; PMCID: PMC284541.

118. Xu C, Kreiswirth BN, Sreevatsan S, Musser JM, Drlica K. Fluoroquinolone resistance associated with specific gyrase mutations in clinical isolates of multidrug-resistant Mycobacterium tuberculosis. J Infect Dis. 1996;174(5):1127-30. PubMed PMID: 8896523.

119. Cambau E, Sougakoff W, Besson M, Truffot-Pernot C, Grosset J, et al. Selection of a gyrA mutant of Mycobacterium tuberculosis resistant to fluoroquinolones during treatment with ofloxacin. J Infect Dis. 1994;170(5):1351. PubMed PMID: 7963747.

120. Kocagoz T, Hackbarth CJ, Unsal I, Rosenberg EY, Nikaido H, et al. Gyrase mutations in laboratory-selected, fluoroquinolone-resistant mutants of Mycobacterium tuberculosis H37Ra. Antimicrob Agents Chemother. 1996;40(8):1768-74. PubMed PMID: 8843279; PMCID: PMC163415.

121. Zhou J, Dong Y, Zhao X, Lee S, Amin A, et al. Selection of antibiotic-resistant bacterial mutants: allelic diversity among fluoroquinolone-resistant mutations. J Infect Dis. 2000;182(2):517-25. doi: 10.1086/315708. PubMed PMID: 10915083.

122.   Liu J, Takiff HE, Nikaido H. Active efflux of fluoroquinolones in Mycobacterium smegmatis mediated by LfrA, a multidrug efflux pump. J Bacteriol. 1996;178(13):3791-5. PubMed PMID: 8682782; PMCID: PMC232638.

123.   Nair S, Maguire W, Baron H, Imbruce R. The effect of cycloserine on pyridoxine-dependent metabolism in tuberculosis. J Clin Pharmacol. 1976;16(8-9):439-43. PubMed PMID: 972198.

124.   Tsukamura M. [Evaluation of cycloserine in the treatment of infections caused by nontuberculous mycobacteria viewed from in vitro experiments]. Kekkaku. 1989;64(5):345-9. PubMed PMID: 2507817.

125.   Kuehl FAJW, Frank J.; Trenner, Nelson R.; Peck, Robert L.; Buhs, Rudolf P.; Putter, Irvin; Ormond, Robert; Lyons, John E.; Chaiet, Louis; Howe, Eugene; Hunnewell, Berl D.; Downing, Geo; Newstead, E; Folkers, Karl. D-4-Amino-3-isoxazolidinone, a new antibiotic. Journal of the American Chemical Society. 1995;77(8):2344-55.

126.   Stammer CHW, Andrew N.; Holly, Frederick W.; Folkers, Karl. Synthesis of D-4-amino-3-isoxazolidinone. Journal of the American Chemical Society. 1995;77(8):2346-7.

127.   Hidy PHH, E B.; Young, Vernon V.; Harned, Roger L.; Brewer, Glenn A.; Phillips, W. F.; Runge, W. F.; Stavely, Homer E.; Pohland, A.; Boaz, H.; Sullivan, H. R. Structure and reaction of cycloserine. Journal of the American Chemical Society. 1955;77(8):2345-6.

128.   Prosser GA, de Carvalho LP. Reinterpreting the mechanism of inhibition of Mycobacterium tuberculosis D-alanine:D-alanine ligase by D-cycloserine. Biochemistry. 2013;52(40):7145-9. doi: 10.1021/bi400839f. PubMed PMID: 24033232; PMCID: PMC3944805.

129.   Prosser GA, de Carvalho LP. Kinetic mechanism and inhibition of Mycobacterium tuberculosis D-alanine:D-alanine ligase by the antibiotic D-cycloserine. FEBS J. 2013;280(4):1150-66. doi: 10.1111/febs.12108. PubMed PMID: 23286234.

130.   Feng Z, Barletta RG. Roles of Mycobacterium smegmatis D-alanine:D-alanine ligase and D-alanine racemase in the mechanisms of action of and resistance to the

peptidoglycan inhibitor D-cycloserine. Antimicrob Agents Chemother. 2003;47(1):283-91. PubMed PMID: 12499203; PMCID: PMC149019.

131. Rist N, Canetti G, Boisvert H, Le Lirzin M. [The BCG antibiogram. Diagnostic value of resistance to cycloserine]. Rev Tuberc Pneumol (Paris). 1967;31(7):1060-5. PubMed PMID: 4988437.

132. Desjardins CA, Cohen KA, Munsamy V, Abeel T, Maharaj K, et al. Genomic and functional analyses of Mycobacterium tuberculosis strains implicate ald in D-cycloserine resistance. Nat Genet. 2016;48(5):544-51. doi: 10.1038/ng.3548. PubMed PMID: 27064254; PMCID: PMC4848111.

133. Park JW, Park SR, Nepal KK, Han AR, Ban YH, et al. Discovery of parallel pathways of kanamycin biosynthesis allows antibiotic manipulation. Nat Chem Biol. 2011;7(11):843-52. doi: 10.1038/nchembio.671. PubMed PMID: 21983602.

134. Kotra LP, Haddad J, Mobashery S. Aminoglycosides: perspectives on mechanisms of action and resistance and strategies to counter resistance. Antimicrob Agents Chemother. 2000;44(12):3249-56. PubMed PMID: 11083623; PMCID: PMC90188.

135. Suzuki Y, Katsukawa C, Tamaru A, Abe C, Makino M, et al. Detection of kanamycin-resistant Mycobacterium tuberculosis by identifying mutations in the 16S rRNA gene. J Clin Microbiol. 1998;36(5):1220-5. PubMed PMID: 9574680; PMCID: PMC104803.

136. Jugheli L, Bzekalava N, de Rijk P, Fissette K, Portaels F, et al. High level of cross-resistance between kanamycin, amikacin, and capreomycin among Mycobacterium tuberculosis isolates from Georgia and a close relation with mutations in the rrs gene. Antimicrob Agents Chemother. 2009;53(12):5064-8. doi: 10.1128/AAC.00851-09. PubMed PMID: 19752274; PMCID: PMC2786337.

137. Ford CW, Zurenko GE, Barbachyn MR. The discovery of linezolid, the first oxazolidinone antibacterial agent. Curr Drug Targets Infect Disord. 2001;1(2):181-99. PubMed PMID: 12455414.

138. Long KS, Vester B. Resistance to linezolid caused by modifications at its binding site on the ribosome. Antimicrob Agents Chemother. 2012;56(2):603-12. doi: 10.1128/AAC.05702-11. PubMed PMID: 22143525; PMCID: PMC3264260.

139.   Richter E, Rusch-Gerdes S, Hillemann D. First linezolid-resistant clinical isolates of Mycobacterium tuberculosis. Antimicrob Agents Chemother. 2007;51(4):1534-6. doi: 10.1128/AAC.01113-06. PubMed PMID: 17242139; PMCID: PMC1855508.

140.   Dey T, Brigden G, Cox H, Shubber Z, Cooke G, et al. Outcomes of clofazimine for the treatment of drug-resistant tuberculosis: a systematic review and meta-analysis. J Antimicrob Chemother. 2013;68(2):284-93. doi: 10.1093/jac/dks389. PubMed PMID: 23054996.

141.   Lechartier B, Cole ST. Mode of Action of Clofazimine and Combination Therapy with Benzothiazinones against Mycobacterium tuberculosis. Antimicrob Agents Chemother. 2015;59(8):4457-63. doi: 10.1128/AAC.00395-15. PubMed PMID: 25987624; PMCID: PMC4505229.

142.   Hartkoorn RC, Uplekar S, Cole ST. Cross-resistance between clofazimine and bedaquiline through upregulation of MmpL5 in Mycobacterium tuberculosis. Antimicrob Agents Chemother. 2014;58(5):2979-81. doi: 10.1128/AAC.00037-14. PubMed PMID: 24590481; PMCID: PMC3993252.

143.   Dauby N, Muylle I, Mouchet F, Sergysels R, Payen MC. Meropenem/clavulanate and linezolid treatment for extensively drug-resistant tuberculosis. Pediatr Infect Dis J. 2011;30(9):812-3. doi: 10.1097/INF.0b013e3182154b05. PubMed PMID: 21378593.

144.   Alahari A, Trivelli X, Guerardel Y, Dover LG, Besra GS, et al. Thiacetazone, an antitubercular drug that inhibits cyclopropanation of cell wall mycolic acids in mycobacteria. PLoS One. 2007;2(12):e1343. doi: 10.1371/journal.pone.0001343. PubMed PMID: 18094751; PMCID: PMC2147073.

145.   van der Paardt AF, Wilffert B, Akkerman OW, de Lange WC, van Soolingen D, et al. Evaluation of macrolides for possible use against multidrug-resistant Mycobacterium tuberculosis. Eur Respir J. 2015;46(2):444-55. doi: 10.1183/09031936.00147014. PubMed PMID: 26022960.

146.   Zumla A, Nahid P, Cole ST. Advances in the development of new tuberculosis drugs and treatment regimens. Nat Rev Drug Discov. 2013;12(5):388-404. doi: 10.1038/nrd4001. PubMed PMID: 23629506.

147.	Koul A, Vranckx L, Dendouga N, Balemans W, Van den Wyngaert I, et al. Diarylquinolines are bactericidal for dormant mycobacteria as a result of disturbed ATP homeostasis. J Biol Chem. 2008;283(37):25273-80. doi: 10.1074/jbc.M803899200. PubMed PMID: 18625705.

148.	Rao SP, Alonso S, Rand L, Dick T, Pethe K. The protonmotive force is required for maintaining ATP homeostasis and viability of hypoxic, nonreplicating Mycobacterium tuberculosis. Proc Natl Acad Sci U S A. 2008;105(33):11945-50. doi: 10.1073/pnas.0711697105. PubMed PMID: 18697942; PMCID: PMC2575262.

149.	Koul A, Dendouga N, Vergauwen K, Molenberghs B, Vranckx L, et al. Diarylquinolines target subunit c of mycobacterial ATP synthase. Nat Chem Biol. 2007;3(6):323-4. doi: 10.1038/nchembio884. PubMed PMID: 17496888.

150.	Huitric E, Verhasselt P, Koul A, Andries K, Hoffner S, et al. Rates and mechanisms of resistance development in Mycobacterium tuberculosis to a novel diarylquinoline ATP synthase inhibitor. Antimicrob Agents Chemother. 2010;54(3):1022-8. doi: 10.1128/AAC.01611-09. PubMed PMID: 20038615; PMCID: PMC2825986.

151.	Matsumoto M, Hashizume H, Tomishige T, Kawasaki M, Tsubouchi H, et al. OPC-67683, a nitro-dihydro-imidazooxazole derivative with promising action against tuberculosis in vitro and in mice. PLoS Med. 2006;3(11):e466. doi: 10.1371/journal.pmed.0030466. PubMed PMID: 17132069; PMCID: 1664607.

152.	Skripconoka V, Danilovits M, Pehme L, Tomson T, Skenders G, et al. Delamanid improves outcomes and reduces mortality in multidrug-resistant tuberculosis. Eur Respir J. 2013;41(6):1393-400. doi: 10.1183/09031936.00125812. PubMed PMID: 23018916; PMCID: PMC3669462.

153.	Manjunatha U, Boshoff HI, Barry CE. The mechanism of action of PA-824: Novel insights from transcriptional profiling. Commun Integr Biol. 2009;2(3):215-8. PubMed PMID: 19641733; PMCID: PMC2717523.

154.	Lechartier B, Hartkoorn RC, Cole ST. In vitro combination studies of benzothiazinone lead compound BTZ043 against Mycobacterium tuberculosis. Antimicrob Agents Chemother. 2012;56(11):5790-3. doi: 10.1128/AAC.01476-12. PubMed PMID: 22926573; PMCID: PMC3486603.

155.   Reddy VM, Einck L, Andries K, Nacy CA. In vitro interactions between new antitubercular drug candidates SQ109 and TMC207. Antimicrob Agents Chemother. 2010;54(7):2840-6. doi: 10.1128/AAC.01601-09. PubMed PMID: 20385864; PMCID: PMC2897281.

156.   Tahlan K, Wilson R, Kastrinsky DB, Arora K, Nair V, et al. SQ109 targets MmpL3, a membrane transporter of trehalose monomycolate involved in mycolic acid donation to the cell wall core of Mycobacterium tuberculosis. Antimicrob Agents Chemother. 2012;56(4):1797-809. doi: 10.1128/AAC.05708-11. PubMed PMID: 22252828; PMCID: 3318387.

157.   Rhee KY, de Carvalho LP, Bryk R, Ehrt S, Marrero J, et al. Central carbon metabolism in Mycobacterium tuberculosis: an unexpected frontier. Trends Microbiol. 2011;19(7):307-14. doi: 10.1016/j.tim.2011.03.008. PubMed PMID: 21561773; PMCID: 3601588.

158.   Eisenreich W, Dandekar T, Heesemann J, Goebel W. Carbon metabolism of intracellular bacterial pathogens and possible links to virulence. Nat Rev Microbiol. 2010;8(6):401-12. doi: 10.1038/nrmicro2351. PubMed PMID: 20453875.

159.   Li K, Schurig-Briccio LA, Feng X, Upadhyay A, Pujari V, et al. Multitarget drug discovery for tuberculosis and other infectious diseases. J Med Chem. 2014;57(7):3126-39. doi: 10.1021/jm500131s. PubMed PMID: 24568559; PMCID: 4084622.

160.   Sharma SK, Mohan A. Extrapulmonary tuberculosis. Indian J Med Res. 2004;120(4):316-53. PubMed PMID: 15520485.

161.   McCarthy KD, Cain KP, Winthrop KL, Udomsantisuk N, Lan NT, et al. Nontuberculous mycobacterial disease in patients with HIV in Southeast Asia. Am J Respir Crit Care Med. 2012;185(9):981-8. doi: 10.1164/rccm.201107-1327OC. PubMed PMID: 22345581.

162.   Bodle EE, Cunningham JA, Della-Latta P, Schluger NW, Saiman L. Epidemiology of nontuberculous mycobacteria in patients without HIV infection, New York City. Emerg Infect Dis. 2008;14(3):390-6. doi: 10.3201/eid1403.061143. PubMed PMID: 18325252; PMCID: 2570812.

163.   Patel SY, Ding L, Brown MR, Lantz L, Gay T, et al. Anti-IFN-gamma autoantibodies in disseminated nontuberculous mycobacterial infections. J Immunol. 2005;175(7):4769-76. PubMed PMID: 16177125.

164.   Raju RM, Raju SM, Zhao Y, Rubin EJ. Leveraging Advances in Tuberculosis Diagnosis and Treatment to Address Nontuberculous Mycobacterial Disease. Emerg Infect Dis. 2016;22(3):365-9. doi: 10.3201/eid2203.151643. PubMed PMID: 26886068; PMCID: 4766907.

165.   Reyrat JM, Kahn D. Mycobacterium smegmatis: an absurd model for tuberculosis? Trends Microbiol. 2001;9(10):472-4. PubMed PMID: 11597444.

166.   Prasanna AN, Mehra S. Comparative phylogenomics of pathogenic and non-pathogenic   mycobacterium.   PLoS   One.   2013;8(8):e71248.   doi: 10.1371/journal.pone.0071248. PubMed PMID: 24015186; PMCID: 3756022.

167.   Zakham F, Aouane O, Ussery D, Benjouad A, Ennaji MM. Computational genomics-proteomics and Phylogeny analysis of twenty one mycobacterial genomes (Tuberculosis & non Tuberculosis strains). Microb Inform Exp. 2012;2(1):7. doi: 10.1186/2042-5783-2-7. PubMed PMID: 22929624; PMCID: 3504576.

168.   Altaf M, Miller CH, Bellows DS, O'Toole R. Evaluation of the Mycobacterium smegmatis and BCG models for the discovery of Mycobacterium tuberculosis inhibitors. Tuberculosis (Edinb). 2010;90(6):333-7. doi: 10.1016/j.tube.2010.09.002. PubMed PMID: 20933470.

169.   Gupta A, Bhakta S. An integrated surrogate model for screening of drugs against Mycobacterium tuberculosis. J Antimicrob Chemother. 2012;67(6):1380-91. doi: 10.1093/jac/dks056. PubMed PMID: 22398649.

170.   Wang R, Marcotte EM. The proteomic response of Mycobacterium smegmatis to anti-tuberculosis drugs suggests targeted pathways. J Proteome Res. 2008;7(3):855-65. doi: 10.1021/pr0703066. PubMed PMID: 18275136.

171.   Chaturvedi V, Dwivedi N, Tripathi RP, Sinha S. Evaluation of Mycobacterium smegmatis as a possible surrogate screen for selecting molecules active against multi-drug resistant Mycobacterium tuberculosis. J Gen Appl Microbiol. 2007;53(6):333-7. PubMed PMID: 18187888.

172.   Bassett IM, Lun S, Bishai WR, Guo H, Kirman JR, et al. Detection of inhibitors of phenotypically drug-tolerant Mycobacterium tuberculosis using an in vitro bactericidal screen. J Microbiol. 2013;51(5):651-8. doi: 10.1007/s12275-013-3099-4. PubMed PMID: 23800952.

173.   Schenone M, Dancik V, Wagner BK, Clemons PA. Target identification and mechanism of action in chemical biology and drug discovery. Nat Chem Biol. 2013;9(4):232-40. doi: 10.1038/nchembio.1199. PubMed PMID: 23508189.

174.   Martinez JL, Baquero F. Mutation frequencies and antibiotic resistance. Antimicrob Agents Chemother. 2000;44(7):1771-7. PubMed PMID: 10858329; PMCID: 89960.

175.   Morlock GP, Plikaytis BB, Crawford JT. Characterization of spontaneous, In vitro-selected, rifampin-resistant mutants of Mycobacterium tuberculosis strain H37Rv. Antimicrob Agents Chemother. 2000;44(12):3298-301. PubMed PMID: 11083630; PMCID: 90195.

176.   Sambandamurthy VK, Wang X, Chen B, Russell RG, Derrick S, et al. A pantothenate auxotroph of Mycobacterium tuberculosis is highly attenuated and protects mice against tuberculosis. Nat Med. 2002;8(10):1171-4. doi: 10.1038/nm765. PubMed PMID: 12219086.

177.   Daugelat S, Kowall J, Mattow J, Bumann D, Winter R, et al. The RD1 proteins of Mycobacterium tuberculosis: expression in Mycobacterium smegmatis and biochemical characterization. Microbes Infect. 2003;5(12):1082-95. PubMed PMID: 14554249.

178.   Leeson P. Drug discovery: Chemical beauty contest. Nature. 2012;481(7382):455-6. doi: 10.1038/481455a. PubMed PMID: 22281594.

179.   Collins L, Franzblau SG. Microplate alamar blue assay versus BACTEC 460 system for high-throughput screening of compounds against Mycobacterium tuberculosis and Mycobacterium avium. Antimicrob Agents Chemother. 1997;41(5):1004-9. PubMed PMID: 9145860; PMCID: 163841.

180.   Larsen MH, Biermann K, Tandberg S, Hsu T, Jacobs WR, Jr. Genetic Manipulation of Mycobacterium tuberculosis. Curr Protoc Microbiol. 2007;Chapter 10:Unit 10A 2. doi: 10.1002/9780471729259.mc10a02s6. PubMed PMID: 18770603.

181.   La Rosa V, Poce G, Canseco JO, Buroni S, Pasca MR, et al. MmpL3 is the cellular target of the antitubercular pyrrole derivative BM212. Antimicrob Agents Chemother. 2012;56(1):324-31. doi: 10.1128/AAC.05270-11. PubMed PMID: 22024828; PMCID: 3256021.

182.   Ioerger TR, Sacchettini JC. Structural genomics approach to drug discovery for Mycobacterium tuberculosis. Curr Opin Microbiol. 2009;12(3):318-25. doi: 10.1016/j.mib.2009.04.006. PubMed PMID: 19481971.

183.   Murry JP, Sassetti CM, Lane JM, Xie Z, Rubin EJ. Transposon site hybridization in Mycobacterium tuberculosis. Methods Mol Biol. 2008;416:45-59. doi: 10.1007/978-1-59745-321-9_4. PubMed PMID: 18392960.

184.   Sassetti CM, Boyd DH, Rubin EJ. Genes required for mycobacterial growth defined by high density mutagenesis. Mol Microbiol. 2003;48(1):77-84. PubMed PMID: 12657046.

185.   Murphy KC. Targeted chromosomal gene knockout using PCR fragments. Methods Mol Biol. 2011;765:27-42. doi: 10.1007/978-1-61779-197-0_2. PubMed PMID: 21815084.

186.   Piccaro G, Poce G, Biava M, Giannoni F, Fattorini L. Activity of lipophilic and hydrophilic drugs against dormant and replicating Mycobacterium tuberculosis. J Antibiot (Tokyo). 2015;68(11):711-4. doi: 10.1038/ja.2015.52. PubMed PMID: 25944535.

187.   Tasneen R, Williams K, Amoabeng O, Minkowski A, Mdluli KE, et al. Contribution of the nitroimidazoles PA-824 and TBA-354 to the activity of novel regimens in murine models of tuberculosis. Antimicrob Agents Chemother. 2015;59(1):129-35. doi: 10.1128/AAC.03822-14. PubMed PMID: 25331697; PMCID: PMC4291340.

188.   Williams K, Minkowski A, Amoabeng O, Peloquin CA, Taylor D, et al. Sterilizing activities of novel combinations lacking first- and second-line drugs in a murine model of tuberculosis. Antimicrob Agents Chemother. 2012;56(6):3114-20. doi: 10.1128/AAC.00384-12. PubMed PMID: 22470112; PMCID: PMC3370712.

189.   Veber DF, Johnson SR, Cheng HY, Smith BR, Ward KW, et al. Molecular properties that influence the oral bioavailability of drug candidates. J Med Chem. 2002;45(12):2615-23. PubMed PMID: 12036371.

190.   Barrett I, Meegan MJ, Hughes RB, Carr M, Knox AJ, et al. Synthesis, biological evaluation, structural-activity relationship, and docking study for a series of benzoxepin-derived estrogen receptor modulators. Bioorg Med Chem. 2008;16(21):9554-73. doi: 10.1016/j.bmc.2008.09.035. PubMed PMID: 18835176.

191.   Owens CP, Chim N, Graves AB, Harmston CA, Iniguez A, et al. The Mycobacterium tuberculosis secreted protein Rv0203 transfers heme to membrane proteins MmpL3 and MmpL11. J Biol Chem. 2013;288(30):21714-28. doi: 10.1074/jbc.M113.453076. PubMed PMID: 23760277; PMCID: 3724630.

192.   Li W, Upadhyay A, Fontes FL, North EJ, Wang Y, et al. Novel insights into the mechanism of inhibition of MmpL3, a target of multiple pharmacophores in Mycobacterium tuberculosis. Antimicrob Agents Chemother. 2014;58(11):6413-23. doi: 10.1128/AAC.03229-14. PubMed PMID: 25136022; PMCID: 4249373.

193.   Ioerger TR, O'Malley T, Liao R, Guinn KM, Hickey MJ, et al. Identification of new drug targets and resistance mechanisms in Mycobacterium tuberculosis. PLoS One. 2013;8(9):e75245. doi: 10.1371/journal.pone.0075245. PubMed PMID: 24086479; PMCID: 3781026.

194.   Jarand J, Levin A, Zhang L, Huitt G, Mitchell JD, et al. Clinical and microbiologic outcomes in patients receiving treatment for Mycobacterium abscessus pulmonary disease. Clin Infect Dis. 2011;52(5):565-71. doi: 10.1093/cid/ciq237. PubMed PMID: 21292659.

195.   Altschul SF, Gish W, Miller W, Myers EW, Lipman DJ. Basic local alignment search tool. J Mol Biol. 1990;215(3):403-10. doi: 10.1016/S0022-2836(05)80360-2. PubMed PMID: 2231712.

196.   Altschul SF, Madden TL, Schaffer AA, Zhang J, Zhang Z, et al. Gapped BLAST and PSI-BLAST: a new generation of protein database search programs. Nucleic Acids Res. 1997;25(17):3389-402. PubMed PMID: 9254694; PMCID: 146917.

197. Doi E, Shibata D, Matoba T. Modified colorimetric ninhydrin methods for peptidase assay. Anal Biochem. 1981;118(1):173-84. PubMed PMID: 7039409.

198. Chow C, Xu H, Blanchard JS. Kinetic characterization of hydrolysis of nitrocefin, cefoxitin, and meropenem by beta-lactamase from Mycobacterium tuberculosis. Biochemistry. 2013;52(23):4097-104. doi: 10.1021/bi400177y. PubMed PMID: 23672214; PMCID: 3750105.

199. Jimenez JI, Canales A, Jimenez-Barbero J, Ginalski K, Rychlewski L, et al. Deciphering the genetic determinants for aerobic nicotinic acid degradation: the nic cluster from Pseudomonas putida KT2440. Proc Natl Acad Sci U S A. 2008;105(32):11329-34. doi: 10.1073/pnas.0802273105. PubMed PMID: 18678916; PMCID: 2516282.

200. Kincaid VA, Sullivan ED, Klein RD, Noel JW, Rowlett RS, et al. Structure and catalytic mechanism of nicotinate (vitamin B3) degradative enzyme maleamate amidohydrolase from Bordetella bronchiseptica RB50. Biochemistry. 2012;51(1):545-54. doi: 10.1021/bi201347n. PubMed PMID: 22214383.

201. Savvi S, Warner DF, Kana BD, McKinney JD, Mizrahi V, et al. Functional characterization of a vitamin B12-dependent methylmalonyl pathway in Mycobacterium tuberculosis: implications for propionate metabolism during growth on fatty acids. J Bacteriol. 2008;190(11):3886-95. doi: 10.1128/JB.01767-07. PubMed PMID: 18375549; PMCID: 2395058.

202. Eoh H, Rhee KY. Methylcitrate cycle defines the bactericidal essentiality of isocitrate lyase for survival of Mycobacterium tuberculosis on fatty acids. Proc Natl Acad Sci U S A. 2014;111(13):4976-81. doi: 10.1073/pnas.1400390111. PubMed PMID: 24639517; PMCID: 3977286.

203. Akiya Furuichi HA, Hiroko Matsukura, Takeshi Oishi, Koki Horikoshi. Purification and Properties of an Asymmetric Reduction Enzyme of 2-Methyl-3-oxobutyrate in Baker's Yeast. Agric Biol Chem. 1985;49(9):2563-70.

204. Lin MC, Wagner C. Purification and characterization of N-methylalanine dehydrogenase. J Biol Chem. 1975;250(10):3746-51. PubMed PMID: 236301.

205.   Palmatier RD, McCroskey RP, Abbott MT. The enzymatic conversion of uracil 5-carboxylic acid to uracil and carbon dioxide. J Biol Chem. 1970;245(24):6706-10. PubMed PMID: 5482775.

206.   Watanabe MS, McCroskey RP, Abbott MT. The enzymatic conversion of 5-formyluracil to uracil 5-carboxylic acid. J Biol Chem. 1970;245(8):2023-6. PubMed PMID: 5440840.

207.   Soong CL, Ogawa J, Sakuradani E, Shimizu S. Barbiturase, a novel zinc-containing amidohydrolase involved in oxidative pyrimidine metabolism. J Biol Chem. 2002;277(9):7051-8. doi: 10.1074/jbc.M110784200. PubMed PMID: 11748240.

208.   Seffernick JL, Erickson JS, Cameron SM, Cho S, Dodge AG, et al. Defining sequence space and reaction products within the cyanuric acid hydrolase (AtzD)/barbiturase protein family. J Bacteriol. 2012;194(17):4579-88. doi: 10.1128/JB.00791-12. PubMed PMID: 22730121; PMCID: 3415516.

209.   Jakoby WB, Bonner DM. Kynureninase from Neurospora: interaction of enzyme with substrates, coenzyme, and amines. J Biol Chem. 1953;205(2):709-15. PubMed PMID: 13129249.

210.   Barbara S Briggs AJK, Celia Whitesitt, Wu-Kuang Yeh, Milton Zmijewski. Discovery, purification, and properties of o-phthalyl amidase from *Xanthobacter agilis*. Journal of Molecular Catalysis B: Enzymatic. 1996;2(1):53-69.

211.   Krieger IV, Freundlich JS, Gawandi VB, Roberts JP, Gawandi VB, et al. Structure-guided discovery of phenyl-diketo acids as potent inhibitors of M. tuberculosis malate synthase. Chem Biol. 2012;19(12):1556-67. doi: 10.1016/j.chembiol.2012.09.018. PubMed PMID: 23261599; PMCID: 3530165.

212.   Abrahams GL, Kumar A, Savvi S, Hung AW, Wen S, et al. Pathway-selective sensitization of Mycobacterium tuberculosis for target-based whole-cell screening. Chem Biol. 2012;19(7):844-54. doi: 10.1016/j.chembiol.2012.05.020. PubMed PMID: 22840772; PMCID: 3421836.

213.   Doerks T, van Noort V, Minguez P, Bork P. Annotation of the M. tuberculosis hypothetical orfeome: adding functional information to more than half of the

uncharacterized proteins. PLoS One. 2012;7(4):e34302. doi: 10.1371/journal.pone.0034302. PubMed PMID: 22485162; PMCID: PMC3317503.

214.   Sivashankari S, Shanmughavel P. Functional annotation of hypothetical proteins - A review. Bioinformation. 2006;1(8):335-8. PubMed PMID: 17597916; PMCID: PMC1891709.

215.   Pan X, Yang Y, Zhang JR. Molecular basis of host specificity in human pathogenic bacteria. Emerg Microbes Infect. 2014;3(3):e23. doi: 10.1038/emi.2014.23. PubMed PMID: 26038515; PMCID: PMC3974339.